Escola de Camins
Escola Tècnica Superior d'Enginyeria de Camins, Canals i Ports
UPC BARCELONATECH

Tesis doctoral – Doctorat d'Enginyeria Civil

Título

Measuring impact loads on rigid coastal structures

Autor

Andrea Marzeddu

Tutores

Francesc Xavier Gironella i Cobos

Agustín Sánchez-Arcilla Conejo

Data

Barcelona 07/03/2016

Índice

Listado de figuras

Listado de tablas

Resumen

Esta tesis se centra en el estudio de efectos de laboratorio que tienen lugar durante la medida de impactos violentos generados por olas rompientes sobre estructuras rígidas. Para su fin, se ha llevado a cabo una extensa campaña experimental en el canal de pequeña escala CIEMito del LIM-UPC BarcelonaTech y se ha realizado más de 4000 ensayos con oleajes regulares. Se ha analizado el efecto de la frecuencia de muestreo, la tipología del sistema de medida y el *layout* experimental en los resultados registrados. Tras confirmar experimentalmente el comportamiento prácticamente aleatorio del fenómeno y, para poder realizar comparativas estadísticamente validas, se ha realizado un alto número de repeticiones del mismo oleaje. Se ha analizado en particular los siguientes efectos:

- Frecuencias de muestreo entre 50 y 19200 kHz
- Células de carga, sensores de presión y un innovador sistema táctil de medidas de presión
- Seis diferentes *layouts* experimentales.

Los máximos resultados de fuerza y presión se han medido siempre a la máxima frecuencia de muestreo y se han obtenido diferencias del orden del 150% con los ensayos muestreados a 50 Hz.

La resultante medida de la fuerza en todo el ancho del canal tiende a subestimar el valor de la fuerza cuando se compara con medidas en la porción central. Aunque en valor promedio los resultados son comparables, en el caso de los sensores de presión los resultados son más dispersos en comparación con los resultados de las células de carga.

El sensor táctil de presión destaca por su elevada densidad espacial (196 sensores en un área de 49cm^2) pero en su contra, requiere de una calibración dinámica y un *set-up* particular para su utilización en agua y para que los resultados sean comparables con los de los sistemas clásicos de medida. Para este trabajo se comparó una calibración con la caída de un martillo y con la caída de un volumen controlado de agua, siendo ésta última la seleccionada para estos ensayos. Entre los resultados obtenidos se destacaque a partir de una comparativa directa entre la integral de las presiones medidas del sensor táctil calibrado y la fuerza medida en la misma área por una célula de carga, se ha evidenciado errores del orden del ±20%. El sensor táctil tiende a subestimar las presiones de pico, aunque si se consideran los valores extremos medidos, los errores son del ±10%. Se ha evidenciado también un efecto de reducción del pico de presión cuando las medidas de presión están acopladas con medidas de células de carga.

Aunque no hay una alternativa perfecta para esta tipología de medidas la combinación de los tres sensores parece la mejor solución posible. Las células de carga dan un resultado directo y muy fiable de la fuerza total, pero su instalación, sobretodo en ensayos de gran escala puede ser complicada. El sensor táctil tampoco se presenta como la alternativa absoluta a los sensores de presión y se aconseja un uso combinado para ensayos que requieran más altos niveles de precisión espacial que en magnitud.

Una frecuencia de muestreo entorno a 4000 Hz en ensayos a pequeña escala presenta la justa combinación entre velocidad de muestreo y cantidad de datos registrados para detectar el fenómeno impulsivo generado por el impacto violento del oleaje en estructuras rígidas. Si se considera que se ha trabajado con una escala de trabajo alrededor entre 1/50 y 1/100, se propone una frecuencia de muestreo a escala prototipo entorno a 500 Hz.

El seguimiento de estas recomendaciones metodológicas permite no sólo generar unas medidas más fiables sino también permitirá una mejor comprensión/evaluación de las posibles incertidumbres en fase de ensayo y análisis de datos. Una correcta medida del fenómeno impulsivo del impacto del oleaje en estructuras rígidas aporta más fiabilidad al proyecto de estructuras rompeolas.

Abstract

The aim of this work is the study of laboratory effects on the measurement of wave impact induced loads on rigid maritime structures. A high number of experiments (more then 4000 using regular wave attacks) have been carried out in the small scale wave flume "CIEMito" in the laboratory of the LIM-UPC BarcelonaTech. The effects on the results of sample frequency, measurement systems and experimental layout has been deeply studied. A high number of repetitions of the same wave attack has been performed in order to have statistically robust results since the almost-random behavior of the studied phenomenon.

- Sample frequencies from 50 to 19200 Hz
- Load cells, pressure transducers and an innovative tactile pressure map
- Six different experimental layouts effects have been tested

The maximum results of force and pressures have been always measured at the maximum sample frequency. Differences of the 150% has been found between the measurements at 50 and 19200 Hz.

The total load measured considering all the width of the flume tends to sub estimate the total force measured only in a slice in the middle of the flume. Even if the average value is comparable, the pressure transducers tends to return much spread results than the load cells.

The tactile pressure mapping system stands out for his very high spatial density (196 sensels in a 49cm^2 area) but an experimental specific calibration and an ad-hoc set-up are necessary for the utilization with water and in order to can collect reliable results comparable with the classic measurement systems. For this work 3 types of calibration methodology have been compared: static, instrumented pendulum and water jets. The last has to be considered the best choice and the selected for the definitive tests. Among all the results the ones to be highlighted are: the integral of pressures (the force applied over the whole sensor) acting on the tactile sensor differ from simultaneous load cell measurements by less than ±20%. The pressure mapping system tends to underestimate the pressure peak. However, if the average values of the 3, 5 and 10 highest peaks are considered they differ by up to ±10%. Has been shown a reduction effect of the pressure peak when pressure measurement systems are coupled with load cells.

A perfect set-up for these kind of measurement hasn't found yet but the combination of the three measurement systems seems to be the best possible solution. Load cells return a direct and reliable result of the total load, but the set-up could be complicated especially at large scales. The pressure mapping system neither seems to be the perfect alternative to the pressure

transducers and a combined use is suggested for these experiments that require a high level of precision both in space and magnitude.

 A sample frequency around 4000 Hz, for small scale experiments, present the right combination between sample density, memory storage and added signal noise for the correct characterization of the impulsive phenomenon of the wave generated violent impact loads on rigid structures. Considering a working scale in between 1/50 and 1/100, a frequency of 500Hz is proposed for measurement at full scale.

Following these methodologic recommendations not only will permit better and more reliable measurement but also will permit a better comprehension/evaluation of the test and analysis uncertainties. In this manner it will be possible to extrapolate, in a reliable way, scale test results to the design process of breakwaters

1. Introducción

1.1. Estado del arte

A finales del siglo pasado creció la atención sobre el fenómeno de los impactos violentos de las olas rompientes sobre estructuras rígidas, como pueden ser, por ejemplo, los diques verticales. Durante esa época se asociaron varios fallos de diques verticales con estos tipos de cargas (Oumeraci, 1994) que se distinguen para su corta duración (ms) y su elevada magnitud. En la bibliografía se han realizado muchos estudios sobre los esfuerzos generados da las olas en rompeolas de todo tipo, empezando por Stevenson (Stevenson, 1886), pero el primero en estudiar los impactos violentos de las olas rompientes en estructuras costeras fue Bagnold (Bagnold, 1939). Tuvieron que pasar más de 20 años para que se desarrollara una formulación para la predicción de dichas cargas (Minikin, 1963), aunque Allsop (Allsop et al, 1996) demostró la inconsistencia de la formulación. En tiempos más recientes Takahashi (Takahashi, 1994, 2002) incorporó nuevos coeficientes en la formulación de Goda (Goda, 1974) que tenían en cuenta la impulsividad de las cargas generadas por olas rompientes. Esta ha sido la primera formulación aceptada de forma generalizada en la ingeniería marítima poniendo las bases y un primer punto de referencia en los inicios de nuestro siglo. Dentro del proyecto Europeo *"Probabilistic Design Tools for Vertical Breakwavers (PROVERBS)* (Oumeraci, 2001) se llevaron a cabo ensayos físicos a gran y pequeña escala en el *GWK* de Hannover (Alemania) y en el *DWF* de la empresa *HR Wallingford* (Reino Unido). Los resultados de estos ensayos fueron utilizados por Allsop (Allsop et al, 1999) para extrapolar una formulación con un enfoque estadístico. Durante un nuevo proyecto llamado *"Violent Overtopping by Waves at Seawalls (VOWS)"*, un nuevo conjunto de datos generados en el canal de gran escala CIEM del LIM-UPC de Barcelona derivó a la generación de una nueva formulación (Cuomo et al, 2010) para el cálculo de las fuerzas y de los momentos generados. Otro gran trabajo se ha realizado durante el proyecto *"Breaking Wave IMpacts on steep fronted COastal STructures (BWIMCOST)"* comparando medidas reales registradas en el *Admiralty Breakwater (Braye Harbour - Channel Islands - Reino Unido)* con medidas a gran y pequeña escala obtenidas en el *GWK* de Hannover (Alemania) y en el canal de oleaje de la Universidad de Plymouth (Reino Unido). Durante este trabajo la atención se centró no sólo en las cargas sino también en el importante papel que juega el aire atrapado, la diferencia entre agua salada y agua dulce y, los efectos de escala (Bullock et al, 2001, 2007) (Bredmose et al 2009, 2015).

El conocimiento de la física implicada en el desarrollo de estos fenómenos es todavía limitado y, como se ha mostrado anteriormente, todas las teorías se basan en resultados de ensayos de laboratorio a escala.

Generalmente se prefiere antes las medidas de presión que las medidas de fuerzas, ya que es posible colocar los sensores en áreas vulnerables, mientras que la adquisición de medidas de fuerzas requiere, especialmente para ensayos a gran escala, preparativos complejos y elevados costes económicos. En la gran mayoría de los ensayos en canales físicos de oleaje que involucran estructuras costeras, se coloca una matriz vertical de sensores de presión en el lado mar de la estructura. Los datos adquiridos se utilizan para la obtención de distribuciones de presión, a partir de los que se calcularán las fuerzas y momentos generados. Sin embargo, los sensores de presión proporcionan una medida puntual y, en muchos casos, por motivos constructivos y económicos no permiten el uso de un gran número de sensores. Al mismo tiempo, la gran variabilidad temporal y espacial, la limitada información sobre la coherencia de los perfiles de presión (tanto vertical como horizontal) y la complejidad geométrica de algunas estructuras modernas, generan la necesidad de medidas con alta densidad tanto espacial como temporal (Peregrine, 2003), (Saruwatari et al. ,2009), (Hull and Müller ,2002). Aparecen también nuevos desafíos cuando hay que ensayar estructuras con geometrías complejas, como es el caso de plataformas petrolíferas, botaolas,… que requieren un detalle afinado de las distribuciones de presión generadas por el impacto violento de una ola rompiente.

1.2. Objetivos

El objetivo principal de esta tesis es mejorar el conocimiento sobre las cargas generadas de olas que rompen violentamente encima de estructuras rígidas. Se pueden visualizar tres objetivos fundamentales a perseguir para cumplir con el objetivo principal.

- Mejorar las técnicas y metodología de medida utilizando la justa combinación de aparatos y la correcta técnica de muestreo
- Utilizar el gran potencial de los ensayos a pequeña escala para evaluar problemas y generar soluciones utilizables a escalas mayores.
- Utilizar los resultados obtenidos para generar confianza y mejorar las técnicas de diseño en la ingeniería de diques.

El eje central de esta tesis se basa en el estudio de efectos de laboratorio que pueden alterar, de forma no natural, los resultados registrados en los modelos físicos. En particular, se focaliza la atención en las medidas de fuerza y presión generadas por los impactos de las olas rompientes encima de diques verticales.

Estos efectos pueden ser de diferentes tipología y naturaleza; hay efectos debidos a las condiciones de contorno (eg. *Teoría de generación de oleaje utilizada y *simplificación/alteración de la geometría del ensayo a escala), efectos debidos a los sistemas

de medidas y adquisición de datos (eg. *Diferentes tipos de sensores y *adecuada frecuencia de muestreo) y efectos debidos a la alteración de la física de los fenómenos (eg. *Utilización de agua dulce en ensayos de hidráulica marítima).

Para realizar este estudio se han ejecutado ensayos físicos en el canal de pequeña escala CIEMito del LIM-UPC y se ha utilizado un modelo simplificado de un dique vertical. Como primera iteración se ensayó un modelo de dique vertical con una protección a pie de estructura y fondo plano. Vistas las dificultades en generar olas estables y al límite de rotura en fondo plano se decidió añadir a la base del dique vertical un plano inclinado con peralte 1/15 de 2.06m de largo y eliminar la protección de pie. Con esta geometría se han realizados todos los ensayos. Para las medidas de fuerzas y presiones se han utilizados tres sistemas de medidas diferentes (*Sensores de presión *Células de carga *Sensor táctil) y los adecuados sistemas de adquisición de datos. Todos los ensayos fueron financiados y encajan en el marco de la Joint Research Activity *"HyRes"* dentro del proyecto Europeo *"Hydralab IV"*.

1.3. Estructura de la tesis

Cada capítulo de este documento se ha estructurado a partir de un artículo de revista/congreso que ya ha sido revisado y publicado o que esté en fase de publicación (*submitted*). Todos los artículos están ordenados en orden lógico (no 100% cronológico) aunque siguen el desarrollo natural del estudio empezando por ensayos y resultados preliminares "sencillos" hasta la adquisición por parte del autor de más experiencia en el campo de estudio y la generación de ensayos más adecuados y resultados más detallados.

El primer artículo *"Impulsive wave loads on rigid structures, an experimental approach"* (Marzeddu et al, 2013) publicado en la revista científica *"Journal of Coastal Research"* tiene dos objetivos principales. El primero es el estudio de las diferencias entre resultados obtenidos con sensores de presión (generación de un perfil vertical de presión con 6 sensores) y células de cargas (medición de la carga total en todo el dique vertical), mientras el segundo es el estudio de los efectos de la frecuencia de muestreo (se midieron las fuerzas y presiones generadas por el mismo oleaje con frecuencias que iban desde los 50 hasta los 19200 Hz). La geometría de estudio, como se comentó anteriormente, era la de un dique vertical con protección a pie de estructura y fondo plano. Se realizaron más de 300 ensayos. El análisis de los resultados de estos primeros ensayos llevó a unas importantes consideraciones. Desde un principio estuvo claro que la generación de olas estables y el límite de rotura en fondo plano era complicado de generar (aunque se logró un oleaje que rompía violentamente encima del dique vertical) y que era necesario un plano inclinado para ayudar a la transformación de la ola y obtener impactos aún

más violentos. La frecuencia de muestreo es muy importante y los valores más altos de presión/fuerza se midieron a la frecuencia de muestreo más alta que permitían los equipos de registro (19200 Hz), aunque resultados con errores aceptables se registraron a partir de frecuencias de 4000 Hz. Se obtuvieron resultados diferentes utilizando los dos sistemas de medida (fuerza/presión). La fuerza medida a partir de los resultados de los sensores de presión siempre excedía a los resultados obtenidos con las células de carga. Estos ensayos dieron paso a las primeras dudas en los resultados obtenidos históricamente con una baja resolución espacial de la matriz de sensores de presión.

Estos resultados condujeron a construir un plano inclinado con pendiente regulable (después de varias pruebas fue seleccionada la pendiente 1/15) para facilitar el *shoaling* y la generación de una ola en el límite de rotura justo a pie de dique. También se modificó el soporte de los sensores de presión/células de carga. En particular se añadieron dos nuevos sensores de presión para aumentar la resolución espacial de las medidas en el área de impacto. Con este set-up se realizaron los ensayos para el segundo artículo: *"Laboratory effects on measurnig impact load on rigid coastal structures"* (Marzeddu et al, 2014a) presentado en el *"3rd IAHR European Congress"* y publicado en sus *proceedings*. Los objetivos siguieron siendo los mismos pero se añadió además de las 300 repeticiones de la ola que impacta violentamente, 20 repeticiones de un oleaje regular no en rotura que generara cargas cuasi estáticas para comprobar y verificar el funcionamiento de los sistemas de medida. Los resultados de estos ensayos resaltaron la enorme variabilidad y la poca repetitividad de los impactos violentos generados por olas que rompen directamente encima de la estructura, mostrando así que se trata de un fenómeno aleatorio. De nuevo los máximos de fuerza y presión se obtuvieron con la máxima frecuencia de muestreo y, además, aumentaron las diferencias entre los resultados obtenidos con los sensores de presión y las células de carga. Por el contrario, con el oleaje regular no en rotura, se evidenció una total repetitividad de los ensayos a través de las medidas de lso sensores y muy pequeñas diferencias entre los dos sistemas de medida durante el análisis de los resultados de fuerzas y presión. Respecto a la resolución espacial de las medidas de presión, las dudas siguen en aumento debido a los diferentes resultados que se pueden obtener utilizando diferentes técnicas de interpolación e integración entre sensores. Se plantean dudas por primera vez de la extrapolación en horizontal de las distribuciones de presión y empieza a crecer la seguridad en que no se pueden extrapolar medidas puntuales de presión tomadas en una columna central del canal a todo su ancho para estos tipos de impactos. Se confirma que, con una alta frecuencia de muestreo, se aumenta la posibilidad de caracterizar de forma correcta los picos de

fuerza/presión y se determina que una frecuencia alrededor de 4000 Hz proporciona un buen compromiso entre cantidad de datos y calidad de los resultados.

De forma cronológica, se inicia una colaboración con el *University College of London* para adaptar el uso debajo del agua de los innovadores (en el campo de la ingeniería marítima) sensores de presión táctiles de Tekscan. Estos sensores permiten densidades espaciales (196 sensores en un área de 49 cm²) inigualables por los sensores de presión, y además son flexibles y se puedan adaptar a geometrías muy complejas. Uno de los puntos clave de esta colaboración fue una estada del autor en Noruega en las instalaciones de *Marintek* para colaborar en los ensayos "*Impact induced pressure distribution at the face of caisson breakwaters under oblique wave attacks: a novel approach*" en el marco del proyecto Europeo *"Transnational Access - Hydralab IV".* Durante estos ensayos se evidenció la necesidad de generar un set-up, una calibración y una manipulación *ad-hoc* del sensor para la utilización debajo del agua. La descripción de los ensayos y los resultados están recopilados en el artículo "*Large scale experiments on the interaction of a caisson breakwater with breaking waves*" (Stagonas et al, *2014),* se ha presentado en el "*Hydralab IV Joint User Meeting*" y está publicado en sus *proceedings*. Para dar respuesta a todas estas preguntas se decide trasladar el novedoso sistema de medida a las instalaciones del LIM-UPC para seguir trabajando con estos sensores y para ejecutar una comparación exhaustiva con los sistemas clásicos de medida.

En el artículo *"Measuring wave impact induced pressures with a pressure mapping system, Part 1: Experimental set-up and calibration"* (Stagonas et al, 2015) enviado a la revista *"Coastal Engineering"* y actualmente en fase de revisión, se explica las modificaciones que se han tenido que realizar para que el sistema táctil de medida de presiones fuese capaz de medir las cargas generadas para el impacto de olas rompiente en estructuras rígidas. Se explica además, el proceso de calibración y se realiza un análisis exhaustivo para la selección del método adecuado de calibración. Los resultados de las pruebas de calibración evidencian la necesidad de una calibración dinámica y de la utilización de agua como material de impacto. La calibración final se realiza con una prueba de caída libre de un volumen controlado de agua. Una vez modificado y calibrado el sensor táctil, se ha utilizado en los ensayos en laboratorio físico para su comparación con los sistemas clásicos de medida.

Del análisis de los problemas de los ensayos precedentes, se decide modificar el *layout* experimental para investigar la importancia de la coherencia horizontal. Se modifica el área de medida de las células de carga, transformándose de todo el ancho del canal (como en los precedentes ensayos) a sólo los 10 cm centrales. De esta manera, el área de medida de los dos

sistemas clásicos acababa siendo comparable. En el artículo *"Effects of measurement system on impact loads on rigid structures"* (Marzeddu et al, 2014b) publicado en los *proceedings* del congreso *"5th conference on the application of physical modelling to port and coastal protection"* se analizan las diferencias en los resultados obtenidos de los tres sistemas de medidas. Después de haber realizado aproximadamente 200 ensayos con dos oleajes regulares se confirmaron las dudas sobre la no coherencia horizontal de este fenómeno, encontrando gran variabilidad entre los resultados registrados en el lateral y en el centro del canal por el sensor táctil. Además, con el sistema de medida de las células de carga en un área menor, el valor promedio de la fuerza registrada con células de cargas se asemeja mucho a los resultados extrapolados da las medidas con sensores de presión. Vista la imposibilidad de medir con los tres sistemas al mismo tiempo en el mismo lugar, y dadas las dimensiones reducidas (7,1 x 7,1 cm) del sistema táctil en comparación con el área de medida de las células de carga, se compararon los resultados del sensor táctil con los resultados de los sensores de presión posicionados en la misma zona de medida en ensayos distintos. Los resultados han sido sorprendentemente buenos y han evidenciado una buena correlación en los puntos comunes de medida. Sin embargo, el sensor táctil evidencía pequeños puntos de altas presiones que claramente los sensores de presión, no presentes en aquel particular punto, no han podido registrar. Del análisis de estos resultados surge también la duda sobre la calidad de las medidas de los sensores de presión cuando están midiendo en una mezcla de aire y agua (típico de las olas en rotura).

Una vez más se decide modificar la disposición experimental de modo que los tres diferentes sistemas de medida puedan registrar todos en el mismo lugar y, si es posible al mismo tiempo, para poder ser comparados de forma directa el uno con el otro. Finalmente se decide hacer coincidir el área de medida de una célula de carga con el área de medida del sensor táctil. Se sobrepone el sensor táctil a la célula de carga de forma que la integral de la distribución de presión del sensor sea exactamente la fuerza medida por la célula de carga. Por otra parte se construye en otro modelo de dique vertical una matriz de sensores de presión en la misma área de medida anterior con la máxima densidad espacial posible (13 sensores en 49 cm^2). Se ensayan separadamente para los dos *layouts* 4 oleajes diferentes con diferentes tipos de rotura y por cada oleaje se realizan 120 repeticiones (para garantizar un valor estadísticamente representativo) alcanzando un total de casi 1500 ensayos. De los resultados de estos ensayos se puede apreciar una buena correlación entre los resultados del sensor táctil y los resultados medidos por la célula de carga, pero aparecen grandes diferencias en comparación con los resultados de los sensores de presión. Surge así la duda de que la presencia de una célula de carga rígidamente conectada con un sistema de medida de presión pueda actuar como un

amortiguador de presión. Se decide por lo tanto evaluar estos efectos montando un número reducido de sensores de presión en el sistema de medida de la célula de carga. Se realizan 240 ensayos. Un análisis preliminar de los resultados evidencia claramente este fenómeno. Todos los resultados y la descripción de los ensayos han formado el último artículo *"Measuring wave impact induced pressures with a pressure mapping system, Part 2: Validation"* (Marzeddu et al, 2015) enviado y en fase de revisión a la revista "*Coastal Engineering*".

En total se han realizado, sólo en el canal de pequeña escala CIEMito del LIM-UPC, entre ensayos de prueba y ensayos "oficiales" más de 4000 test y, como anécdota, considerando aproximadamente un recorrido de 20m para ir de un sistema de adquisición a otro 2 veces por ensayo, se ha recorrido aproximadamente unos 160 Km en 3 años para la realización de este trabajo.

Bibliografía

Allsop, N.W.H., Kortenhaus, A., Oumeraci, H., McConnell, K., 1999. New design methods for wave loading on vertical breakwaters under pulsating and impact conditions. Proc. Coast. Struct. '99, Santander, Spain. Balkema Rotterdam 592–602.

Allsop, N.W.H., Vicinanza, D., McKenna, J.E., 1996. Wave forces on vertical and composite breakwaters Strategic , 1–94.

Bagnold, R.A., 1939. Interim report on wave pressure research. J. Inst. Civ. Engrs. 12, 202–226.

Bredmose, H., Bullock, G.N., Hogg, a. J., 2015. Violent breaking wave impacts. Part 3. Effects of scale and aeration. J. Fluid Mech. 765, 82–113. doi:10.1017/jfm.2014.692

Bredmose, H., Peregrine, D.H., Bullock, G.N., 2009. Violent breaking wave impacts. Part 2: modelling the effect of air. J. Fluid Mech. 641, 389. doi:10.1017/S0022112009991571

Bullock, G.N., Crawford, A.R., Hewson, P.J., Walkden, M.J.A., Bird, P.A.D., 2001. The influence of air and scale on wave impact pressures. Coast. Eng. 42, 291–312. doi:10.1016/S0378-3839(00)00065-X

Bullock, G.N., Obhrai, C., Peregrine, D.H., Bredmose, H., 2007. Violent breaking wave impacts. Part 1: Results from large-scale regular wave tests on vertical and sloping walls. Coast. Eng. 54, 602–617. doi:10.1016/j.coastaleng.2006.12.002

Cuomo, G., Allsop, N.W.H., Bruce, T., Pearson, J., 2010. Breaking wave loads at vertical seawalls and breakwaters. Coast. Eng. 57, 424–439. doi:10.1016/j.coastaleng.2009.11.005

Goda, Y., 1974. New Wave Pressure Formulae for Composite Breakwaters. Proc. 14th Int. Coast. Eng. Conf. 3, 1702–1720.

Hull, P., Müller, G., 2002. An investigation of breaker heights, shapes and pressures. Ocean Eng. 29, 59–79. doi:10.1016/S0029-8018(00)00075-5

Marzeddu, A., Gironella, X., Conejo, A.S., 2013. Impulsive wave loads on rigid structures , an experimental approach. J. Coast. Res. doi:10.2112/SI65-xxx.1

Marzeddu, A., Gironella, X., Sachez-Arcilla, A., Sutherland, J., 2014a. Laboratory effects on measuring impact loads on rigid coastal structures, in: 3rd IAJH. pp. 1–9.

Marzeddu, A., Stagonas, D., Gironella, X., Conejo, A.S.Y., 2014b. Effect of measurement systems on impact loads on rigid structures, in: Proceedings 5th Conference on the Application of Physical Modelling to Port and Coastal Protection.

Marzeddu, A., Stagonas, D., Gironella, X., Sánchez-Arcilla, A., 2015. Measuring wave impact induced pressures with a pressure mapping system, Part 2: Validation. Coast. Eng.

Minikin, R.R., 1963. Winds, Waves and Maritime Structures, 2nd edition. Charles Griffin, London, UK.

Oumeraci, H., 1994. Review and analysis of vertical breakwater failures - lessons learned. Spec. Issue Vert. Break. 22, 3–29. doi:10.1016/0378-3839(94)90046-9

Oumeraci, H., Allsop, N.W.H., De Groot, M., Crouch, R., Voortman, H., Vrijling, H., 2001. Probabilistic design tools for vertical breakwaters. Swets & Zeitlinger, Amsterdam : (ndl).

Peregrine, D.H., 2003. Water - Wave Impact on walls. Annu. Rev. Fluid Mech. 35, 23–43. doi:10.1146/annurev.fluid.35.101101.161153

Saruwatari, A., Watanabe, Y., Ingram, D.M., 2009. Scarifying and fingering surfaces of plunging jets. Coast. Eng. 56, 1109–1122. doi:10.1016/j.coastaleng.2009.08.007

Stagonas, D., Marzeddu, A., Buccno, M., Calabrese, M., Banfi, D., Vicinanza, D., Kofoed, J.P., Pecher, A., Frigaard, P., Pakozdi, C., 2014. Large Scale Experiments on the Interaction of a Caisson Breakwater with Breaking Waves, in: HYDRALAB IV Joint User Meeting.

Stagonas, D., Marzeddu, A., Gironella, X., Sánchez-Arcilla, A., Muller, G., 2015. Measuring wave impact induced pressures with a pressure mapping system, Part 1: Experimental set-up and calibration. Coast. Eng.

Stevenson, T., 1886. The design and construction of harbours 3rd edition. Adam Charles Black.

Takahashi, S., Tanimoto, K., Shimosako, K., 1994. A Proposal of Impulsive Pressure Coefficient for Design of Composite Breakwaters. Proc. Int. Conf. Hydro-Technical Eng. Port Harb. Constr. Port Harb. Res. Institute, Yokosuka, Japan, 489–504.

2. Enfoque experimental

En este capítulo se describen los primeros pasos y los primeros ensayos realizados. Durante estos ensayos se focaliza la atención sobre todo en la toma de confianza con los nuevos sistemas de medidas adquiridos en el laboratorio. Se utiliza un *layout* experimental sencillo constituído por un fondo plano y un dique vertical instrumentado con protección al pie. Se realizan ensayos para analizar los efectos de la frecuencia de muestreo en las medidas de los impactos de las olas rompientes. Se realiza una primera comparativa entre los dos tipos de sensores utilizados. Se identifican dificultades en la generación de una ola en límite de rotura estable en fondo plano. Después de muchas pruebas se detecta una condición de ola que genera un impacto pero lejos de ser un impacto violento como los que se lograrán generar posteriormente. Los resultados están publicados en el artículo "*Impulsive wave loads on rigid structures, an experimental approach*" en la revista "*Journal of coastal research*"

Marzeddu, Andrea, Xavier Gironella i Cobos, and Agustin Sánchez-Arcilla y Conejo. "Impulsive wave loads on rigid structures, an experimental approach." *Proceedings 12th International Coastal Symposium (Plymouth, England). Journal of Coastal Research, Special Issue*. No. 65. 2013.

Abstract

Within the European project 'Hydralab IV', HyRes we aim to improve the characterization of wave loads on rigid structures and the associated response by carrying out some laboratory experiments. Wave loads on rigid structures are divided into quasi static loads and impact loads. If the physics of quasi-static loads due to waves is well known, this cannot be said the same for wave impact loads. A comprehensive method to design maritime rigid structures under impact loads does not exist yet and the actual design method suggests avoiding scenarios where impact loads can take place. In the last decade, some laboratory experiments have been carried out; however some questions remain still unanswered. The use of different sensors can lead to significant changes in the results and an "exhaustive comparison" between dissimilar types of sensors has not been done yet. Even the magnitude of these forces can be underestimated during a laboratory test just for the choice of sample frequencies which are too low. This paper describes the experiments performed on a small scale flume at UPC on a scaled vertical breakwater in order to compare the results of pressure transducers and force load cells. Moreover, a high frequency sampler (up to 20 KHz) was used in order to understand the importance of sample frequency on the magnitude of the results. A simplified scenario has been set up in order to make the data analysis easier.

2.1. Introduction

In the last few years, increasing attention has been given by various authors to the phenomena of wave impact on rigid structures and particularly on vertical breakwaters. Only recently the failure of a caisson breakwater caused by a wave impact has been analyzed in depth (Oumeraci, 1994) and since that time a more focused approach on the consequences of pulsating loads and on the dynamic response of the structures has started. A lot of historical research has been carried out regarding wave forces on seawall starting from Stevenson (Stevenson, 1874). It was Bagnold (Bagnold, 1939) who was the first to focus the attention on wave impacts on coastal structures. The first to develop a prediction method for waves that breaks directly onto a vertical breakwater was Minikin (Minikin, 1963), but Allsop (Allsop et al., 1996) demonstrated the inconsistency of the formula. Takahashi (Takahashi, 1994), extended the Goda formula (Goda, 1974) including the impulsive force parameter setting the benchmark in the calculation of pulsating loads on vertical breakwaters. Within the European project PROVERBS laboratory tests, at large and small scales, were run at the GWK of Hannover, Germany and at DWF at HR Wallingford, UK. The results of these experiments have led to the Allsop formula (Allsop et al., 1999) in which a statistical approach was used. A new data set of large scale experiments performed at the LIM-UPC Barcelona, Spain, under the project Violent Overtopping by Waves at Seawalls (VOWS), led to a new formulation (Cuomo et al, 2010). Using both data sets of PROVERBS and VOWS, a statistic evaluation of impact loads on caisson breakwaters based on the joint probability was presented (Cuomo et al, 2011). An extended work has been done also over the effects of fresh water, trapped air, laboratory and scale effects (Bullock et al, 2001) using the comparison between field measurements at the Admiralty Breakwaters at Braye Harbour in the Channel Islands. A scaled 1:25 physical model test was carried out, at the University of Plymouth, UK. In this paper, a simple study case of a vertical breakwater with toe protection was tested in a small scale flume at the UPC under regular wave attacks in order to find an impulsive load condition. Once the impulsive condition was found, a comparison between pressure sensors and load cells was made and a brief study over the influence of the sample frequency and the natural frequency of vibration of the structure itself was performed. A comparison with the existing formulations was done.

2.2. Methodology

The experiments have been carried out in the CIEMito wave flume of the Laboratori D'Enginyeria Maritima (LIM) of the Universitat Politecnica de Catalunya (UPC). The flume is 18m long, 0.38 m

wide and 0.56 m high. It is equipped with a piston type wave maker driven by software developed at LIM/UPC that allows generation of regular and random waves characterized by a target spectrum as well as a target wave time series. A scaled model of a vertical breakwater has been built and tested against regular wave attacks.

The flume has a flat bottom and the breakwater has a smooth toe protection in order to simulate a rubble mound toe protection (Figure 2.1).
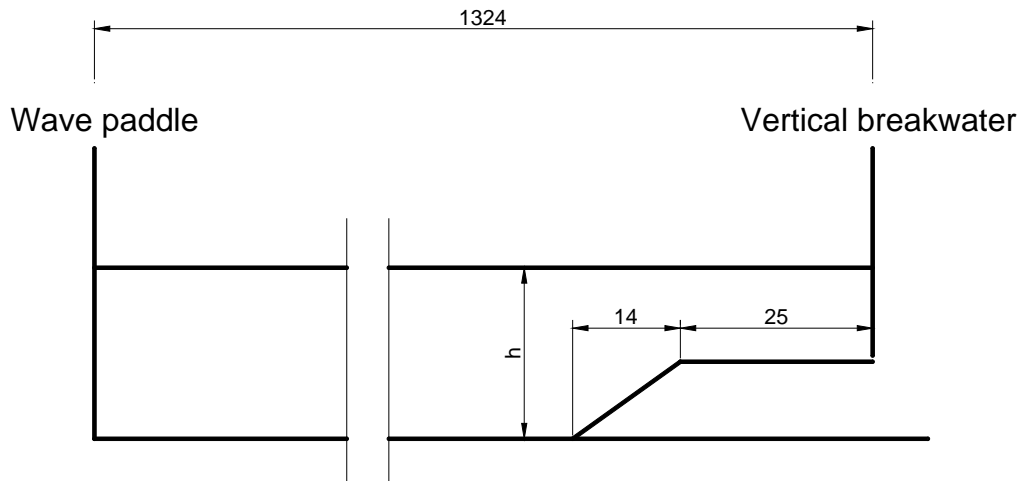
Figure 2.1: Dimensions in cm and position of the vertical breakwaters in CIEMito wave flume.

The vertical wall of the breakwater has been equipped with six pressure sensors and was held also with two load cells, in order to record the pressure and the total force at every wave attack at the same time. The load cells have been fixed at a superstructure of the wave flume with a reticular structure in order to avoid possible movements.

2.2.1. Instrumentation

The instrumentation used during the experiments was composed of:

- Six pressure sensors P8AP by HBM ©
- Two load cells Z6 by HBM ©
- Six wave gages

The P8AP is an absolute pressure transducer based on a strain gauge sensor with a measuring span of 10 bars and an accuracy class 0.3. The P8AP are IP67, that means they are weatherproof but not waterproof and for this reason a box that isolates the sensors from the water is needed.

20 holes were added to the front wall so as to be able to try different patterns of pressure sensors positions. Six holes were plugged with the pressure sensors and the others are plugged with screws in a manner that the front wall will be waterproof and continuous.

After some tests using various positions of the pressure sensors, the definitive pattern was defined with the six pressure sensors placed on the same vertical and with a distance between each sensor of 25 mm.

 The Z6 by HBM is a bending beam load cell with a nominal load of 50 Kg and an accuracy of 0.009 % of the maximum capacity. The load cells were mechanically fixed to the protecting box of the pressure sensors and fixed at the reticular structure described before. It is very important that the mechanical connection should be very rigid in order not to absorb any force and affect the measurement.

A reticular structure fixed on a super structure of the wave flume (independent from the wave flume itself) is used because in a reticular structure there are just normal forces and the nodes are fixed (Figure 2.2).

Figure 2.2: Reticular structure that constrains the load cells

The stiffness of the load cells should be much lower than the stiffness of the reticular structure in order to deform itself and to perform the right measure of the force.

The coupling of the two load cells in two different positions is needed in order to obtain time series of the total force, the momentum and the application point of the force.

Both pressure sensors and load cells are connected at a Quantum X MX840A data acquisition system by HBM. The MX840A is an 8 channel data acquisition system that can record at a maximum sample frequency of 19.2 KHz. The possibility to connect the six pressure transducers

and the two load cells in the same acquisition system and sample at a very high speed is crucial in order to be able to compare the results obtained from both together.

Wave motions were measured by using 6 resistive wave gages, with an accuracy of 0.1 mm, positioned in front of the vertical breakwater in order to measure the generated wave, the wave in front of the structure and decompose incident/reflected waves with the Mansard and Funke method (Mansard, 1980).

A schematic with the position of all the sensors is exposed at (Figure 2.3).
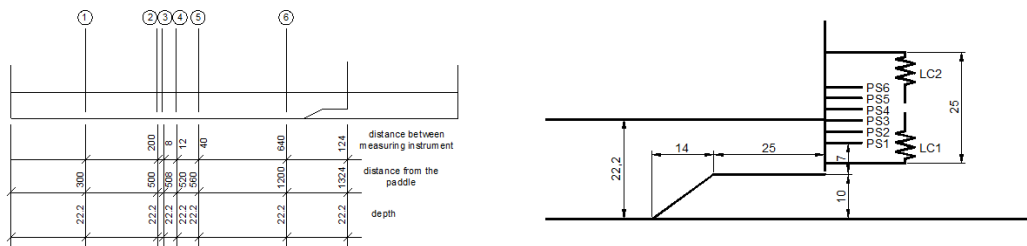
Figure 2.3: Left: Wave gage positions. Right: Pressure sensor and load cell positions. (dimensions in cm)

2.2.2. Wave test conditions

A water depth of 0.22 m was used and ten regular waves were performed during each wave attack. As explained above a flat bottom was used. Previous tests with a wave height bigger than 0.12m was discarded because breaks in front of the paddle and waves smaller than 0.1m, never produce impact conditions.

In a flat bottom it is not so easy to reach impact conditions and for that reason a wide range of regular wave conditions (86 tests) were tested in order to find the one with the right impulsive conditions.

The wave attack H=0.11m T=0.9s has been chosen after analyzing the conditions that have produced at least one impact state in the register. In this register, it is clearly an impulsive situation (Figure 2.4).
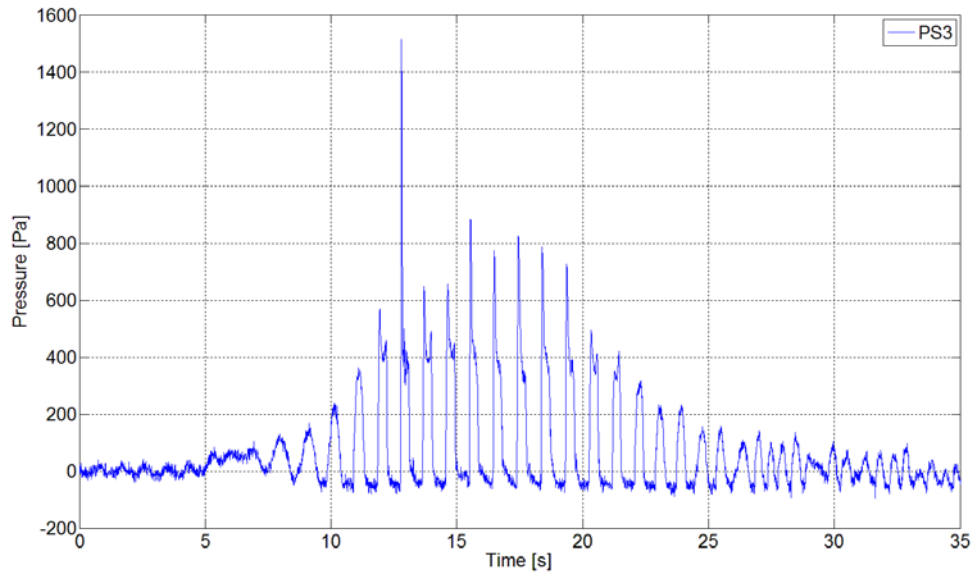
Figure 2.4: Time series of the pressure sensor PS3 for the conditions H=0.11 T=0.9 with the clear impact.

All the following comparisons were made using this wave attack as the standard.

2.2.3. Analysis

The analysis that has been performed consists of the following parts:

- **Calculation of the total force and momentum with the two load cells**. Both load cells give the force in their respective application point. Every load cell behaves like a fully restrained beam to one end and a free end to the other. The stiffness is known and for this reason knowing the deformation is possible to derive the applied force at the free end. Once the forces are known in two points is known the total force, which is the sum of the two forces.

- **Calculation of the total force and momentum with the six pressure sensors.** Every sensor gives the pressure in one point. A linear interpolation is done between one pressure value and another. All the area between the lower and the upper pressure sensors is covered, but there is no data in the part under the lower pressure sensor and over the upper pressure sensor. In order to cover these two areas an extrapolation was performed. In the lower part an extrapolation with a spline using the values of the PS1 and PS2 was done. In the upper part an extrapolation using the PS5 and PS6 was done, but not admitting negative pressure values and when the pressure values were positive, pressure above the higher part of the vertical wall were not taken into account. To maintain the same integration domain between pressure sensors and load cells, values higher than the maximum height of the vertical wall are excluded too. An integral covering the obtained pressure distribution was applied in order to calculate the total force using the pressure sensors. For the calculation of the application point of the total force and consequently the moment, a

weighted average on the areas of the pressure diagram between one sensor and another was done, allowing the calculation of the application point of the total force with simple calculations.

- **Identification and analysis of the natural frequency of vibration of the vertical wall.** Once the total force and moment are calculated with the load cells and with the pressure sensors, it is necessary to know if some deformations of the load cells are due to the natural frequency of vibration of the vertical wall. The system is elastic and for that reason every oscillation due to the elasticity of the system should be filtered. In order to know the natural frequency of vibration of the vertical wall a particular test was done. Without water and with a rubber hammer the surface has been hit as close as possible to the water surface recording with the load cells. The hammer causes vibrations and the recorded time series is characterized by damped oscillations. The frequency of these oscillations is constant and equal to the natural frequency of vibration of the vertical wall. This frequency need to be filtered from the results in order not to take into account these oscillations that are not a consequence of the wave impact.

- **Comparison between pressure sensors and load cells with error calculation.** The pressure sensors does not present, in the data sheet, an accuracy class good enough for the small scale used in these experiments. Indeed, previous tests have shown a better resolution and a possibility to apply these kinds of transducers for the pressure measurements at such small scales of work. Undoubtedly a comparison with suitable sensors is needed. For that reason a double measure with both load cells and pressure sensors has been done. The pressure sensors are useful for the evaluation of the pressure distribution on the vertical wall and for the identification of the impact point. To evaluate the performance of the pressure sensors and the analysis method utilized to compute the total force, a comparison between the result obtained with the load cells and the pressure sensor was done. This comparison consists of an evaluation of the error during the impact and during all the time series. The statistic parameters utilized are:

$$RMAE = \frac{\langle |Y - X| \rangle}{\langle |X| \rangle} \qquad (1)$$

where X is a set of N observed data and Y a set of predicted data. The angular brackets denote an average and |X| is the modulus of X.

A RMAE value of zero implies a perfect match between predictions and observations. This will never, in practice, be achieved as the RMAE includes contributions from the measurement error. The simplest approach to estimate the relative effect of observational errors is to compare the observational error to the mean absolute error. Another approach

taken to reduce the influence of the observational errors is to subtract the observed error OE from each absolute error, thus defining an adjusted RMAE:

$$ARMAE = \frac{\langle |Y-X|-OE \rangle}{\langle |X| \rangle} \qquad (2)$$

In this case of study the observed data correspond to the total force calculated with the load cells whereas the predicted data is the total force calculated with the pressure sensors. Sutherland et al. (2004) propose a classification and a categorization of the ARMAE error (Table 2.1).

Range of ARMAE	Classification
< 0.2	Excellent
$0.2 - 0.4$	Good
$0.4 - 0.7$	Reasonable
$0.7 - 1$	Poor
> 1	Bad

Table 2.1: Error classification and categorization of the ARMAE statistic. (Sutherland et al, 2004)

- **Influence of the sample frequency.** As a definition an impulsive condition is something that has a short duration; in the case of a wave that impacts on a vertical wall the duration of the impact is unknown and the use of a sample frequency that is too low can lead to a sub estimation of the force peak. For that reason a very high frequency acquisition system is recommended in order to avoid non-quantifiable errors. Using the same experiments, the repeatability should be no different and guaranteed to perform the same test several times and analysing the differences between the two experiments with the same statistic as explained before. Once the repeatability was guaranteed performing an error analysis based on the root mean square error, various tests made under the same conditions were recorded at different sample frequencies from 19200 Hz to 50 Hz and the differences were analysed.

- **Comparison of the results with formulations.** A comparison between the obtained data, the Takahashi (Takahashi, 1994) distribution and the Allsop formula (Allsop et al., 1996) was made taking into account the differences between the experimental set-ups and the scale of work.

2.3. Preliminary results

2.3.1. Natural frequency of vibration

As was explained in the previous section, a test to find out the natural frequency of vibration of the vertical wall was performed. From this test it was found that the natural frequency of vibration of the vertical wall was between 12 and 14 Hz.

2.3.2. Load cells and pressure sensors comparison

Following the explanations described in the analysis section, a comparison of the calculated total force has been done between the load cells and the pressure sensors. Some results of this comparison are presented in Figure 2.5.
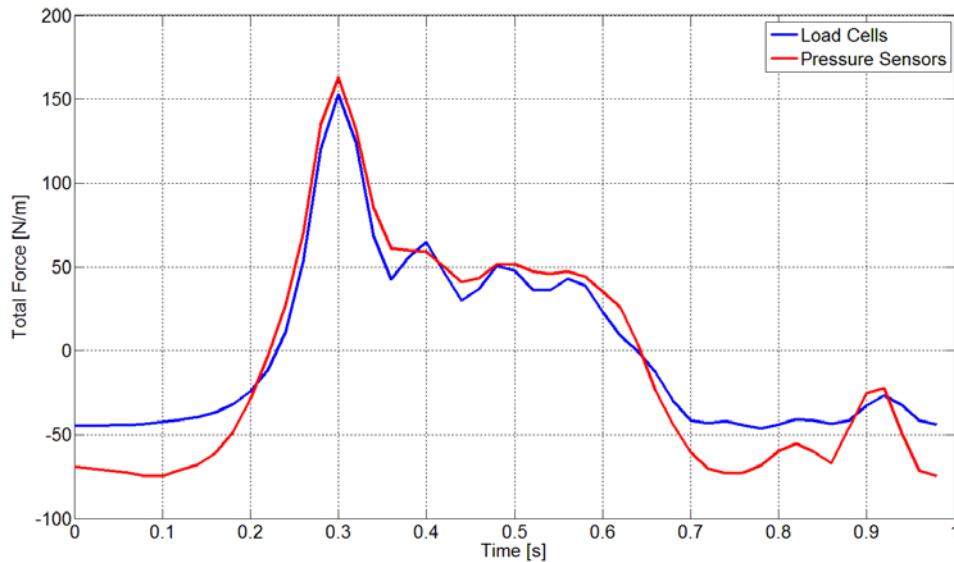
Figure 2.5: Impulsive condition. Comparison between load cells and pressure sensors.

Analyzing the figure is possible to see that the peak during one wave period is well represented, but the sinus of the wave does not seem so good. This is due to the zero offset performed at the pressure sensor in order to cleanse the measure of all the sensors to the hydrostatic pressure. This is because the load cells are in equilibrium with the water on both sides of the wall and for that reason the hydrostatic force is not measured. The problem appears in the sinus of the wave when a pressure sensor that in static conditions is wet becomes dry. The difference between the hydrostatic pressure and the atmosphere pressure is computed as a negative pressure. This kind of comparison is performed to use the results of the pressure sensors in order to have the pressure distribution on the vertical wall during an impact. For that reason it is preferable to have the right measure on the peak and a known error on the sinus (condition less dangerous for the wall). In order to quantify the quality of the results was the previous explained statistic parameter has been used. To calculate the *ARMAE* parameter it is important to define the observed error *OE*. In this case the observed values are the one calculated with the load cells (more precise than the pressure sensors) and their observed error is the double of the precision of the single load cell. from the data sheet of the z6 *OE* must to be set to 0.044 n. considering only the time series range where the total force is positive (water at still level or above), the value of the *ARMAE* parameter is 0.16 that corresponds to an excellent in the classification

proposed by (sutherland et al, 2004). AS evolution of the *ARMAE* parameter is plotted below (figure 2.6). It is also possible to consider that in the quasi-static part of the impact time series (flat part after impulse in figure 2.5) there are some oscillations in the load cells graph.
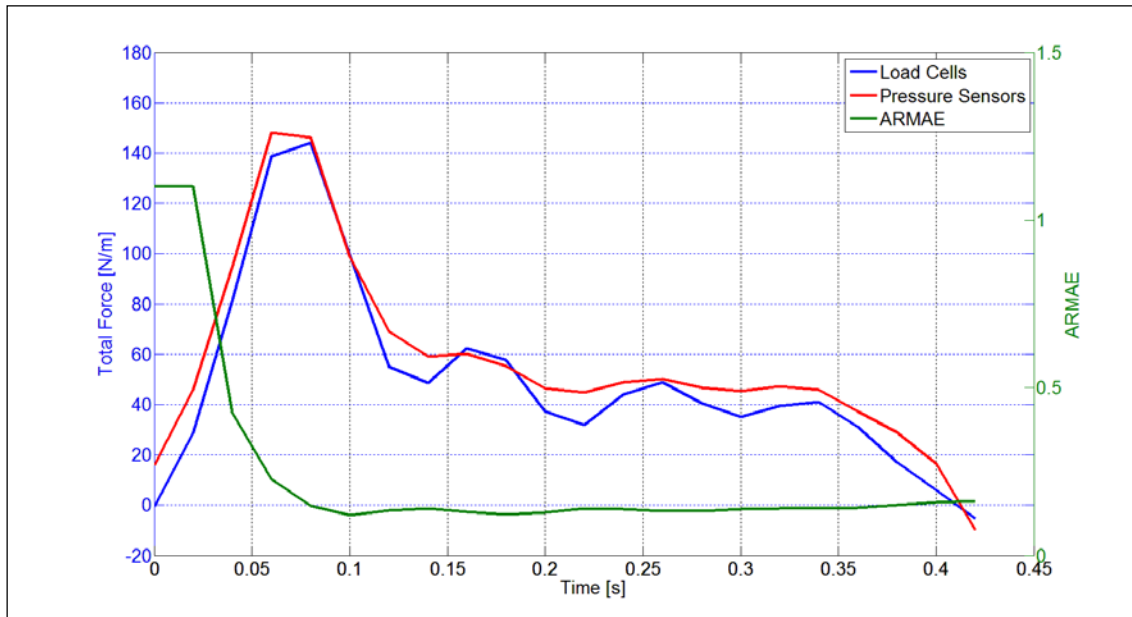
Figure 2.6: Evolution of the ARMAE parameter.

Considering the previous results on the natural frequency of vibration of the plate and considering that those oscillations correspond to a frequency of 12 Hz, it is possible to assume that those oscillations are caused by the natural frequency of vibration of the vertical wall. Considering also the last assumption it is possible to say that the results obtained with the load cells and with the pressure sensors are similar and comparable in the part of the time series range where the forces are positive.

2.3.3. Sample frequency influences

Before performing the analysis on the influence of the sample frequency on the results, it is important, as already said before, to analyse the results of the repeatability of the experiments. Ten different time series with the same paddle movement were analysed in order to confirm that the generated time series is always the same with an acceptable error. A comparison was made for the generated waves and for the total force (Figure 2.7).
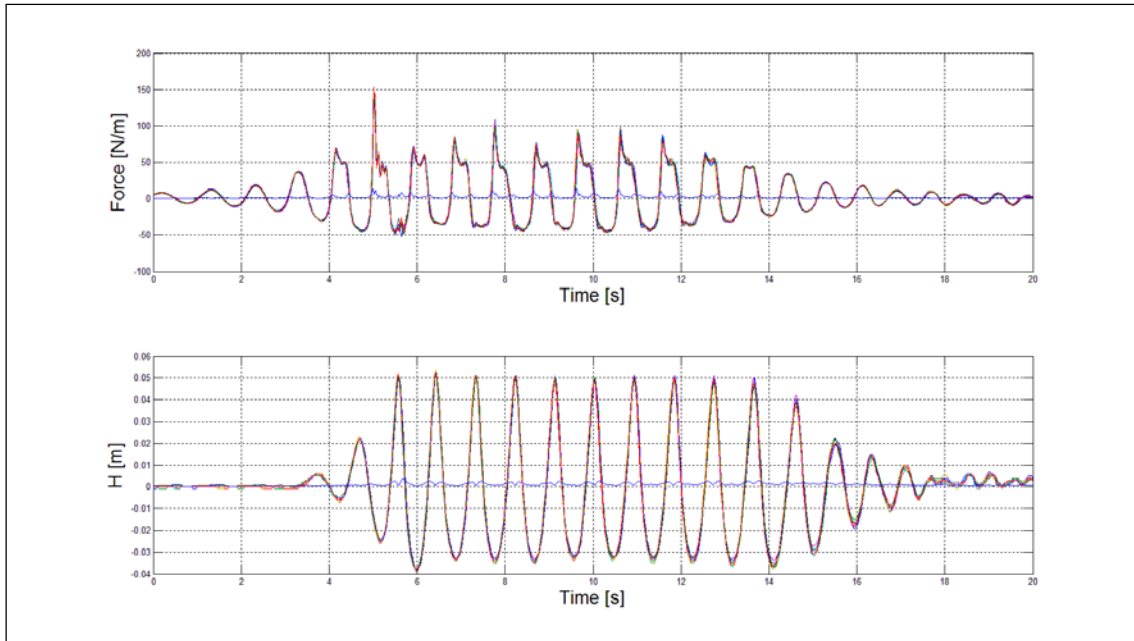
Figure 2.7: Test repeatability: Total force on the vertical wall (up). Generated wave at 3 m from the wave paddle (down). In both figures there are plotted the 10 time series (in colors) and the computed RMS (in blue).

A maximum error of 4% in the total force and of 6% in the generated wave was found. With this error it is possible to assume that the experiments are repeatable and the results obtained are representative. As is known, the impulsive conditions are extremely fast and as can be seen for the same wave impact condition (Figure 2.8) the maximum force sampling at 50 Hz is around 150 N/m but the maximum force sampling at 19200 Hz is 220 N/m. This is a 150 % more.
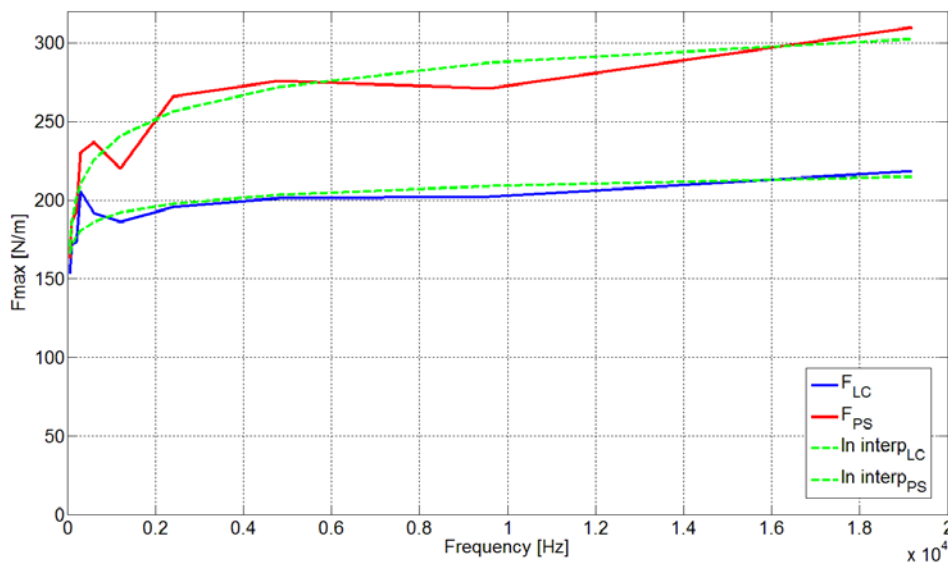
Figure 2.8: Sample frequency analysis. In blue and red there are the recorded data and in green a logarithmic interpolation of the dataset.

It is also possible to see some dispersion in the dataset at the frequencies between 300 and 600 Hz. This is a normal occurrence because of the sampling at a low frequency. It does not mean

that it is impossible to catch the peak, but it means that the probability of detecting the peak is smaller. Furthermore, is possible to say that small increases in the total force are predictable for increases in the sample frequency (over 19200 Hz). Is important to remember that a 400 fold increase of the sample frequency leads to a 1.5 fold increase of the total force. The sample frequency also influences on the noise level present in the signal. The electrical pollution in the environment is captured by the cables that are working as antennas. This electrical noise has, for definition, amplitude and infinite frequencies, for that reason, pushing up the sample frequency can be a problem for the measure itself as more frequencies capture more noise. In the study case the load cells have a shorter cable than the pressure sensors and for this reason they capture less noise.

2.3.4. Results against the existing formulation

The most used formulation for the calculation of the pressure distribution on a vertical wall is the Goda formula (Goda, 1974) but it does not take into account the impulsive condition. For that reason Takahashi in 1996 has performed some tests and has introduced some modifications in order to consider the impulsive condition. The modified formula gives the following results:

- F = 211 N/m
- Pmax = 980 Pa (at SWL)
- Pb = 657 Pa (at the base of the vertical wall)
- h = 0.135 (height reached by the water above SWL)

The Cuomo (2010) formula instead gives the values of the maximum impact force (Fimp) and of the quasi-static force (Fqs) but does not give the pressure distribution. The results are:

- Fimp = 938 N/m
- Fqs = 378 N/m

The overall forces of the study case are listed in Table 2.2 taking into account the variability of the results with the sample frequency.

FLC [N/m]	FPS [N/m]	Pmax [Pa]	Sample Freq. [Hz]
153	163	1052	50
172	186	1273	100
173	193	1512	200
206	230	2014	300
192	237	2231	600
186	220	1882	1200
196	266	2445	2400
201	276	2423	4800
202	271	2584	9600
218	310	2644	19200

Table 2.2: Experimental results: Total Force computed with the load cells (F_{LC}) and the pressure sensors (F_{PS}) varying the sample frequency

2.4. Conclusions

From these tests it is possible to draw some discussions referred to in the preliminary results. It is possible to assume that the load cells and the pressure sensors give comparable results, especially at a low sampling frequency where the noise does not play an important role as is "filtered" by the low sample frequency. When increasing the sample frequency this filter is less effective against the noise that affects, with greater magnitude, the pressure sensors than the load cells. The global behavior remains comparable, but a lot of noise appears in the pressure sensor time series with mean amplitude of approximately 30 N/m (Figure 2.9).
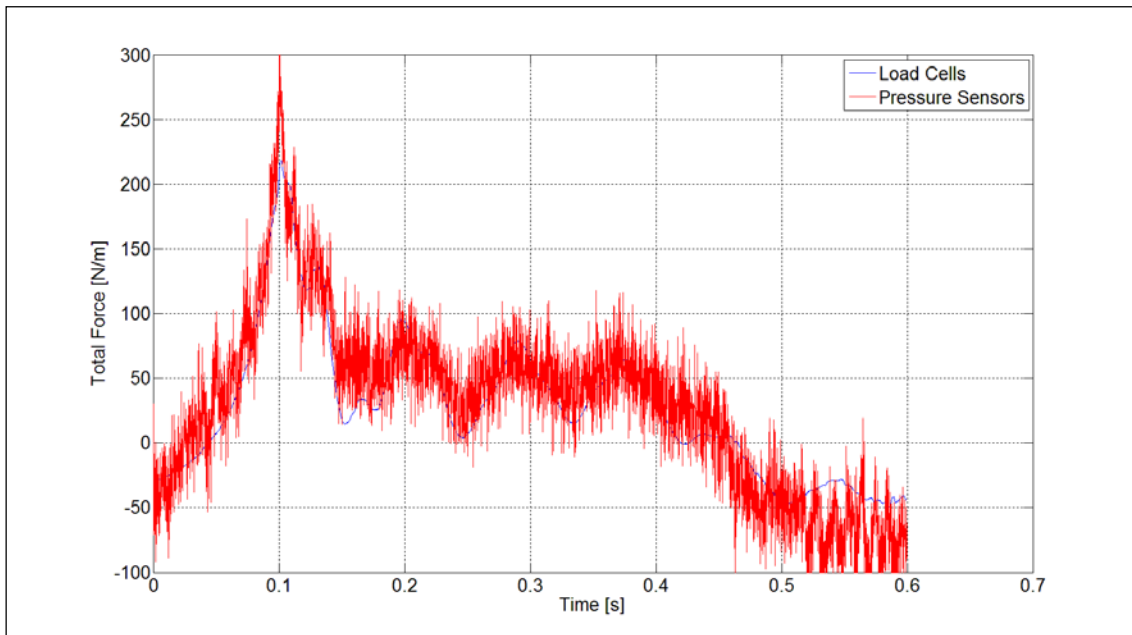
Figure 2.9: Load cells and pressure sensors comparison; at a sample frequency of 19200 Hz a lot of noise appears in the time series of the load cells.

That affects clearly the measure of the peak if a variation of 60 N/m is not negligible as in the present study case. That behavior of the pressure sensors can be associated with the length of the cable. As said before the cable can work as an antenna that captures all the electric signals and a longer cable is a more receptive antenna. The length of the cables of the pressure sensors were 6m instead of the 3m for the cables of the load cells. The sample frequency does not just affect the level of noise in the signal, but also influences the value of the force peak recorded during the impact. A growth of the sample frequency implies a higher value of the maximum total force, as it can be seen in Figure 2.8, both using the load cells and the pressure sensors to calculate it, although with some differences between both systems of measure. Comparing the experimental results (Table 2.2) with the results of the classical formulations it is possible to assume that the formula of Takahashi is comparable with the maximum force calculated with the load cells at the maximum sample frequency. Nevertheless, the maximum pressure is not comparable because of the pressure distribution that Takahashi uses. The Takahashi (2002) pressure distribution is averaged, and it does not present a peak above the water level according to the results. Also the maximum height reached by the water is overestimated. That means that the total force is comparable but not the pressure distribution and the momentum. The Cuomo formula (2010) instead returns values one order of magnitude higher than the recorded ones. It is possible to associate these differences to the scale of work: Takahashi (2002) has worked at a comparable (a bit bigger) scale for the physical model. Instead the experiments used by Cuomo (2010) to develop his formula are performed in the big scale flume of the UPC that is approximately 6 times longer than the CIEMito flume. Furthermore the configuration used in the experiments of Takahashi (2002) is similar to the one used in this paper, instead Cuomo (2010) uses a slope beach (1/13 slope) that allows a better development of the wave in order to reach an impact condition. Also in the Cuomo (2010) experiments a toe protection is not present. All these differences can lead to different results.

2.5. Future works

More exhaustive experiments need to be done in the near future. A sloping beach will be used so as to improve the development of the wave and reach "more impulsive" conditions and higher values of the total force. With the utilization of a sloped beach a higher depth at the generation zone can be used that permits to generate higher waves and longer periods avoiding the wave breaking at the generation area. Generation of focused waves and the utilization of nonlinear theory of generation can be implemented in order to improve the knowledge and to analyze the differences with linear theory generation. Irregular waves also need to be tested and analyzed in order to sweep a wide range of conditions.

References

Allsop, N.W.H., Kortenhaus, A., Oumeraci, H. & McConnell, K. 1999. New design methods for wave loading on vertical breakwaters under pulsating and impact conditions, *Proc. Coastal Structures '99*, (Santander, Spain). *Balkema Rotterdam*, pp. 592-602.

Allsop, N.W.H. & Vicinanza, D. 1996. Wave impact loadings on vertical breakwaters: development of new prediction formulae, *Proceedings 11th International Harbour Congress*.

Allsop, N.W.H., Vicinanza, D. & McKenna, J.E. 1996. Wave forces on vertical and composite breakwaters, *vol. Strategic Research Report SR 443*. (HR Wallingford), pp. 1-94.

Bagnold, R.A. 1939. Interim report on wave pressure research, *J. Inst. Civil Engrs*, vol. 12, pp. 202-226.

Bullock, G.N., Crawford, A.R., Hewson, P.J., Walkden, M.J.A. & Bird, P.A.D. 2001. The influence of air and scale on wave impact pressures, *Coastal Engineering*, vol. 42, no. 4, pp. 291-312.

Bullock, G.N., Obhrai, C., Peregrine, D.H. & Bredmose, H. 2007. Violent breaking wave impacts. Part 1: Results from large-scale regular wave tests on vertical and sloping walls, *Coastal Engineering*, vol. 54, no. 8, pp. 602-617.

Cuomo, G., Allsop, W., Bruce, T. & Pearson, J. 2010. Breaking wave loads at vertical seawalls and breakwaters, *Coastal Engineering*, vol. 57, no. 4, pp. 424-439.

Cuomo, G., Allsop, W. & Takahashi, S. 2010. Scaling wave impact pressures on vertical walls, *Coastal Engineering*, vol. 57, no. 6, pp. 604-609.

Cuomo, G., Piscopia, R. & Allsop, W. 2011. Evaluation of wave impact loads on caisson breakwaters based on joint probability of impact maxima and rise times, *Coastal Engineering*, vol. 58, no. 1, pp. 9-27.

Goda, Y. 1974. New Wave Pressure Formulae for Composite Breakwaters, *Proceedings of the 14th International Coastal Engineering Conference*,(Copenhagen, Denmark), vol. 3, pp. 1702-1720.

Mansard, E.P.D. & Funke, E.R. 1980. The measurement of incident and reflected spectra using a least squares method, *Proceedings of the 17th Coastal engineering Conference,* (Sydney, Australia), vol. 1, pp. 154-172.

Minikin, R.R. 1963. *Winds, Waves and Maritime Structures*. 2nd edition. Charles Griffin, London, UK.

Oumeraci, H. 1994. Review and analysis of vertical breakwater failures — lessons learned, *Coastal Engineering*, vol. 22, no. 1–2, pp. 3-29.

Stevenson, T. 1874. *The design and construction of harbors*, 2nd edition. Black, London.

Sutherland, J., Walstra, D.J.R., Chesher, T.J., van Rijn, L.C. & Southgate, H.N. 2004. Evaluation of coastal area modelling systems at an estuary mouth, *Coastal Engineering*, vol. 51, no. 2, pp. 119-142.

Takahashi, S., Tanimoto, K. & and Shimosako, K. 1994. A Proposal of Impulsive Pressure Coefficient for Design of Composite Breakwaters, *Proceedings of the International Conference on Hydro-Technical Engineering for Port and Harbor Construction*. (Port and Harbour Research Institute, Yokosuka, Japan) , pp. 489-504.

Takahashi, S. 2002. *Design of vertical breakwaters*. Port and airport research institute - Japan.

3. Efectos de laboratorio

Los efectos de laboratorio que se analizarán en este capítulo son principalmente dos: el efecto del sistema de medida (células de carga y sensores de presión) y, en segundo lugar, el efecto de la frecuencia de muestreo. Aprendiendo de los errores de los primeros ensayos se construye un nuevo *layout* experimental incluyendo un plano inclinado como aproximación al dique vertical instrumentado. Este nuevo *layout* permite la generación de impactos más controlados y violentos. Se añade también un sensor de presión en la zona de impacto para mejorar la densidad espacial de las medidas de presión y así caracterizar mejor la distribución de presión. La descripción de los ensayos, la presentación y el análisis de estos resultados están publicados en el artículo "*Laboratory effects on measuring impact loads on rigid coastal structures*".

Marzeddu, A., Gironella, X., Sánchez-Arcilla, A., & Sutherland, J. (2014). Laboratory effects on measuring impact loads on rigid coastal structures. In *Proceedings of the 3rd IAHR Europe Congress, 2014, Porto-Portugal.*

Abstract

Some small scale laboratory experiments were carried out in order to detect laboratory effects during the measurement of wave loads on rigid structures. Wave loads on rigid structures are divided into quasi static loads and impact loads. The procedure that will be demonstrated in this paper, the measure of quasi static loads is fairly easy and not affected by the sample frequency. Instead the measure of impact loads is very difficult and some laboratory effects can strongly influence the results and lead at an unsafe estimation of the total load. Particularly, the use of different equipment and sensors can lead to significant differences in the results, so, for this reason, a comparison between load cells and pressure transducers recorded under the same wave conditions were made. Impulsive wave loads are very fast and are characterized by a very short rise time (some milliseconds) and the results, also under regular waves attack, are very scattered. For that reason a higher frequency sampler (up to 19.2 KHz) was used in order to study how the use of different sample frequencies can lead to very different results. In principle the utilization of a sample frequency that is too low can lead again to an unsafe estimation of the total load and affect the design process. Besides, due to the large scatter on the data, a deterministic approach is inadvisable and some repetitions of the same wave conditions are needed in order to characterize well the studied phenomena. The obtained results show the probabilistic performance inherent to the impact loads phenomena as a source of the scattered results.

3.1. Introduction

In the last few years, increasing attention has been given by various authors to the phenomena of wave impact on rigid structures and particularly on vertical breakwaters. Only recently the failure of a caisson breakwater caused by a wave impact has been analyzed in depth (Oumeraci, 1994) and since that time a more focused approach on the consequences of pulsating loads and on the dynamic response of the structures has started. A lot of historical research has been carried out regarding wave forces on seawall starting from Stevenson (Stevenson, 1874). It was Bagnold (Bagnold, 1939) who was the first to focus the attention on wave impacts on coastal structures. The first to develop a prediction method for waves that breaks directly onto a vertical breakwater was Minikin (Minikin, 1963), but Allsop (Allsop et al., 1996) demonstrated the inconsistency of the formula. Takahashi (Takahashi, 1994), extended the Goda formula (Goda, 1974) including the impulsive force parameter setting the benchmark in the calculation of pulsating loads on vertical breakwaters. Within the European project PROVERBS laboratory tests, at large and small scales, were run at the GWK of Hannover, Germany and at DWF at HR Wallingford, UK. The results of these experiments have led to the Allsop formula (Allsop et al., 1999) in which a statistical approach was used. A new data set of large scale experiments performed at the LIM-UPC Barcelona, Spain, under the project Violent Overtopping by Waves at Seawalls (VOWS), led to a new formulation (Cuomo et al, 2010). Using both data sets of PROVERBS and VOWS, a statistic evaluation of impact loads on caisson breakwaters based on the joint probability was presented (Cuomo et al, 2011). An extended work has been done also over the effects of fresh water, trapped air, laboratory and scale effects (Bullock et al, 2001) using the comparison between field measurements at the Admiralty Breakwaters at Braye Harbour in the Channel Islands. A scaled 1:25 physical model test was carried out, at the University of Plymouth, UK. In this paper, a simple study case of a vertical breakwater with an approaching 1/15 sloped beach was tested in a small scale flume at the UPC under regular wave attacks in order to find impulsive load conditions. Different impulsive conditions were generated and analyzed and one of the strongest one was selected in order to perform a comparison between pressure sensors and load cells and a study over the influence of the sample frequency was performed.

3.2. Experimental Set-Up

The experiments have been carried out in the CIEMito wave flume of the Laboratori D'Enginyeria Maritima (LIM) of the Universitat Politecnica de Catalunya (UPC). The flume is 18m long, 0.38 m wide and 0.56 m high. It is equipped with a piston type wave maker driven by software developed at LIM/UPC that allows generation of regular and random waves characterized by a

target spectrum as well as a target wave time series. A scaled model of a vertical breakwater has been built and tested against regular wave attacks. The flume has a flat bottom and an approaching 1/15 sloped beach that end at the toe of a simplified vertical breakwater. A water depth of 0.285m was used. The vertical wall of the breakwater has been equipped with eight pressure sensors and was held also with two load cells, in order to record the pressure and the total force at every wave attack at the same time. The load cells have been fixed at a superstructure of the wave flume with a reticular structure in order to avoid possible movements. The experimental set-up is shown in Figure 3.1.
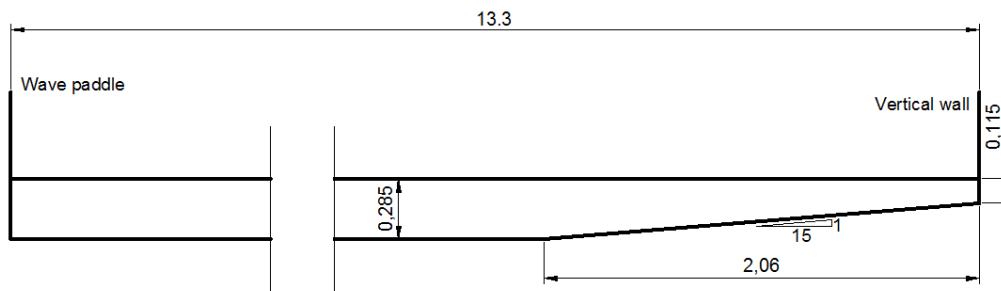
Figure 3.1: Experimental lay-out CIEMito wave flume (all dimension in m)

3.2.1. Instrumentation

The instrumentation used during the experiments was composed of:

- Eight pressure sensors P8AP by HBM ©

- Two load cells Z6 by HBM ©

- Eight wave gages

The P8AP is an absolute pressure transducer based on a strain gauge sensor with a measuring span of 10 bars and an accuracy class 0.3. The P8AP are IP67, that means they are weatherproof but not waterproof and for this reason a box that isolates the sensors from the water is needed. 20 holes were added to the front wall so as to be able to try different patterns of pressure sensors positions. Eight holes were plugged with the pressure sensors and the others are plugged with screws in a manner that the front wall will be waterproof and continuous.

After some tests using various positions of the pressure sensors, the definitive pattern was defined with six pressure transducers placed with a spacing of 2.5 cm and, slightly above the water level (impact zone) the distribution became denser adding another sensor between the third and the fifth, reducing the spacing at 1.25 cm. Another sensor (the eighth) has been added

5 cm above the seventh sensor in order to have an accurate estimation of the higher part of the pressure distribution and make the comparison with the load cells more precise (Figure 3.2).

The Z6 by HBM is a bending beam load cell with a nominal load of 50 Kg and an accuracy of 0.009 % of the maximum capacity. The load cells were mechanically fixed to the protecting box of the pressure sensors and fixed at the reticular structure described before. It is very important that the mechanical connection should be very rigid in order not to absorb any force and affect the measurement.

A reticular structure fixed on a super structure of the wave flume (independent from the wave flume itself) is used because in a reticular structure there are just normal forces and the nodes are fixed (Figure 3.3). The stiffness of the load cells should be much lower than the stiffness of the reticular structure in order to deform itself and to perform the right measure of the force.

The coupling of the two load cells in two different positions is needed in order to obtain time series of the total force, the momentum and the application point of the force. The static scheme of the two load cells is shown in Figure 3.2.
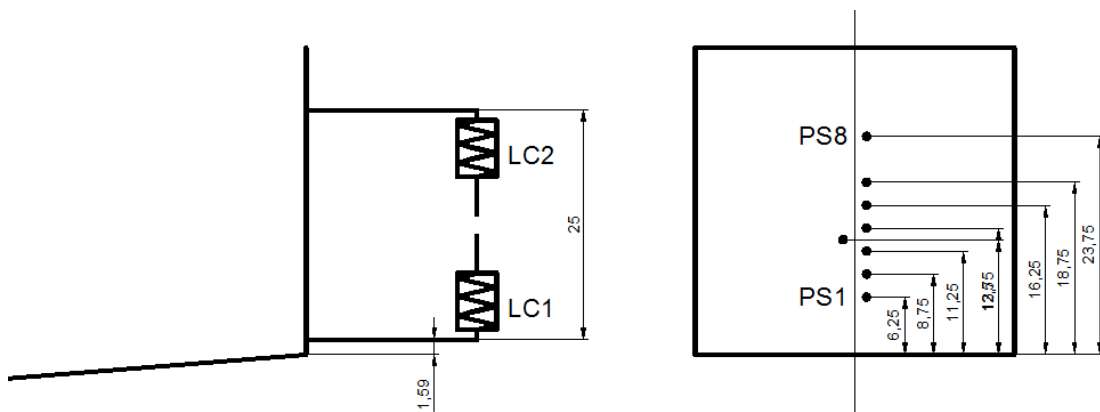
Figure 3.2: Load cell and pressure transducers set-up on the vertical wall (all dimension in cm)

Figure 3.3: Vertical wall mounted in the CIEMito wave flume

Both pressure sensors and load cells are connected at two Quantum X MX840A data acquisition system by HBM. The MX840A is an 8 channel data acquisition system that can record at a maximum sample frequency of 19.2 KHz. The possibility to connect the eight pressure transducers and the two load cells in the same acquisition system and sample then at a very high speed is crucial in order to be able to compare the results obtained from both together and well analyze the results.

Wave motions were measured by using 8 resistive wave gages, with an accuracy of 0.1 mm, positioned in front of the vertical breakwater in order to measure the generated wave, the wave in front of the structure and decompose incident/reflected waves with the Goda and Suzuki method (Mansard, 1980).

3.2.2. Wave test conditions

In order to guarantee an impulsive wave load condition a series of preliminary tests were made. These tests consist in 120 different regular wave conditions executed in a manner to find a benchmark wave and a control wave. The characteristics of the benchmark wave are that the wave generated loads should be both impulsive and reach higher pressure level so as to ensure that the noise level on the pressure transducers signal will be small enough. The control wave is a wave attack which should lead to quasi-static loads and will be used to control the proper functioning of the measurement system. Wave periods from 1 to 3 seconds with a spacing of 0.2

seconds and wave heights from 0.09 to 0.16 m with spacing of 0.01 m were tested. Each time series is composed by 9 waves divided in 2 ramp-up waves 5 regular waves and 2 ramp-down waves.

The selected wave conditions are:

Benchmark wave:

- H=0.15 m T=2.1 s

Control wave:

- H=0.08 m T=1 s

In order to study the effect of the sample frequency 300 repetitions of the same benchmark wave were done. Once the first repetitions were done, clearly appear that the results of the total force presented a large spread. For that reason two controls were done. The first one was on the generated waves and appears that the repeatability were almost perfect with a maximum RMSE of 0.0015m in accordance with the wave gages measurement error. The second control was the one on the reliability of the measurement system. As explained before a control wave that generates quasi-static loads were tested and again, almost perfect match were found on the recorded total force. The maximum RMSE found is 2N, comparable with the amplitude of the signal noise at the sample frequency of 19.2 KHz.

3.3. Analysis methodology

3.3.1. Load cells

The load cells give as a result the force applied at their extreme, and solving the static scheme in Figure left, is possible to obtain with a simple calculation the total force applied on the wall. This result is very robust as no calculation and no analysis are needed.

Once the time series of the total force applied on the vertical wall is calculated is important to identify the peaks of the 5 regular waves in time and magnitude. The ramp-up and ramp-down will not be analyzed for neither load cells nor pressure transducers.

3.3.2. Pressure transducers

The analysis required to obtain the total force from the pressure sensors is a little more complicated. The time series of the pressure transducers, especially at high sample frequency, is noisier and the magnitude of the pressure is highly variable sensor by sensor. For that reasons, the automatic identification of the peaks does not return unique results. Since the pressure transducers and the load cells are triggered in the same DAQ, it was decided to use the time of

the load cells in order to identify the peaks on the pressure transducers. All the pressure transducers time series do not reach the peak at the same instant and not at the same instant of the load cells. To overcome this problem, a time windows of plus or minus 1/50 seconds was applied at the load cells peak time in order to identify the maximum peak on the time series recorded with the pressure transducers. Good results were achieved and are showed as an example in Figure 3.4.
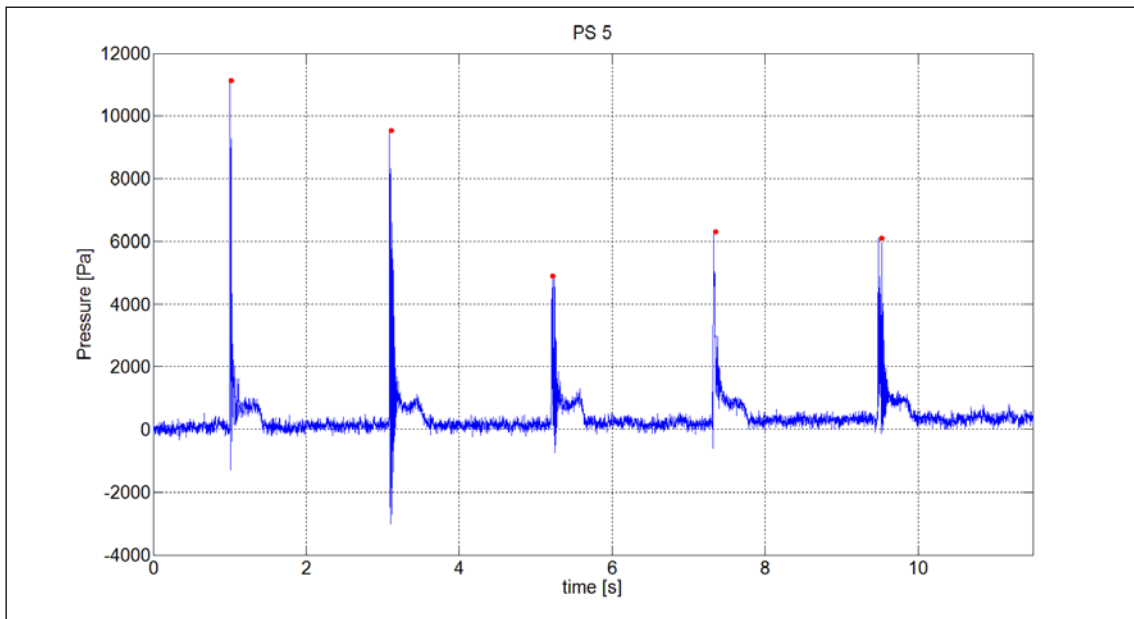
Figure 3.4: Peak determination in the pressure transducers time series by controlling the load cell peak time

Once the peaks are determined, a vertical distribution of the pressure on the vertical wall is needed in order to can compare the results with the ones obtained with the load cells. Three different approaches have been used in order to interpolate the data between pressure sensors and extrapolate, if it is the case, under the first and over the last pressure transducer:

- Linear extrapolation over the upper sensor and under the lower sensor and linear interpolation between the measured pressures (case A).
- Linear interpolation between the measured pressures with no extrapolation (case B)
- Rectangular distribution between measured pressures with no extrapolation (case C).

The three different approaches are graphically explained in Figure 3.5
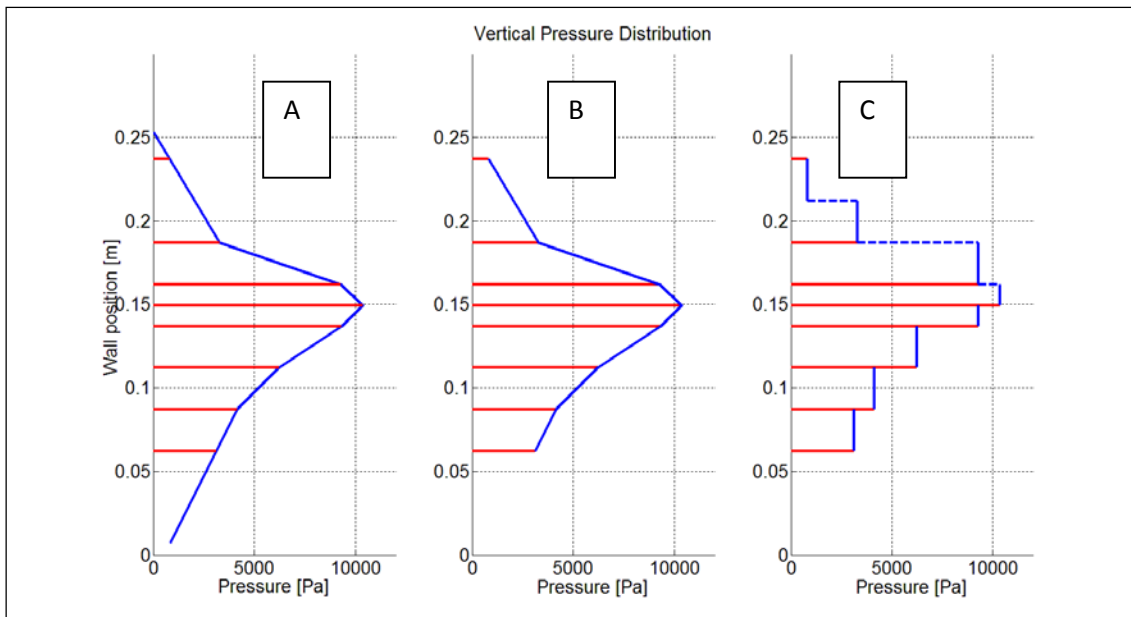
Figure 3.5: Vertical pressure distribution – interpolation approaches

The total force is obtained by integrating the vertical distribution.

3.4. Results

Once the total force is calculated from the load cells and from the pressure transducers is it possible to perform an analysis of how the sample frequency used affects the magnitude of the impulsive loads. In principle is important to remember that the utilization of a lower sample frequency reduces the probability to capture the peak but this probability is never zero.

The results were analyzed wave by wave and considering the 300 repetition of the 5 regular waves we can consider 1500 unique regular waves. Considering the 10 tested sample frequencies, it is possible, for every sample frequency to apply each statistical analysis to 150 unique regular waves.

In Figure 3.6 it is shown the sample frequency against the dimensionless total force calculated from the load cells and from the three different integration methods of the pressure vertical distribution. It is easy to see that the spread on the force data is large if the measures are done with both the load cells or with the pressure transducers. The spread on the data is larger on all the cases in which the force is calculated from the vertical pressure distribution. It seems that the behavior of the maximum force recorded at every sample frequencies increases with the increase of the sample frequency, tough again that this increment is larger if the force is obtained from the vertical pressure distribution. Differences are appreciable also if the integral of the vertical pressure distribution is calculated with the three different methods. If the

increment of the force calculated with the load cells, passing from 1.2 KHz to 19.2 KHz, goes from about 10%, to almost the 50% if the case A integration method is considered (Figure 3.6).
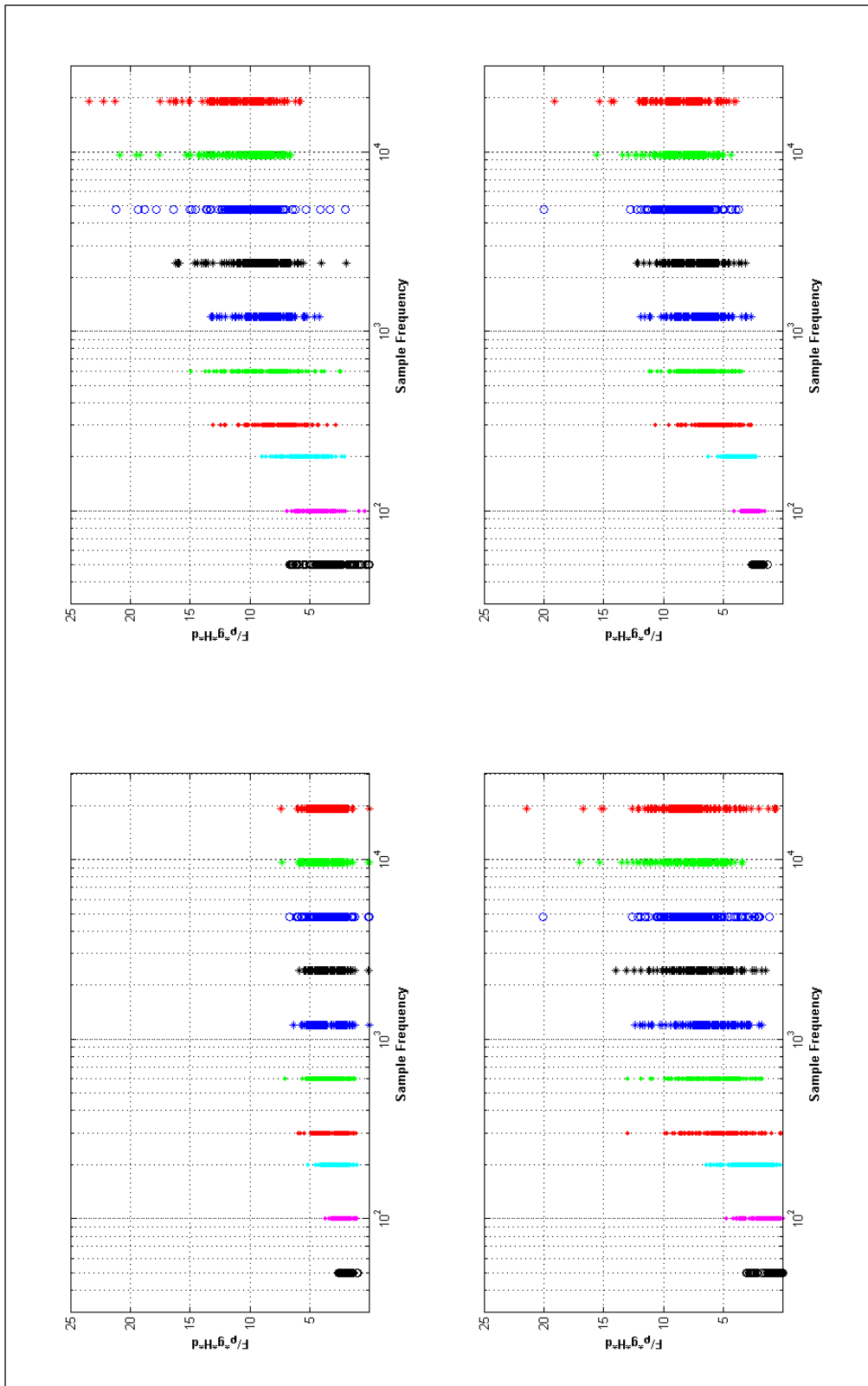
Figure 3.6: Sample frequency against dimensionless force From the upper-left corner clockwise: Force obtained from the load cells – Force calculated with the integral of the pressure vertical distribution Case A – Case B – Case C

In Figure 3.7 the dimensionless force calculated from the load cells against the frequency of occurrence is plotted. The results are shown for the 10 different tested sample frequencies. The statistical distribution seems close to the normal distribution for the sample at 50 and 100 Hz but it flattens and spreads when increasing the sample frequency, moving away from the normal distribution. The behavior at higher frequency seems totally random with similar patterns and a low probability (< 5%) to "catch" a smaller or a larger force peak. From both figures is possible to see that the maximum recorded force was recorded for the maximum sample frequency (19.2 KHz) and again, the maximum spread on the data is notable at the maximum sample frequency. It appears that, Figure 3.7 shows some trend to a "double pseudo-normal distribution" around a valley zone when increasing the sample frequency.

3.5. Conclusions

From the presented results some important considerations on laboratory effects to understand wave loads can be derived. First of all it is important to focus on the differences on the results obtained with the two different types of sensors. The pressure transducers seem to be affected by the presence of the air in the water during impact situations, presenting, a larger spread in the collected data. Instead, the load cells are not affected by this phenomenon as they measure directly the force over the entire wall and they not enter in contact with the wave itself. Also the different methods of integration of the pressure vertical distribution may affect the results introducing another degree of incertitude on the calculation of the force. Considering here that the results obtained with the load cells are more robust, it seems that the simplest type of integration, the rectangular one (case C Figure), is the one that may lead to better results in a general situation.
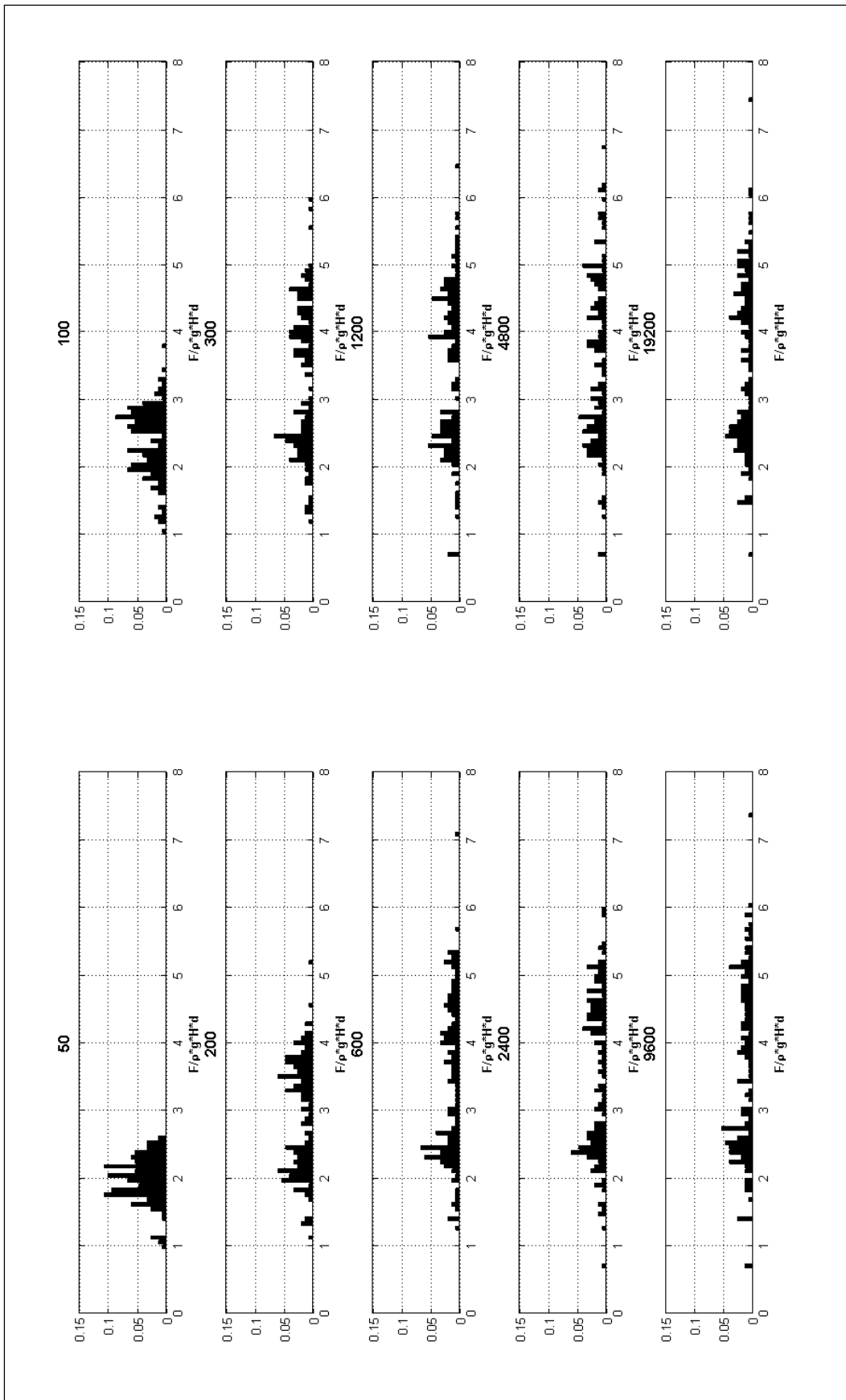
Figure 3.7: Dimensionless total force against the probability of occurrence for the different sample frequencies

Considering now the results obtained with the load cells is possible to assume that the impact loads have an almost random component without any particular behavior. In a train of the 5 regular waves, while the 5 wave are almost the same at the toe of the structure, is impossible to assure which wave in the train will produce the maximum force and it is almost impossible to predict a priori a deterministic value of the maximum force. For these tests the error passing from 1.2 KHz to 19.2 KHz, is about 10%. This error could be considered acceptable, despite the spread on the data that is large. Thus it is important to sample at higher frequency in order to have a higher probability to "catch" the peak (Figure 3.7). Also a lot of repetitions of the same test series are needed in order to be sure to complete a valid statistical analysis of the phenomena and to estimate an extreme value of the force.

Acknowledgments

References

Allsop, N. W. H., Kortenhaus, A., Oumeraci, H., & McConnell, K. (1999). 'New design methods for wave loading on vertical breakwaters under pulsating and impact conditions'. Proc. Coastal Structures '99, Santander, Spain. Balkema Rotterdam, 592–602.

Allsop, N. W. H., Vicinanza, D., & McKenna, J. E. (1996). 'Wave forces on vertical and composite breakwaters', Strategic, 1–94.

Bagnold, R. A. (1939). 'Interim report on wave pressure research', J. Inst. Civil Engrs., 12, 202–226.

Bullock, G. N., Crawford, A. R., Hewson, P. J., Walkden, M. J. A., & Bird, P. A. D. (2001). 'The influence of air and scale on wave impact pressures'. Coastal Engineering, 42(4), 291–312. Doi:10.1016/S0378-3839(00)00065-X

Cuomo, G., Allsop, W., Bruce, T., & Pearson, J. (2010). 'Breaking wave loads at vertical seawalls and breakwaters'. Coastal Engineering, 57(4), 424–439. doi:10.1016/j.coastaleng.2009.11.005

Goda, Y. (1974). 'New Wave Pressure Formulae for Composite Breakwaters'. Proceedings of the 14th International Coastal Engineering Conference, 3, 1702–1720.

Goda, Y., & Suzuki, Y. (1976). 'Estimation of incident and reflected wave in random wave experiments', 15th International Coastal Engineering Conference (pp. 828–845).

Minikin, R. R. (1963). 'Winds, Waves and Maritime Structures, 2nd edition', Charles Griffin, London, UK.

Oumeraci, H. (1994), 'Review and analysis of vertical breakwater failures lessons learned', Special Issue Vertical Breakwaters, 22(12), 3–29. doi:10.1016/0378-3839(94)90046-9

Takahashi, S., Tanimoto, K., & and Shimosako, K. (1994). 'A Proposal of Impulsive Pressure Coefficient for Design of Composite Breakwaters', Proceedings of the International Conference on Hydro-Technical Engineering for Port and Harbor Construction, Port and Harbour Research Institute, Yokosuka, Japan,, 489–504.

4. Ensayos a gran escala

En este capítulo se presenta una serie de ensayos a gran escala que se han llevado a cabo durante la estancia del autor en las instalaciones de MARINTEK-SINTEF (Trondheim, Noruega). Las instalaciones de MARINTEK destacan por la piscina "Ocean Basin Laboratory" de 80x50 m y una profundidad máxima de 10m. Los ensayos han sido financiados por la Comunidad Europea dentro del programa "Transnational Acces – Hydralab IV". Durante esta estancia se ha ensayado una estructura con pared vertical y protección de pie sobre fondo plano (no fué posible construir un plano inclinado en la piscina). La estructura ha sido instrumentada con dos tipos de sensores de presión, células de carga y el innovador sensor táctil de presión, capaz de generar mapas de presión a alta densidad espacial. La descripción de los ensayos, la presentación y el análisis de estos resultados estén publicados en el artículo "*Large scale experiments on the interaction of a caisson breakwater with breaking waves*".

Stagonas, D., Marzeddu, A., Buccno, M., Calabrese, M., Banfi, D., Vicinanza, D., Kofoed, J.P., Pecher, A., Frigaard, P., Pakozdi, C., 2014. Large Scale Experiments on the Interaction of a Caisson Breakwater with Breaking Waves, in: HYDRALAB IV Joint User Meeting.

Abstract

Tests looking at the interaction of a caisson breakwater with steep, breaking waves are outlined here. 4 different wave generation methodologies were employed allowing for experiments with regular, irregular, focused and tailored made waves. The emphasis, however, is given in tests with focused waves, which resulted in impulsive conditions at the face of the caisson. Amongst our objectives was to look at the mechanisms occurring when a wave breaks at the structure and to investigate the validity of tactile pressure sensors. As such, for all experiments, pressure, force and surface elevation measurements were complimented with high speed and high definition video records. In addition, a pressure mapping system employing tactile pressure sensors was deployed in combination with force panels, both positioned at still water level. Although at a very early stage, data analysis yields promising results.

4.1. Introduction

Although caisson breakwaters are mainly deployed in deep waters, the high irregularity of real sea states suggests that they will still be subject to the effects of breaking waves. High and steep approaching waves may break at the face of the structure and induce forces with magnitudes more than 5 times greater than quasi-static loads and rise times in the order of 1ms. For this, contemporary design guidelines suggest that within a probabilistic framework the effect of breaking waves must be considered, e.g. Oumeraci (1994), Allsop et al. (1996c) and Oumeraci et al. (2001). Based on hydraulic tests and field observations, extensive methodologies for the prediction of pulsating and impulsive loads have been developed, e.g. Goda (1985) and with

continuous research their accuracy increases, Cuomo et al. (2010), Frigaard et al. (1998). Nevertheless, knowledge on the complex hydrodynamic mechanisms involved and on the coherence of the pressures induced upon breaking is still not well advanced. Observations on the former indicate that three different mechanisms occur during the impact of a wave at a structure with vertical face, impact pressure generation, up-rush/downfall and wave reflection but further understanding is limited. With regards to impact induced pressures, Hull and Muller (2002) reported that maximum pressures occur near or at still water level, however the spatial resolution of their experimental measurements was subject to the limitations of instrumentation (pressure transducers) used. In the current work, the interaction of a caisson breakwater with high and steep waves is investigated. It is envisaged that the data produced will aid on further understanding the mechanisms occurring during the impact and form a very useful set for the validation of CFD models. In the same time the use of tactile pressure sensors may provide unique data on the coherence of impact induced pressures. It is anticipated, that the further validation required for the use of such sensors will come through their combined use with force panels.

In the remainder, the experimental arrangement and the tests conducted are described in section 4.2, preliminary results of the ongoing analysis are presented in section 4.3, while section 4.4 gives a summary of the work.

4.2. Methods

4.2.1. The experimental arrangement

All hydraulic model tests reported here were conducted in the Ocean Basin (80x50x10m), at Marintek, in Tronheim Norway, Figure 4.1.The basin is equipped with a floating bed and the water depth can be reduce to 10m. All tests for the specific project were conducted at a water depth ≤ 1m; namely tests were conducted with water depths of 1m, 0.90cm, 0.85cm and 0.82cm. It should, however, be noted that at the water depth at the wavemaker remains at all times fixed to 10m and it is sharply reduced to the working level at a distance of about 2.5m from the wavemaker. The model caisson was made of steel and its center (x=y=z=0) was located 34.74m from the wavemaker. The caisson was mounted on a steel base comprising of a 1:3 slope at the shoreward side (towards the wavemaker), a 1:1.5 slope at the seaward side and a plateau, which in turn was welded on the bed in order to provide the required rigidity, Figure 4.2.
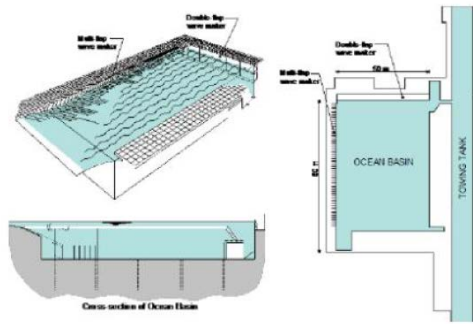
Figure 4.1: The Ocean Basin at Marintek   *Figure 4.2: The model Caisson*
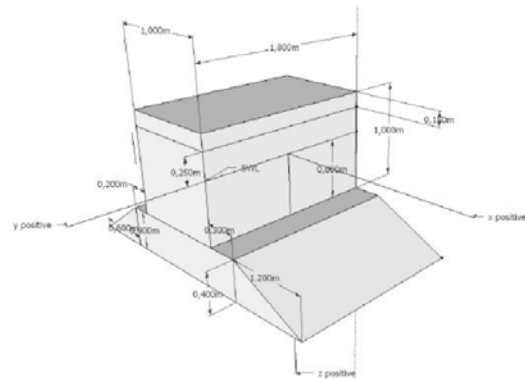
4.2.2. Instrumentation

In total, 50 channels were sampled instantaneously. Amongst them:

- 21 wave gauges positioned between the wavemaker and the structure and at the structure; sampled at 200Hz and filtered at 20 Hz.

- 11 pressure transducers placed on the model caisson at areas where pulsating conditions were anticipated. All 11 transducers were sampled at 2.4 kHz and the signals were filtered at 250Hz.

- 8 HBM P8AP pressure transducers placed on the model caisson at areas where impulsive conditions were anticipated. All 8 transducers were sampled at 9.6kHz and the signals were filtered at 2kHz.

- 6 accelerometers measuring the horizontal and vertical acceleration of the wall, the panel and the beam used to stiffen the area where the force panels were located. All accelerometers were sampled at 9.6 kHz and filtered at 2 kHz.

In addition to the wave gauges, the model caisson is equipped with four different types of pressure measuring instruments. 11 pressure transducers, UNIK 5000 and 8 HBM P8AP pressure transducer are installed at the front, left section of the box and at the back; for the latter 4 of the 11 UNIK 5000 are used. In the same time, 4 force panels, 45x45mm, are placed at SWL and 2 pressure pads, 71x71mm are positioned on top of 2 of the force panels, Figure 4.3. Finally, 6 accelerometers were placed inside the model caisson and behind the latter 2 force panels. At this point it should be noted that the pressure pads are sampled by an independent data acquisition system at a frequency of 4032Hz; the two data acquisition systems are manually 'synchronized'. The location of all pressure and force measuring equipment is illustrated in Figure 4.3.
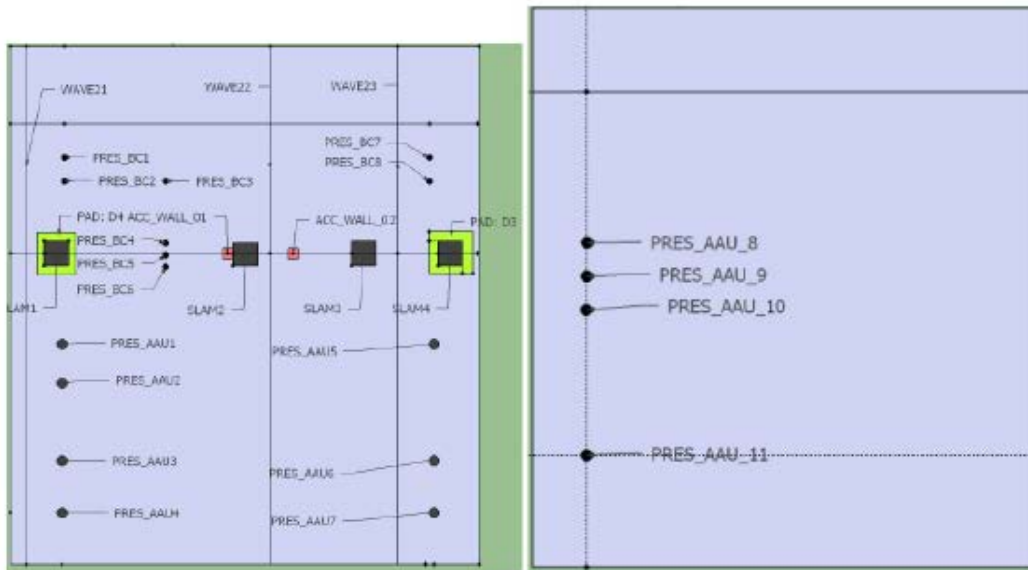
Figure 4.3: Positioning of the force and pressure measuring equipment: the tactile pressure sensors employed with for the pressure mapping system where placed on top of the force panels and they are depicted here within the yellow frame

In addition, video records of the wave propagation and the interaction of the wave(s) with the model caisson were generated with two high definition cameras and one high speed (200fps) and high definition camera. All three cameras were located at the side of the basin and an example of the records acquired is given in Figure 4.4.
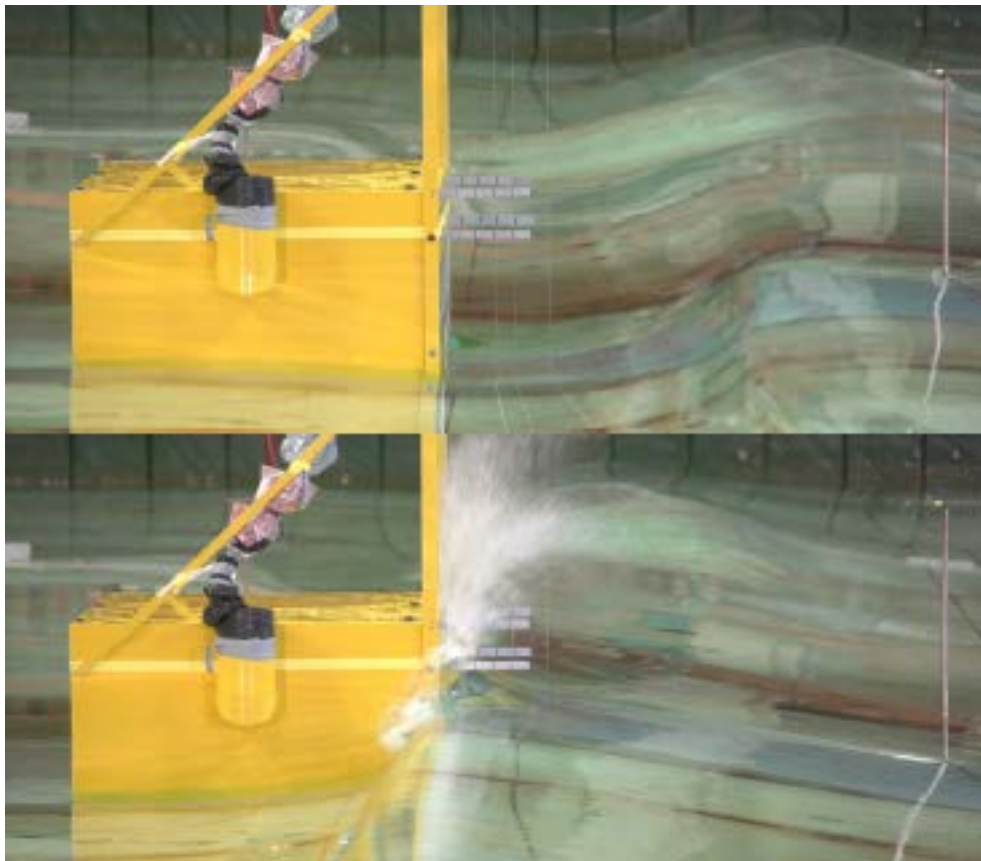
Figure 4.4: Snap-shot from video records acquired with the high speed/high definition camera

4.3. Overview of the test program and preliminary results

The test program was set-up with the aim to initially define the wave conditions giving the steepest waves with the highest possibility to break at the structure. As such tests with regular, irregular and tailor made waves were initially conducted without the model caisson; the input signal for the tailor made waves was very kindly provided by Prof. Alessandro Toffoli. Accordingly it was decided that emphasis was to be given in tests with focused waves which resulted in steeper waves near the structure. For the generation of focused wave the methodology described in Baldock et al (1996) was employed. Experiments were conducted with various combinations of *. the theoretical focusing point with *. the linear wave height at focus and *. the water depth. Although laborious and time consuming, this procedure resulted in nearly-breaking, breaking and broken waves. Figure 4.4 gives an example of a focused wave breaking at the caisson. The methodology followed for the analysis of the videos is described in Vousdoukas et al. (2012). In principle, the water jet position is monitored by sampling pixel intensities along vertical transects on the caisson and along horizontal transects on the rulers Figure 4.5. The jet velocity is derived from the time history of the jet's tip position (red line in Figure 4.5), and its thickness is estimated as a function of the length of the blade/ruler remaining exposed to air (blue and green lines in Figure 4.5). Figure 4.5 gives an overview of the result following the analysis. The first subplot presents the evolution of the jet/wave at the face of the caisson, the subplot in the middle refers to the first ruler (blue line in Figure 4.5) and the lower subplot to the second ruler (green line in Figure 4.5). Here, the velocity and thickness of the highly aerated part of the jet was calculated to about 7m/s and 0.05m respectively.
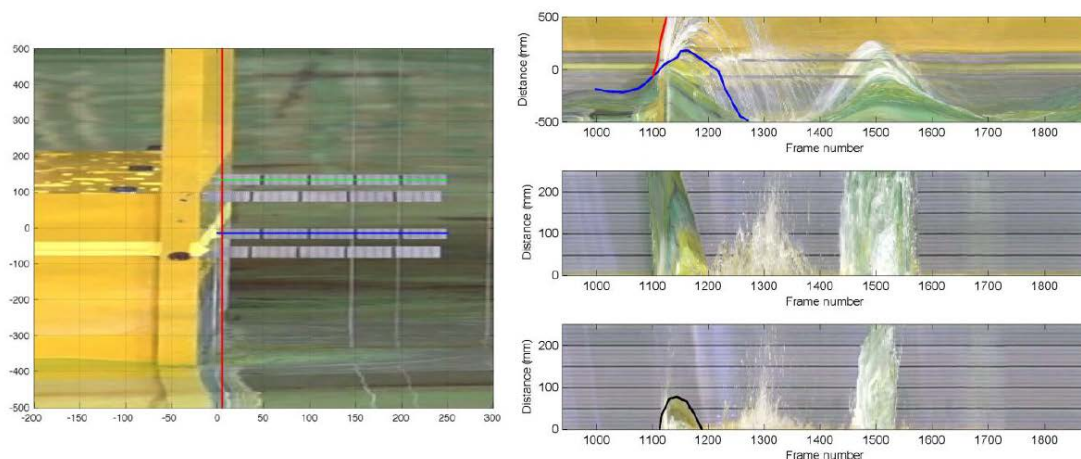
Figure 4.5: Upper image: Transect locations along the caisson and the rulers. Lower image: water jet spatial (distance on x) and temporal (frame number on y) evolution on the face of the caisson (first subplot corresponding to the red line), ruler 1 (second subplot, blue line) and ruler 2 (third subplot, green line).

Examples of surface elevation and pressure measurements are presented in Figure 4.6; measurements at the middle of the caisson are only considered here.
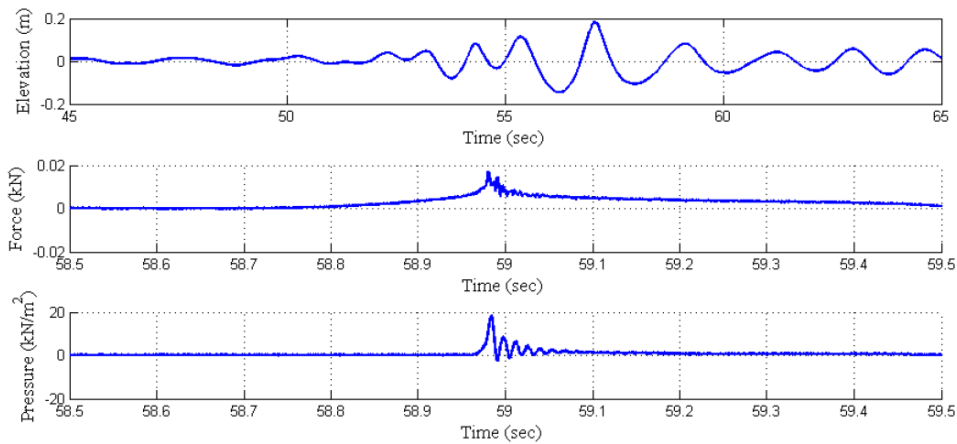
Figure 4.6: Examples of surface elevation, force and pressure measurements

For this project, pressure pads were also used in combination with force panels. This formed the base for an extended, ongoing collaboration between UCL, UPC and University of Southampton which looks deeper on the details of the use of pressure pads. The performance of the pressure pad is compared against load cell measurements for impacts generated with a pendulum but also for impacts generated by water jets, Figures 4.7 and 4.8 respectively.
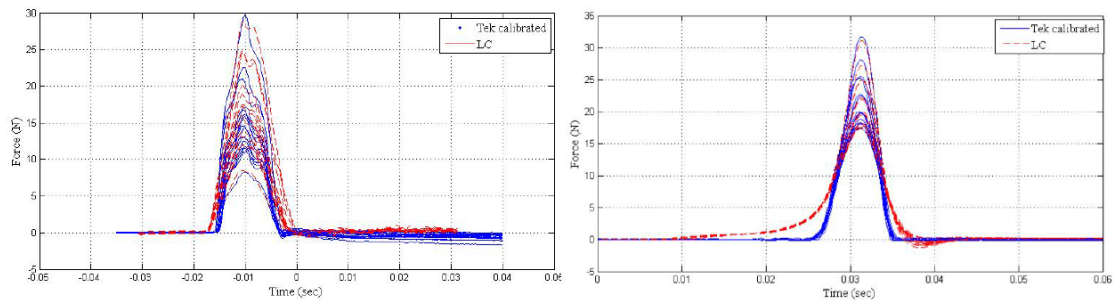
Figure 4.7: Load cell (with red) and tactile pressure sensor (with blue) measurements for impacts with a pendulum; on the left tests conducted at UCP and on the right tests conducted at Marintek
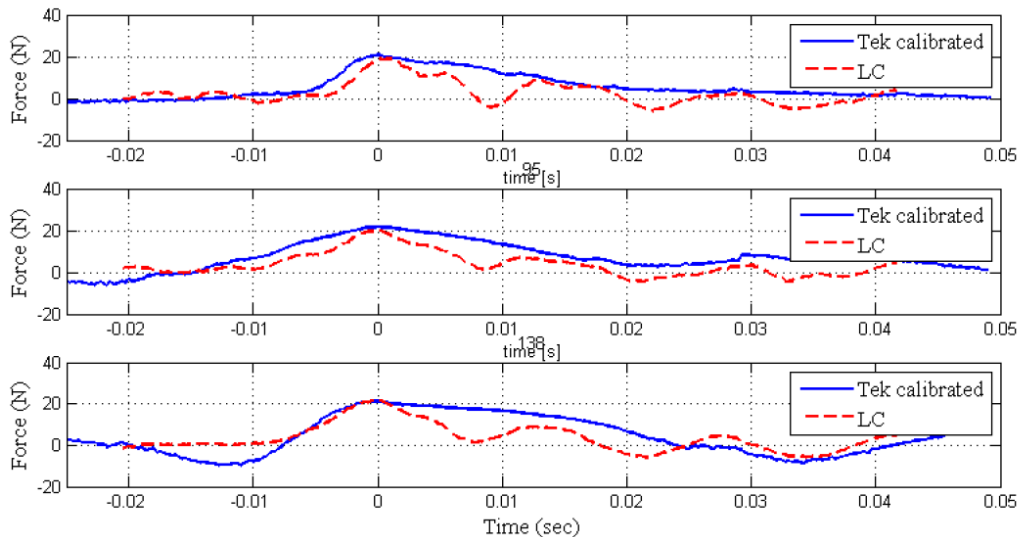
Figure 4.8: Example time histories of load cell (red line) and tactile pressure sensor measurements (blue line) for impinging water jets; the load cell was sampled at 4.8kHz and the tactile sensor at 4kHz.

4.4. Summary

This work looks at the interaction of a caisson breakwater with steep and breaking waves. Emphasis is given on tests employing focused waves, which resulted in impulsive conditions at the structure. Pressures, forces and surface elevation were measured at multiple locations and the interaction of the incoming wave with the caisson was recorded at high speed and high definition. In addition a pressure mapping system was used in conjunction with force panels. It is anticipated that the analysis of the data will provide further insights on the evolution of the mechanisms involved when a wave breaks at vertical structure. In the same time, this work formed the base of an ongoing collaboration between UCL, UPC and the University of Southampton, which at the finer details of the use of the pressure mapping system; this research effort has already yielded promising results.

Acknowledgement

References

Allsop, N.W.H., Vicinanza, D., 1996. Wave impact loadings on vertical breakwaters: development of new prediction formulae. Proc. 11th Int. Harbour Congress, Antewerp, Belgium

Baldock TE, Swan C, Taylor PH, 1996, A laboratory study of nonlinear surface waves on water, Royal Society of London. Philosophical Transactions A. Mathematical, Physical and Engineering Sciences, Vol:354, ISSN:1364-503X, Pages:649-676

Cuomo, G., Allsop, W., Bruce, T., Pearson, J., 2010.Breaking wave loads at vertical seawalls and breakwaters. Coast. Eng. 57, 424–439. Frigaard, P., Burcharth, H.F. and Kofoed, J.P., 1998. Wave impacts on caisson breakwaters situated in multidirectionally breaking seas. Proc. of ICCE98, ASCE, Orlando.

Goda, Y., 1974. New wave pressure formulae for composite breakwater. Proc. of 14th Int. Conf. Coastal Eng., Copenhagen, Denmark. ASCE, New York, pp. 1702–1720.

Hull, P., Müller, G., 2002. An investigation of breaker heights, shapes and pressures. Ocean Eng. 29, 59–79.

Oumeraci, H., 1994. Review and analysis of vertical breakwater failures — lessons learned Special Issue on Vertical Breakwaters Coastal Eng. 22, 3–29.

Oumeraci, H., Kortenhaus, A. Allsop, N.W.H., De Groot, M.B., Crouch, R.S., Vrijling, J.K., Voortman, H.G., 2001. Probabilistic Design Tools for Vertical Breakwaters. Balkema, Rotterdam. 392 pp.

Shiravani, C., Vousdoukas, M., Schimmels, S., Stagonas, D. 2014. A methodology for measuring velocity and thickness of wave-induced up-rushing jets on vertical seawalls and superstructures.Proc.34th Conf. Coastal Engineering.Seoul, Korea (accepted)

Vousdoukas, Wziatek, Almeida (2012): Coastal vulnerability assessment based on video wave run-up observations at a meso-tidal, reflective beach. Ocean Dyn. 62: 123-137.

.

5. Propuesta de una nueva tecnología: Introducción al sensor táctil y resultados preliminares.

Después da la experiencia adquirida por parte del autor con el sensor táctil de presión durante la estancia en las instalaciones de MARINTEK, se decide proseguir el trabajo trasladando el sistema de medida a los laboratorios del LIM-UPC. En este capítulo se describe una primera fase de ensayos donde se evalúa la posible utilización del sensor táctil en canales de pequeña escala. En esta primera fase, que llevará a ensayos más completos, se hace una comparativa indirecta entre este innovador sistema de medida y los sistemas de medida clásicos. Se utiliza una calibración sencilla ero que proporciona resultados aceptables. La descripción de los ensayos, la presentación y el análisis de estos resultados están publicados en el artículo *"Laboratory effects on measurnig impact load on rigid coastal structures".*

Abstract

Laboratory experiments were carried out in small scale wave flume to evaluate the performance of the measuring system on the estimation of impact loads on rigid structures. Three different measuring system were used: two classical (array of pressure transducers on a vertical line and load cells) and one innovative system (Pressure Mapping System). Two different regular wave attacks were repeated 80 times each in order to consider the natural variability of the phenomena in the analysis. Good agreement were found in the comparison of the mean total force measured with the load cells and calculated with the vertical distribution derived by the pressure transducers measurements. A bigger scatter on the data is present on the results obtained from the pressure transducers. Also good agreement in terms of envelope of vertical pressure distribution is found between pressure transducers and the Pressure Mapping System. Some differences are appreciable between the two systems in the impact zone slightly above the SWL. The tactile system (PMS) return higher values in this zone most probably due to the higher spatial resolution.

5.1. Introduction

The correct measurement of impact loads on rigid structures is one of the most intriguing challenges for a maritime physical modeller. Traditionally the measurement of impact loads is indirectly conducted through the use of one or more array(s) of pressure transducers. The vertical pressure distribution is accordingly recorded and the impact load is estimated as the integral of the measured pressures. The use of such arrays is to present the preferred method

for measuring wave induced pressures and it was previously used in break through works that led to the development by Goda of his vastly used formula for the calculation of both pulsating and impulsive pressures and loads (Goda 1985, Takahashi et al., 1994). Nonetheless, in 1996, Allsop (Allsop et al., 1996) used load cells to directly measure the total force induced under by waves on a vertical structure instead of indirectly estimating it by pressure measurements.

Although, since their introduction, both aforementioned measuring methods/systems have been exhaustively used, a comprehensive comparison between them has not been previously performed. However, past experience on the measurement of impact loads on rigid structures with different techniques, indicates that substantial differences (Bullock *et al.*, 2007) on the results can occur.

In this paper three different measuring systems are designed and compared. The first two are based on the "standard" methods for load measurements mentioned above, whilst the third one involves the use of tactile pressure sensors, a newly technique introduced in this field of pressure measuring system (Stagonas et al. 2012). Two benchmark wave cases are chosen in order to compare the performance of all systems under two critical impact loads (impulsive wave). In order to overcome problems related to the stochastic nature of the phenomenon (Marzeddu et al. 2014), the performance of all systems is statistically assessed repeating each of the two wave cases 80 times.

5.2. Methods

5.2.1. The experimental layout

The experiments have been carried out in the CIEMito wave flume of the Laboratori d'Enginyeria Maritima (LIM) of the Universitat Politecnica de Catalunya BarcelonaTech (UPC). The flume is 18m long, 0.38 m wide and 0.56 m high. It is equipped with a piston type wave maker driven by software developed at LIM/UPC that allows generation of regular and random waves characterized by a target spectrum as well as a target wave time series. A scaled model of a vertical breakwater has been built and tested against regular wave attacks. The flume has a flat bottom and an approaching 1/15 sloping beach that ends at the toe of a simplified vertical breakwater. During the tests 0.285m water depth was used. The vertical wall is segmented in 3 parts, with the central part being physically separated and dynamically isolated from the two side parts (Figure 5.1). The central part of the breakwater is also equipped with eight pressure sensors (Figure 5.1) and is mounted on two, rigidly fixed, load cells (Figure 5.1).This, allows for simultaneous pressure and the total force measurements. Initially, the tactile pressure sensor is fixed on the left side part (Figure 5.1) but experiments are also conducted with the tactile

pressure sensor located on the central part and the pressure transducers and the load cells mounted on the left side.
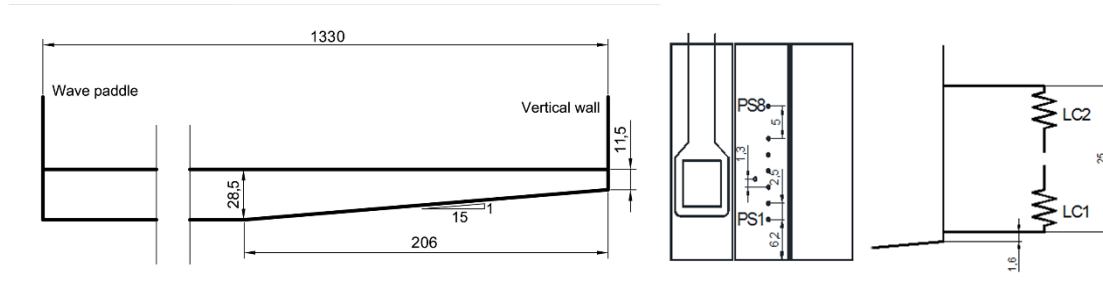
Figure 5.1: Left: Experimental layout - Center: (Front view) Pressure transducers and tactile sensors position – Right: (Lateral view) Load cells position (all dimensions in cm)

5.2.2. Instrumentation

The instrumentation used during the experiments is composed of:

- Eight pressure sensors P8AP by HBM ©

- Two load cells Z6 by HBM ©

- One tactile pressure sensors, model number 9550 by Tekscan ©

- Eight wave gages

The P8AP is an absolute pressure transducer based on a strain gauge sensor with a measuring span of 10 bars and an accuracy class 0.3. The fundamental resonance frequency is 12 KHz.

The Z6 by HBM is a bending beam load cell with a nominal load of 50 Kg and an accuracy of 0.009 % of the maximum capacity.

The 9550 operates in a similar manner to a variable resistor of an electrical circuit. When no load is applied the resistor experiences a very high resistance, which gradually reduces as the applied load increases. The 9550 is a sensor that includes 196 sensing points over an area of 7.11×7.11cm.

After a series of previous tests, in order to asses the impact point of the wave on the vertical wall, the tactile sensor was mounted slightly above the SWL and 7.5 mm under the pressure transducer PS3 (Figure 5.2).
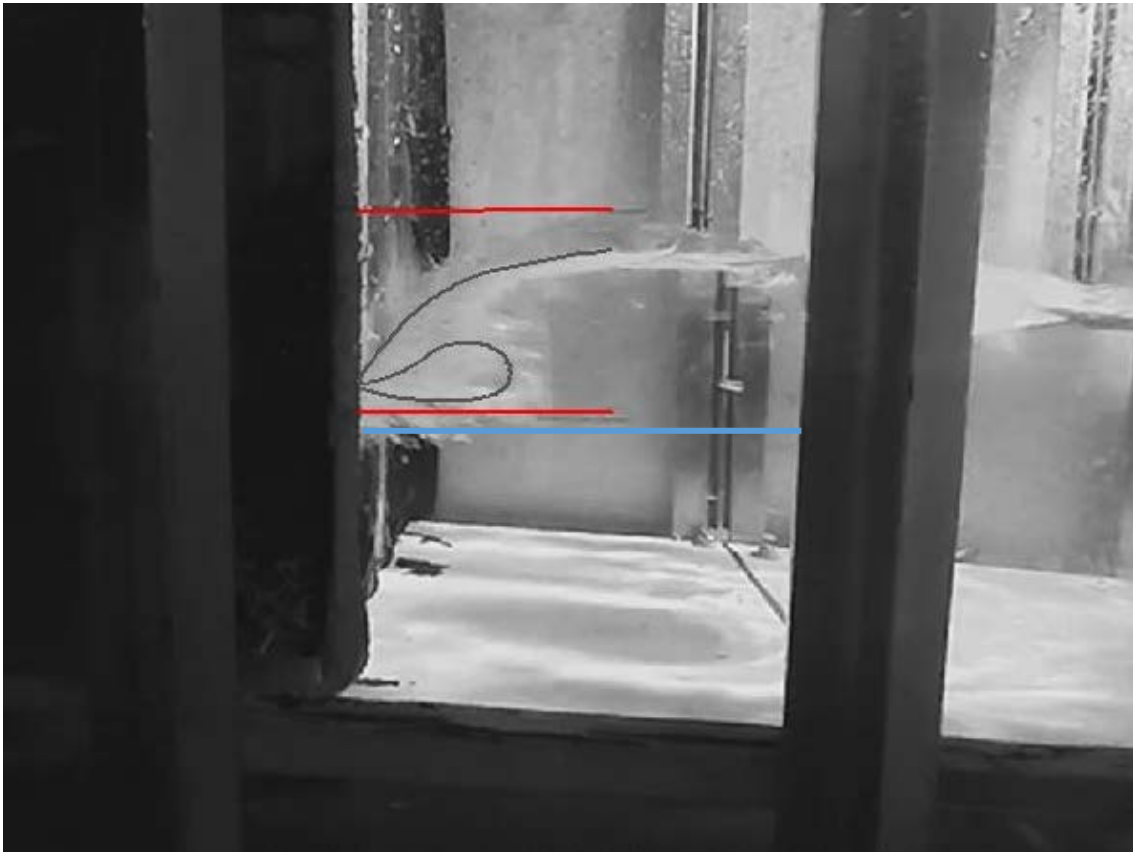
Figure 5.2: Wave impact example. Position of the tactile transducer (red line) and the SWL (blue line).

All the experiments were performed with a sample frequency of 4.8 KHz for the load cells and pressure transducers, at 4 KHz for the tactile pressure sensor and at 40 Hz for the wave gauges.

5.2.3. Description of the experiments

Before running the experiments three different calibrations were done in order to understand the behavior of the tactile transducer under different conditions. A first static calibration was performed loading the sensor with a column of water, a second quasi static calibration with a dynamometric hammer and a third fully dynamic calibration with a drop test. The three calibration methods give extremely different results. The last method seems to be the one much closer to the reality of a wave impact (mixture of air and water impacting on a reduced area) and for this reason this one has been used for the comparison of the tactile pad results with the pressure transducers.

Both the load cells and the pressure transducers were previously calibrated by HBM.

Two different regular waves time series were tested. Each time series is composed by 4 waves divided in 2 ramp-up waves 2 regular waves and 1 ramp-down waves.

The selected target wave conditions are:

- Impulsive wave n1:   H=0.16 m T=2.4 s
- Impulsive wave n2:   H=0.16 m T=2.3 s

80 repetition of the two wave attacks were performed in order to guarantee a good statistic of the phenomena.

5.3. Results

In order to compare correctly the results of the pressure/force measurements, it is important to assess the good repeatability of the wave attacks. To do that all the time series for all the sensors were synchronized using cross correlation. The mean time series of 80 wave attacks was calculated for each wave gauge and the root mean square error was computed. The repeatability is almost perfect with an RMSE of 1mm that is comparable with the measurement error of a resistive wave gauge. An example with 20 time series compared is shown in Figure 5.3.
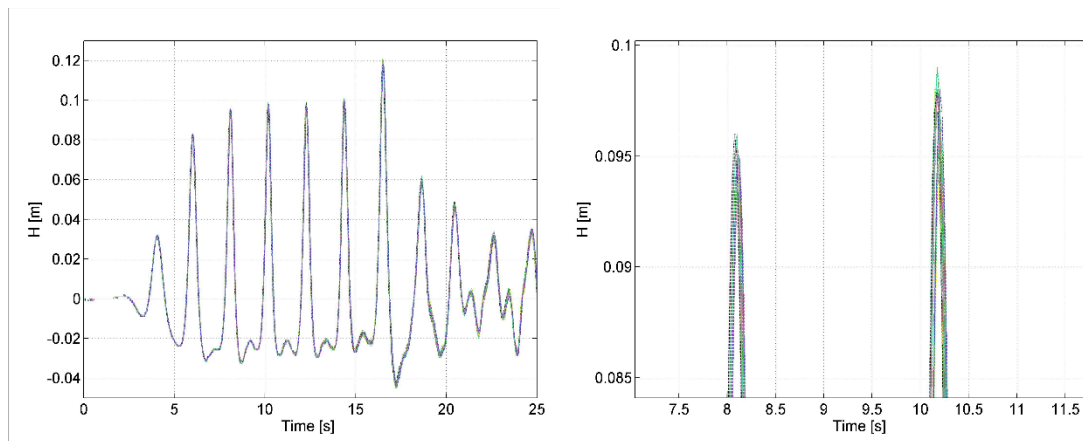
Figure 5.3: Example of the repeatability of the generated waves.

Once the repeatability is assessed, it is possible to compare different results from different sensors. A comparison between pressure transducers and tactile pressure sensor and another comparison between vertical pressure distribution and total force measured with load cells will be performed.

5.3.1. Total force

As evaluated in (Marzeddu et al. 2014) the measurement of the total force using pressure transducers is affected by the interpolation method used in between measures and the extrapolation method used to compute the pressures where the measure was not made directly. From previous experience it was seen that is more safe, to not extrapolate pressure measurements under the lower transducer and over the upper one. This happens because the quasi-static pressures recorded far from the impact zone (lower and upper transducers) are more affected by the electrical noise on the signal when the sample frequency is high. Two

interpolation methods will are used in order to compute the total force, the first one using linear interpolation between pressure transducers measurements and the second one using rectangular distribution around the measured pressure (Figure 5.4).
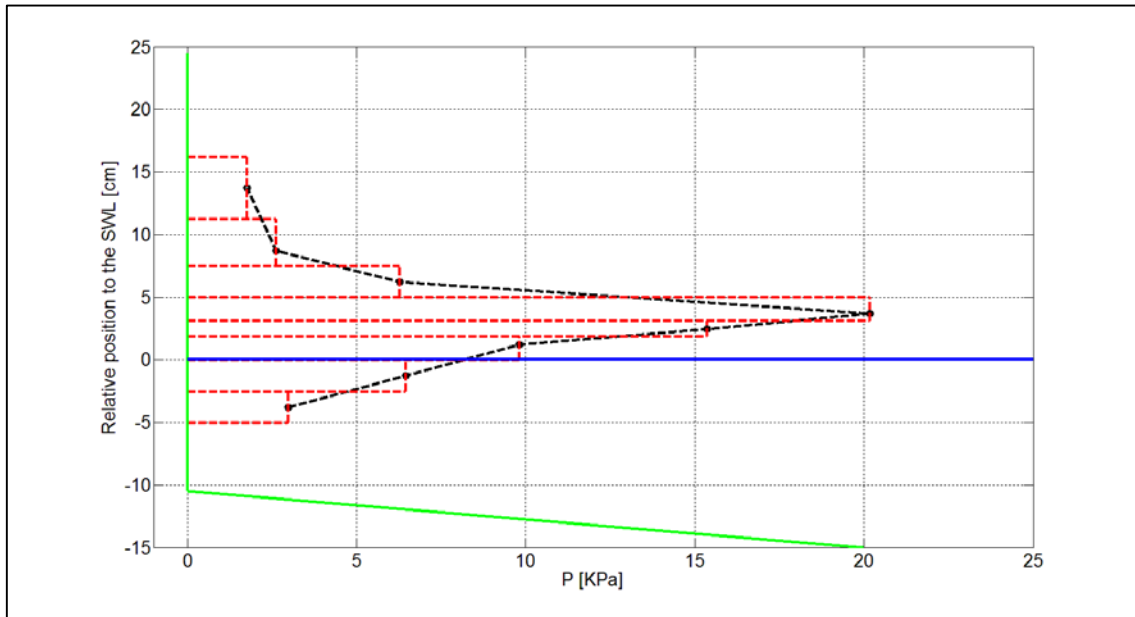
Figure 5.4: vertical pressure distribution computation - red: rectangular interpolation - black: linear interpolation

A brief analysis of the results shows a big variability of the single test but a good agreement on the mean value. Results are summarized in Table 5.1

	mean [N/m]	std_dev [N/m]	Min [N/m]	Max [N/m]
PT	781	168	491	1234
LC	787	55	647	929

Table 5.1: Total force comparison between the results from Pressure Transducers and Load Cells

When the mean value of the measured total forces (load cell measurements) is compared against the mean for the calculated forces (the integral of the pressures recorded by the transducers) a relatively good agreement is observed, Table 5.1. However, a wave by wave analysis reveals that discrepancies of up to 25% are possible with the pressure transducers giving larger estimates for the peak total force.

5.3.2. Pressures

Impact induced pressure values acquired by the pressure transducers are also compared against those recorded by the tactile pressure sensor. The comparison reported here refers to 80 wave impacts recorded with the tactile pressure sensor placed in the middle of the model seawall (Figure 5.1). The tactile sensor was accordingly replaced with an array of 8 pressure transducers and another 80 impacts were recorded. On the right hand side of Figure 5.5, the 15680 (196

sensels × 80 impacts) peak pressure records are plotted (red circles) as a function of the relative location (physical location minus the water depth) of each sensel (pressure sensing unit for the tactile system). The dashed black line corresponds to the highest peak pressures recorded by the pressure transducers for all 80 impacts, in total 640 measurements (8 transducers × 80 impacts); black dots indicate the relative location of the transducers. On the left hand side of Figure 5.5, only the highest peak pressures reported by the sensels located at and near the physical location of the pressure transducer array are plotted. In total, the pressure profiles for 3 sensel arrays are presented (colored lines) along with that for the array of pressure transducer (dashed black line).
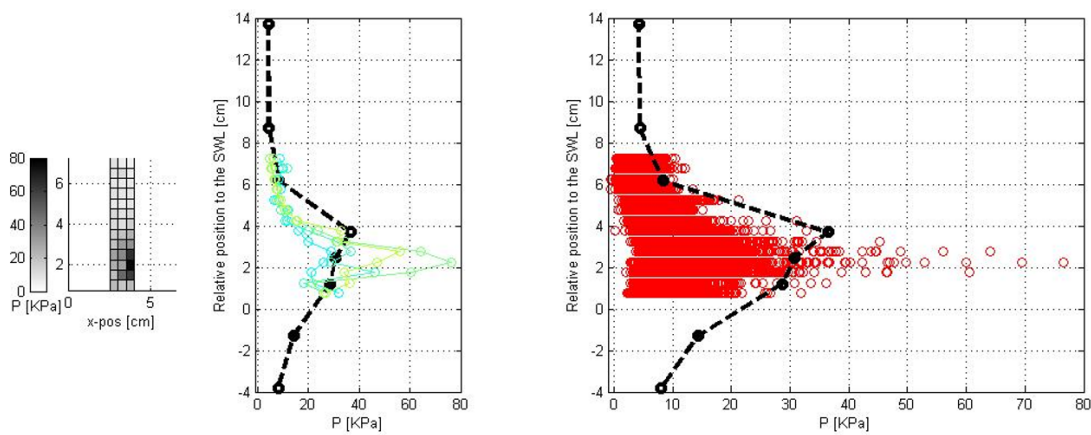
Figure 5.5: Comparison of the vertical pressure distribution (envelope) between pressure transducers (Black line) and tactile system (Color lines). Left: Comparison considering only the columns over the pressure transducers – Right (all measured peaks by the tactile system (red) against vertical pressure distribution envelope from the pressure transducers (black))

Overall, and given the stochastic nature of the phenomenon, the comparison between the two instruments is satisfactory. The general shape of the pressure profile remains fairly similar for both instruments but for the impact zone near SWL, the tactile pressure sensor returns pressures up to two times higher than the maximum peak pressure recorded by the transducers. Although the number (about 20) of these pressures is very small compared to the overall number of tactile pressure measurements (6720 for the area near SWL), a satisfactory explanation for their existence cannot yet been given. However, it should be noted that the majority of these extreme pressures occurred at areas located in-between the (physical) horizontal location of the pressures transducers but the most extreme values were recorded by arrays of sensels located at or adjacent to the physical location of the pressure transducer array, Figure 5.5.

5.4. Summary

Although this work is not yet complete, our preliminary data suggest that:

- Load cell measurements present less variability, while they do not require any post-calculation assumptions.

- Pressure transducer/load cell force calculations/measurements compare well with each other only when the mean total force of a number of tests is considered. On a wave-by-wave basis, the pressure transducer measurements resulted in up to 25% higher calculations for the peak of the total force.

- The use of tactile pressure sensors can provide valuable information with regards to the coherence of impact induced pressures; the occurrence of extreme pressures is currently under investigation.

- Ongoing research gives emphasis to the effect of the pressure coherence on the total force calculation. This is expected to shade more light on the discrepancies observed between pressure transducer/load cell indirect/direct measurements.

Acknowledgments

References

Allsop, N. W. H., Vicinanza, D., & McKenna, J. E. (1996). 'Forces on vertical breakwaters and related structures', Strategic Research Report SR 443. Wallingford.

Bullock, G. N., Obhrai, C., Peregrine, D. H., & Bredmose, H. (2007). 'Violent breaking wave impacts. Part 1: Results from large-scale regular wave tests on vertical and sloping walls'. Coastal Engineering, 54(8), 602–617. doi:10.1016/j.coastaleng.2006.12.002

Goda, Y. (1985). 'Random seas and design of maritime structures'. University of Tokio Press.

Stagonas, D., Muller, G., Ramachandran, K., Schimmels, S., & Dane, A. (2012). 'Distribution of impact induced pressures at the face of uniformly sloped sea dikes: preliminary 2d experimental results'. In Proceedings of the 33rd International Conference on Coastal Engineering (pp. 1–7).

Takahashi, S., Tanimoto, K., & and Shimosako, K. (1994). 'A Proposal of Impulsive Pressure Coefficient for Design of Composite Breakwaters'. Proceedings of the International

Conference on Hydro-Technical Engineering for Port and Harbor Construction, Port and Harbour Research Institute, Yokosuka, Japan, 489–504.

Marzeddu, A., Gironella, X., Sánchez-Arcilla, A., Sutherland, J. (2014). 'Laboratory effects on measuring impact loads on rigid coastal structures'. Proceedings of 3rd IAHR Europe Congress, Porto, Portugal.

6. Propuesta de una nueva tecnología: montaje y calibración

Después de los ensayos a gran escala y de los preliminares a pequeña escala (donde se llegaron a estropear cuatro sensores táctiles por el contacto involuntario con el agua), se ve claramente la necesidad de un *set-up* y de una calibración *ad-hoc* para esta tipología de sensores. En este capítulo se prueban diferentes calibraciones estáticas, dinámicas y con diferentes materiales que generan el impacto. Se describe también el montaje utilizado para la instalación y la protección del sistema de medida táctil. La descripción de los ensayos, la presentación y el análisis de estos resultados se encuentran en el artículo *"Measuring wave impact induced pressures with a pressure mapping system, Part 1: Experimental set-up and calibration"* *(Submitted)*

Stagonas, D., Marzeddu, A., Gironella, X., Sánchez-Arcilla, A., Muller, G., 2015. Measuring wave impact induced pressures with a pressure mapping system, Part 1: Experimental set-up and calibration. Coast. Eng. (Submitted)

Abstract

This, two-part work, investigates the use of a pressure mapping system for hydraulic model tests involving wave impacts on rigid structures. To present, single point measurements are acquired using pressure transducers but the pressure mapping system tested here has the capacity to provide pressure distribution maps with a very high spatial resolution, e.g. 196 measuring points over an area of 50cm^2, at a relatively high sampling frequency (4kHz), while the flexibility of the sensors utilized by the system is considered as an additional comparative advantage. On the other hand, the system is not water-proof, it has a low digital resolution - 8bit instead of 24bit for pressure transducers – and requires an experiment specific calibration. In this first part we describe and propose an experimental set-up and a calibration methodology suitable for measuring wave impact induced pressures and loads. The proposed calibration rig employs impinging water jets and combines measurements from the pressure mapping system with simultaneous load cell measurements. For impact induced pressures ranging from about 3 to 70kPa the minimum, mean±std and maximum RMSE is 0.15, 1.08±0.57 and 5.4kPa, respectively. The pressure integral is also compared to simultaneous load cell measurements and for forces ranging from about 5 to 50N the minimum, mean±std and maximum RMSE reported is 0.0053, 1.49±1.23 and 6.7N. In the second part, the use of the pressure mapping system in conjunction with the proposed set-up and calibration methodology for mapping and measuring wave impact induced pressures and loads is validated.

6.1. Introduction

Short in duration and high in magnitude pressure pulses are induced by waves impacting on marine structures such as vertical seawalls. Despite increased awareness on the importance of impact pressures for the design of coastal (Oumerachi et al (2001)), offshore structures (Wienke and Oumeraci (2005)), ships (Paik and Shin (2006)) and WEC's (Vicinanza et al. (2014)), the knowledge on the mechanics of breaker-structure interaction is limited and existing design formulae and guidelines are derived from and suggest the consideration of experimental results.

The quality of the information provided by hydraulics model tests involving breaking waves interacting with structures is limited by the uncertainties introduced due to the high spatial variability of impact pressures. Existing knowledge on the latter is largely based on pressure transducer measurements but the number of transducers employed is limited by financial and practical - as for example model size, shape and transducer size reasons. For coastal structures and tests at various scales the number of transducers typically employed ranges between 5 to 15, see for example Grune (1992), Hull and Muller (2002), Bullock et al. (2007).

Although a consensus regarding the profiles of impact pressures has been reached, details on the vertical and horizontal coherence of pressures are not yet known and thus force and moment calculations are based on simplifying assumptions. Uncertainties increase further for structures with arbitrary geometries, like for example wave recurves, ships or wave energy converters and although approaches using Computational Fluid Dynamic methods have been recently proposed further knowledge on the local distribution of impact pressures is still required.

The present work explores the aspects of using a pressure mapping system in hydraulic model tests involving waves breaking on a vertical structure. The main advantage of such a system is its capacity to produce very high spatial resolution pressure maps at a relatively high sampling frequency, for example 196 measurements over an area of 50cm^2 at a rate of 4kHz. The flexibility and adaptability of the sensor to the shape of the structure is an additional advantage, see for example Stagonas et al (2014b). On the other hand, the system is not water-proof and has a low digital resolution of 8bit. In the same time, and to the best of the authors knowledge this is the first time that such a system is proposed to map wave impact induced pressures and thus a comprehensive validation is not yet available.

The first part of this work discusses the details of the pressure mapping system and proposes an experimental set-up and a calibration methodology suitable for hydraulic model tests involving waves impacting on structures. Experimental results with more than 1000 wave impacts are

presented in the second part (Marzeddu et al. (2015)) where peak pressure distribution maps and force measurements are compared with pressure transducer and load cell data.

In the remainder, the pressure mapping system used in this work is described first and a review of the existing literature follows in sections 6.2 and 6.3. The proposed experimental set-up and calibration rig and methodology are presented in section 6.4. Section 6.5 presents and discusses results associated to the operation and performance and the calibration accuracy of the system. The paper concludes with a summary of suggestions on the application and calibration of the pressure mapping system for physical model tests considering wave impacts.

6.2. The pressure mapping system

A small number of manufacturers for pressure mapping systems exist but the system investigated in this work was purchased by *TekScan*^{TM}. *TekScan*^{TM} offers a variety of pressure mapping systems but the only one capable of achieving high sampling frequencies is the *TekScan I-Scan*^{TM} used here. The *TekScan I-Scan*^{TM} pressure mapping system consists of three main parts, *. The data acquisition hardware, *. The tactile sensor(s) and *. The data acquisition, display and analysis software.

6.2.1. Data acquisition hardware

The data acquisition hardware is essentially the interface between the tactile sensor and the data acquisition software. The sensor is attached to the *VersaTek*^{TM} *Handle*, which scans the sensing elements of the tactile sensor and reads their individual resistance. The *Handle* has a digital resolution of 8bit and controls the scanning sequence, the sampling frequency and, for some systems, the sensitivity of the sensor. An 8-port hub is used to convert the analogue signal to digital transfer it to a PC via a USB port. The *I-Scan*^{TM} system allows for the simultaneous use of up to 8 handles / sensors but only one is used in this work.

6.2.2. The tactile sensor

The standard tactile sensor manufactured by *TekScan*^{TM} is flexible, for example see Figure 6.1c, has a thickness of 0.1mm and is formed of two polyester sheets. A number of electrically conductive electrodes can be found on the inner sensor side of each sheet and for the sensor types employed here they are arranged as columns (front sheet) and rows (back sheet), Figure 6.1.
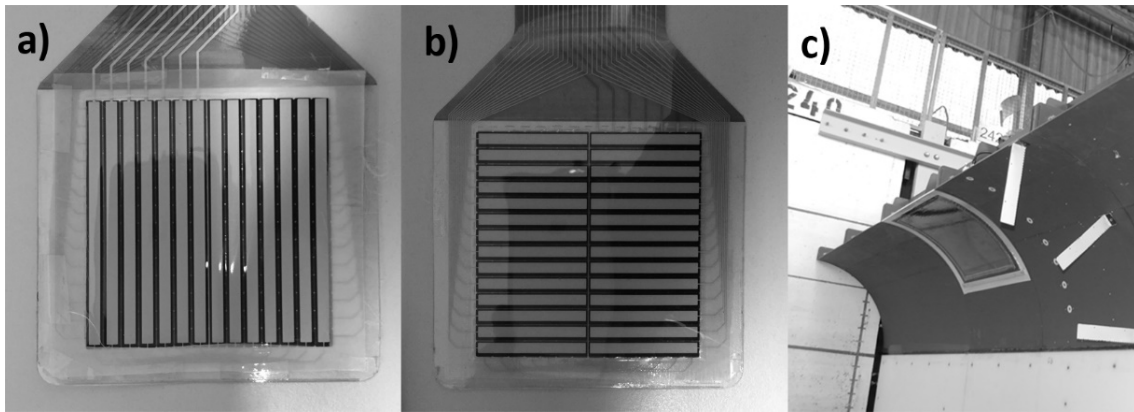
Figure 6.1: (a) Front (b) back of the 9500 tactile sensor. (c) 4550 tactile sensor fixed on the underside of recurved crown seawall large scale physical model, Stagonas et al. (2014a)

The two polyester sheets are thermos-glued together, Figure 6.2, and the cross section of the rows and columns creates a matrix-based tactile sensor; as an example, the sensor with model number 9500 used in this work is formed of a 14×14 matrix, Figure 6.1a and 6.1b. The width of each row and the distance between the columns and rows varies from sensor to sensor and for the model sensor 9500 is 3.3mm and 5.1mm, respectively.

When two electrodes intersect they form a sensing element or a sensel as it is referred to by *TekScan^{TM}*. Each sensel consists of an active area where the applied load is measured and a 'dead' area surrounding the active area, where the no electrode intersection exists. The resistance of every sensel is an inverse function of the applied load and when no load is applied the resistance measured is maximum. Regardless of the extent of the active area loaded, pressure is calculated as force over area, where however the summary of the 'live' and 'dead' part of sensel is considered, Figure 6.2.

The system reads every sensel individually and reports its output as a digital value ranging in linear steps from 0 to 255 (8bit). Once the maximum digital output is reached the sensing element is considered by the system as saturated and any further increase in the wave load will not register. According to the manufacturer, sensors with a nominal range of 0-15 kN/m^2 all the way up to 0-175MN/m^2 are available but information for the maximum non-damaging for the sensor/sensel load is not available.

All sensels have the same response time of 20μs and the system scans sensel arrays (rows or columns) in a timely manner, starting with, e.g., the columns located nearest to the control circuit (handle); the scanning sequence varies between sensors as it depends on the arrangement of electronics. This, in combination with the existence of a residual voltage between subsequent time steps introduce a time lag in the measurements, the maximum value of which is 1/sampling frequency and occurs for the sensels located nearest and furthest to the

control circuit (Tekscan 2008). The sampling rate is a function of the number of sensels and it decreases as the number of sensels increases.
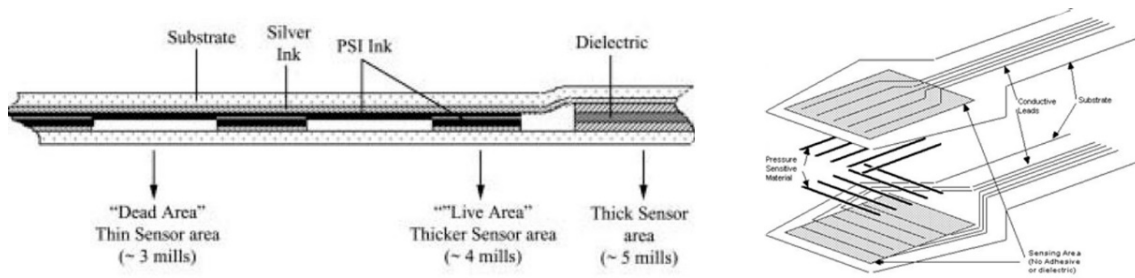
Figure 6.2: Sketch of the tactile sensor cross section (left), exploded (right) - (Tekscan 2003)

The system investigated can sample 44 sensels at 20 kHz each or 196 sensels at 4kHz.

Figure 6.2 presents a conceptual drawing of the cross section of a tactile sensor, which consists of four layers; the two polyester sheets and the rows and columns (indicated as PSI Ink). The active area of each sensel is thicker than its 'dead' area due to the coexistence of all four layers. This entails that the accuracy of the measurement depends on the uniformity of the load applied and thus on the nature of the medium transferring the load on the sensor. In other words, the output recorded by the system will be different if the same load is transferred by a solid material (e.g. steel plate), a partially compliant material (e.g. rubber), or a fully compliant material (e.g. water).

Sensor size, resolution and shape can vary greatly, while the production of bespoke sensors is also possible. Nonetheless, upon manufacturing of every sensor a small amount of air is trapped in the area enclosed by the two substrates. When a load is applied on the sensor the air escapes from areas of high load to unloaded areas or areas with lower load. Under certain conditions, e.g. when a rapid, high magnitude load is applied over a large part of the sensor, violently displaced air can destroy the sensor by causing the two substrates to come apart. Accordingly, larger in size sensors are equipped with ventilation channels, which are essentially a series of gaps between the two polyester sheets and allow for the air to escape without damaging the sensor.

For smaller in size sensors, the amount of entrapped air is considered to be small and the integrity of the sensor is not endangered and ventilation channels are not required. Indeed, compression tests conducted for this work (not presented here) using an Instron hydraulic testing system showed that when the model sensor 9500 is overloaded the air escapes from the measuring to the non-measuring part of the sensor forming a pocket of air between the two polyester sheets; it is noted that for all tests a gradually varying and not a rapidly applied load was used. Nevertheless, when a load is uniformly applied over the full measuring area of the sensor a cushioning effect is caused as the air is spread between the polyester sheets and

prevents the intersection of the electrodes, Figure 6.2, affecting the performance of the sensor, section 6.4.2.

Finally, according to the manufacturer the sensels within a sensor are not identical and as such if the same load is applied a differences on the digital outputs for each sensel can be observed. For this reason, a procedure termed equilibration is suggested by TekScan® (Tekscan 2008). During equilibration, a load is uniformly applied on part of the sensor and a scale factor is attribute to each sensel so as its digital output will be equal to the average digital output of all loaded sensels. The equilibration factor is unique for each sensel and cannot be transferred from one sensel to the other. Accordingly a complete sensor equilibration will require all sensels to be loaded and this can constitute a challenging task when the sensor is not equipped with ventilation channels.

6.2.3. The data acquisition software

The Tekscan software provided with the *I-Scan^{TM}* pressure mapping system is used to control, the settings of the system (e.g. sampling frequency), data acquisition (start/stop), and to display, process and store the data acquired. The software also incorporates the unique, for each sensor, set of drivers and has specific build in options for sensor calibration and equilibration. For the former, two options are offered a single point linear and a two point power calibration. For the linear calibration the application of a single known load is required and the calibration coefficient is calculated considering 0 as a second point on a load over sensor digital output graph. For the power calibration the application of two known loads is required and a curve of the form $y=\alpha x^b$ is fitted on the data.

In contradiction, up to 10 known loads can be used to equilibrate the sensor. The loads used for equilibration should, however, be evenly spread over the loaded area of the sensor. Both calibration and equilibration can be applied either in real time upon data acquisition or during data post processing. We note in passing that for this work the commercial software was used only for data acquisition, whilst sensor calibration and equilibration and data post processing was done externally.

6.3. Literature review

Pressure mapping systems such as the *Tekscan, I-Scan^{TM}* system combine the comparative advantages of high spatial resolution for force/pressure measurements, flexible and thin sensors and real-time time feedback. To present, their range of application includes examples from the automotive, the Geotechnical Engineering and the Biomechanical sectors. Nevertheless, since the early days of their uses aspects related to their accuracy have been reported in the literature, Otto et al. (1999).

Bachus et al. (2006) compared the accuracy of the *Tekscan I-Scan*^{TM} for measuring contact area, force and pressure with that of *Fuji Prescale Film*, see also Hoffmann and Decker (2005). Known loads were generated with a servo hydraulic Instron materials testing machine and were applied on an 8500 model sensor through a cylindrical peg. In agreement with Fregly and Sawyer (2003), Bachus et al. (2006) reported errors in area, force and pressure measurements ranging from -3% to 4%, 1 to 4%, and -1 to 5%, and   concluded that the *Tekscan I-Scan*^{TM} system can be used with confidence and it is more accurate *Fuji Prescale Film*.

Wilson et al. (2003) and Wilson et al. (2006), used the *Tekscan I-Scan*^{TM}system equipped with a *5051* and *6900* model sensors to measure facet loads in the spine. In contradiction to Bachus et al. (2006), the authors did not conduct a custom calibration but they also used the calibration protocols available in the *Tekscan Software*. The linear calibration was shown to be more accurate than the power calibration function and the errors reported for compressive loads of 100, 50 and 25N were 18±9% (mean ± standard deviation), 35±7% and 50±9%. The limited accuracy of the sensor was attributed to the small range of the applied loads compared to the nominal range of the sensor, and to the development during testing of non-uniform stress distribution not accounted for during calibration. Wilson et al. (2006), suggested that extrapolating past the calibration range can reduce the accuracy of the calibration. In agreement with the work of Baer et al. (2004), Wilson et al. (2006) also speculated that better calibration results can be yielded if calibration algorithms are produced and used for each sensel instead of using a universal algorithm for the whole sensor; for the remainder of this work the former will be referred to as a sensel-by-sensel calibration and the latter as a global calibration.

More recently, Brimacombe et al. (2009) studied the effects of the calibration method on the accuracy of the *Tekscan I-Scan*^{TM} system used in biomechanical applications. Instron materials testing machine was used to generate known loads and the two calibration protocols of the *Tekscan* software were compared with custom, user-defined calibration approaches. In contradiction to Wilson et al. (2006), the *Tekscan* software power calibration yielded more accurate results than the linear calibration. Nevertheless, Brimacombe et al. (2009) also employed a ten-point cubic polynomial calibration and a three-point quadratic polynomial calibration. It was concluded that the former yields the best results and that both user-defined calibration protocol results are more accurate than those returned for the *Tekscan* methods; the ten-point cubic polynomial calibration and the three-point quadratic polynomial calibration were about five and two times more accurate.

Similar results are reported by Palmer et al. (2009) who compared different calibration protocols using the *Tekscan I-Scan*[TM] system with the *5315* model sensor. Palmer et al. (2009) applied the system in large scale laboratory, soil-structure interaction tests. The sensor was wrapped around a buried pipe and an actuator based experimental arrangement was used to displace laterally the pipe in the soil. The loads measured by the *I-Scan*[TM] system were compared with independent load measurements. The accuracy levels reported for acting pressures exceeding 15% of the sensor's upper bound pressure were within 10% of the applied pressure, see also Paikowsky and Hajduk (1997). As such, the use of tactile pressure sensors (*Tekscan I-Scan*[TM] system) was characterized as accurate and versatile for measuring normal stresses. It was, however, highlighted that before accurate measurements were to be acquired the shear stresses transmitted on the sensor had to be eliminated or mitigated.

Palmer el al. (2009) also reported a creep in the measurements which begun approximately 120sec after loading. In agreement with previous studies, Paikowsky and Hajduk (1997) and Otto et al. (1999), the creep reduced significantly for acting pressures higher than 15% of the sensor's upper bound pressure. For static loads and similar loading times, *Tekscan* sensors have been reported to experience a time dependent drift which is known to vary from 0 to 3% of the applied load per log time, Tekscan (2008).

Ouckama and Pearsall (2011) used an array of *Tekscan Flexiforce* sensors in order to evaluate the impact performance of ice hockey helmets. In contradiction to previous works, they employed ramp-increasing loads generated using a material testing machine at its maximum speed (750N/s) and calibrated the sensors with non-static loads. *Flexiforce* sensors consist of a single sensing element but use the same technology as the *Tekscan* tactile pressure sensors used for this and for all other studies referred to here. For the calibration, a 3rd order polynomial with the best fit was found and the RMS error reported was smaller than 1.5% of the maximum measuring range. A favorable comparison to individual load cell measurements, RMS error within 5% of the upper measuring range, was also reported for tests involving hemispherical impactors impinging on an array of *Flexiforce* sensors.

For a similar study Ouckama and Pearsall (2012) replaced the calibration rig of Ouckama and Pearsall (2011) with a rig involving the guided linear drop of a head formed mass on the sensors. The new rig was able to generate impact loads with contact times (approx. 12.1ms) similar to those expected during the actual experiments. Once more the 3rd order polynomial fit with the best fit on the calibration data was found and the RMS error reported was 2.8% of the maximum measurement range. Ouckama and Pearsall (2012) used an array of 25 *Flexiforce* sensor in order

to evaluate the performance of sport helmets by capturing the impact induced force distribution. When the interpolated force results from the array of sensors were compared with load cell measurements the captured force was recorded to be 87± 12% of the global force.

More recently, the *Tekscan I-Scan^TM* pressure mapping system was used for underwater and breaking wave related studies. Stagonas et al. (2012) and Stagonas el al. (2014b) applied a tactile sensor (sensor model *5315*) at the surface of a seadike and a wave recurve to map the distribution of wave induced pressures. Both experimental expeditions were conducted in the large scale wave flume (GWK) of the FZK institute in Hanover, Germany and they were supported financially by the European Hydralab IV Integrating activity. There, an appropriate set-up to protect the sensor from direct contact with water was developed; for a more detailed description see also Ramachandran et al. (2013).

In addition, Lu et al. (2013) used the same system to map the distribution of pressures and loads induced during the collision of ice on rigid structures. The authors reported inaccuracies on measuring peak loads and attributed them to inappropriate calibration of the system. It should, however, be emphasized that in agreement with the work of Ouckama and Pearsall (2012) no temperature related effects were recorded. For experiments involving, wave impacts, the sudden change in temperature and the transition from a dry to a wet state is known to introduce errors (thermal peaks) in pressure transducer measurements, Kim et al. (2015)

Overall, the review of the existing literature suggests that the *Tekscan I-Scan^TM* pressure mapping system has the potential to provide reliable pressure and load measurements. Although a consensus has not been reached regarding the most appropriate order (linear or higher order) of the calibration it is commonly acceptable that a multi-level user-defined calibration yields more accurate results than any of the available *Tekscan* calibration protocols. Users should consider the range of anticipated pressures when making decisions about the calibration range and the nominal range of the sensor. The linearity (or not) of the response of *Tekscan* sensors may vary for a given pressure range, see also Tekscan (2008), and higher inaccuracies were reported for the smaller acting loads, Bachus et al. (2006). Calibration algorithms are affected by the shape and nature/compliance of the medium/material used for calibration and the load/pressure application time, e.g. 120sec

It is, however, stressed that all calibration protocols and errors reported in the existing literature refer to the overall sensor and not to individual sensels; the main focus of all studies was on the global/overall measured load/pressure and not on the details of its distribution. For the latter, calibration algorithms and errors may differ, see for example Brown et al. (2004). In the same

time, the user should be aware that readings may be subject to a creep or drift, which however is reported to occur only for relatively long application times.

With regards to the current work, the (model number) 9500 *Tekscan* tactile pressure sensor selected had the smallest pressure range available, 0-35kPa, and was able, in combination with the *Tekscan I-Scan^{TM}* system to provide a maximum sampling rate of 4 kHz. In addition, time dependent effects are not expected as, at a small scale experimental level, the rise and duration time of wave impact induced pressures are known to vary between 1 and 15ms, see for example Hattori et al. (1994). Finally, the pressures/loads developed during the impact of a wave, and especially for the vertical structure used here, will act normal to the sensor. Although the water rushing-up the vertical wall may induce shear stresses, they occur outside the dynamic part of the event and thus do not fall within the focus of this study. For the calibration rig described below, water-jets are employed for the generation of short duration loads acting normal to the sensor and thus a good correlation between the calibration and the experiment is entailed.

6.4. Experimental apparatus and methodology

The review of the existing literature indicates that the accuracy of the calibration for the *Tekscan* sensors depends on the nature of the medium used to transfer the pressure/load on the sensor, the type (dynamic or static) of the acting pressures, and the calibration range with respect to the range of the anticipated pressures.

The rig described and proposed employs impinging water-jets to induce dynamic pressures on the sensels of the tactile pressure sensor. The pressure pulses generated by impinging water jets resemble very closely those expected in experiments with waves breaking on rigid structures, see for example Figure 7.7 and Figure 7.8 in Marzeddu et al. (2015). A sharp increase from 0 to maximum occurs during the first moments of the impact and subsequently the pressure decreases as the pulse transcends from a dynamic to a quasi-static phase.

A photograph of the proposed calibration arrangement is shown in Figure 6.3.
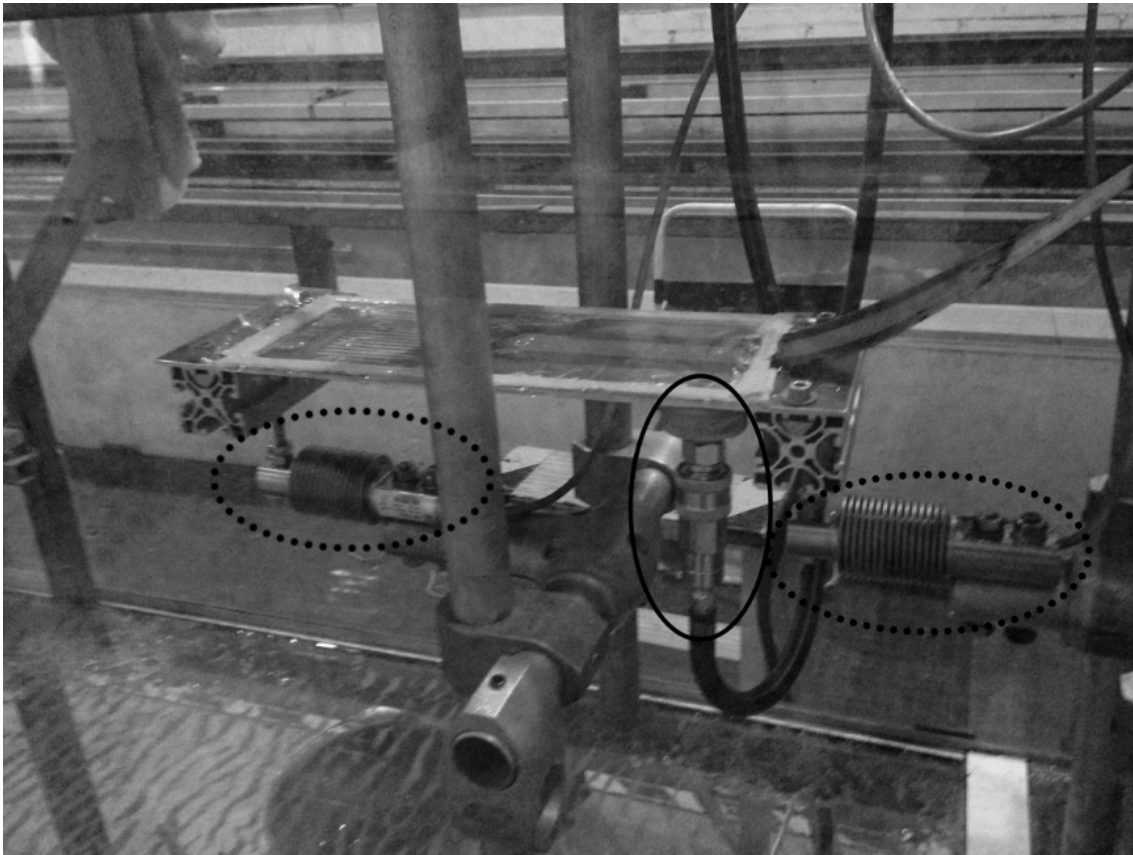
Figure 6.3: Calibration Rig. The vacuum valve (solid circle), the tactile sensor, and the two load cell (dashed circle) are also shown

Free falling water-jets are generated when the water contained in a PVC tube is released. The *Tekscan* sensor is firmly fixed below the tube, on a 3mm thick aluminum plate. The shape and magnitude of the pressure pulses induced by the free falling water-jets is a function of the distance of the tube from the sensor and the amount of water contained in the tube, while the location and size of the impact area is a function of the location and the diameter of the tube. Therefore, some control over both the former and the latter is possible. The extend of this control, however, is restricted by 1. the stochastic nature of the event which entails a range of pressures for the impacts repeated with the same parameters and, 2. for the rig used here, the manual positioning and water-release system.

As the sensor is not water-proof adequate protection from water is provided by placing the sensor in a vacuum bag (Minimatic bag 0.05 mm) and a secondary protection layer is created using a transparent, compliant foil (vacuum film NBF-740-LFT 0.05 mm). In the experimental arrangement described in Stagonas et al. (2012), Stagonas et al. (2014a, b), and Ramachandran et al. (2013) protection from water was provided using a watertight, high endurance Kapton foil carefully fixed on the structures. Since, however, such a high performance foil was not available during the current study a vacuum bag is used in addition to the foil in order to re-assure protection from water.

The vacuum is generated using a pump connected to the back side (not shown in Figure 6.3) of the aluminum plate. Ramachandran et al. (2013) has shown that the response of the sensor changes when a vacuum is employed but remains the same for different levels of vacuum. For the calibration tests presented in this work and for all experiments in Marzeddu et al. (2015) a constant vacuum level of 40 kPa was used. This was found to be the minimum level of vacuum for which air removed from:

- between the sensor and the mounting plate
- between the sensor, the bag and the external foil
- inside the sensor; for this work the 9500 model (provided without ventilation channels) was perforated in-house

Nevertheless, the use of a vacuum pump introduces a high frequency noise with a distinct frequency of 25Hz and a low pass filter is used to remove it from the acquired time history.

A pair of HBM Z6FC3 bending beam load cells arranged in series are used to measure the water-jet impact induced load. In contradiction to pressure transducers, load cells allow for the simultaneous measurement of loads with the *Tekscan I-Scan^{TM}* pressure mapping system. Since the impact area is measured by the *Teskan* sensor, loads can be converted to pressures and be used for pressure calibration. A series of ad-hoc tests using a mallet and a variety of water-jet impacts has shown that the excitation frequency of the load cells-aluminum plate system is significantly higher than the frequencies measured during the calibration tests and the wave experiments of Marzeddu et al. (2015).

For the calibration tests presented and for calibrating the results in Marzeddu et al. (2015), water-jets were generated using two tubes with diameters of 18.6 and 31.7 mm. The tubes were positioned at fixed vertical distance of 0.8m from the sensor, and for each diameter 150 water-jet impacts were generated.

6.4.1. The calibration methodology

The following steps are proposed for the calibration of the pressure mapping system using the rig described above:

- The sensor is subject to water-jet impacts (300 for this occasion) and loads are simultaneously measured by the sensor and the load cells.
- For each impact, the mean pressure acting on the sensor is calculated by dividing the force recorded by the load cells with the area measured by the tactile pressure sensor, eq. 1 and eq. 2.

- The digital output of a sensel is considered equal to the calculated pressure multiplied by a weighting factor, eq. 4. Here, the assumption is made that at the time instant of the measured (by the load cells) peak force the contribution of the pressures recorded by each sensel to the overall load acting on the sensor is equal to the ratio of the digital output of the sensel over the mean digital output of the sensor, eq. 3.
- Calibration curves fitting best on the digital output-weighted pressure data are defined for every sensel. The global (overall) calibration of the sensor is also possible by equilibrating the sensor and combining the datasets for all sensels, Figure 6.4.
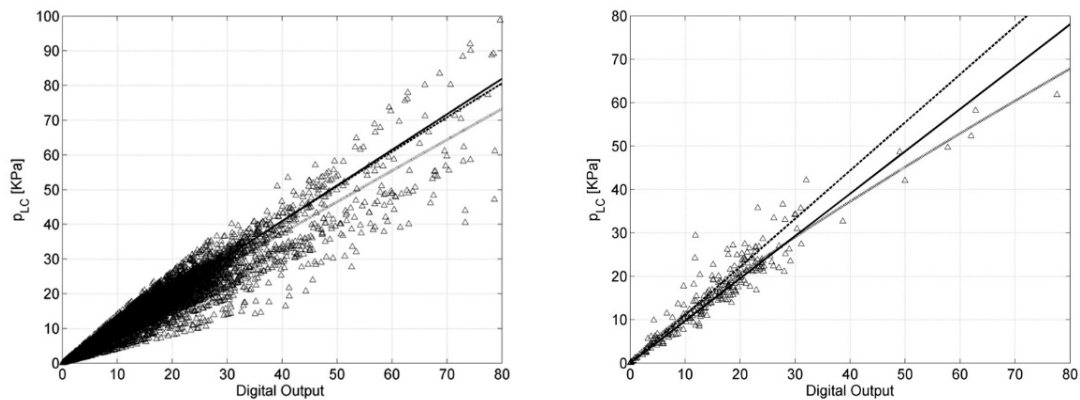
Figure 6.4: On the left, weighted peak pressure plotted over the digital output of all sensels; data set used for a global calibration. On the right, weighted peak pressure over the digital output of a single sensel; data used for the calibration of the specific sensel in a sensel-by-sensel calibration. For both subplots, black solid line: linear, black dotted line: 2nd order polynomial, and grey dashed line: power law.

Figure 6.5 shows the digital output of all active sensels at the time instant of the measured peak force.
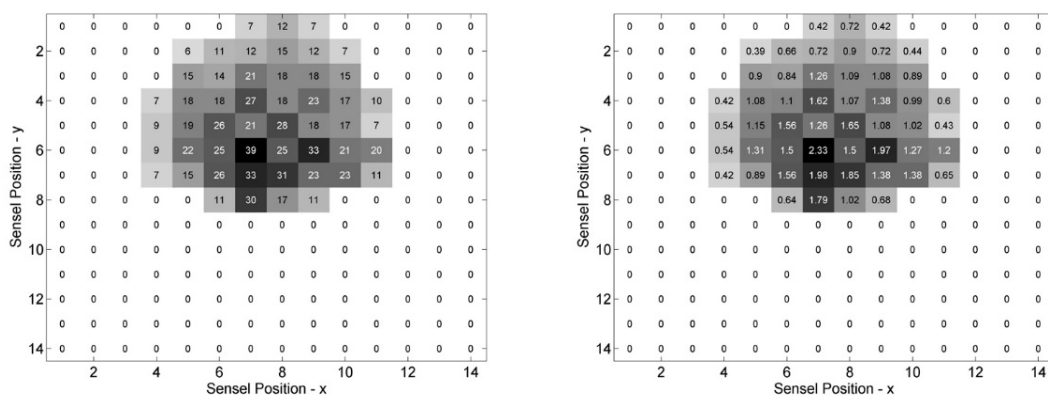
Figure 6.5: Digital output (Left) and weighting factor (Right) for the sensels activated by an impinging water-jet at the time instant of the peak load; x and y are defined in a unitless 14x14 matrix.

The highlighted area A is calculated as:

$$A = N * A_{sensel}$$

Eq. 1

where,

- N: is the number of active sensels
- A_{sensel}: is the sensel area, equal to 26 mm²

and is used to calculate the mean pressure from the load cell measurement, as:

$$P_{LC} = \frac{F_{PLC}}{A}$$

Eq. 2

where,

- F_{PLC}: is the peak force measured by the load cell
- P_{LC}: is the mean pressure acting on the tactile sensor at the time F_{PLC} occurs

The pressure in Eq. 2 is referred to as P_{LC} since it is calculated considering an area (A_{sensel}) larger than the actual area over which the pressures are measured. The contribution of each sensel is estimated as:

$$C_{i,j} = 1 - \frac{\overline{DO} - DO_{i,j}}{\overline{DO}}$$

Eq. 3

where,

- $C_{i,j}$: is the contribution factor for a sensel with horizontan (x) and vertical (y) coordinates i, j, respectively. With i = 1…14 and j = 1…14.
- $DO_{i,j}$: is the digital output of a sensel with horizontal (x) and vertical (y) coordinates i, j.
- $\overline{DO}$: is the mean of the digital output of all sensels active at the time instant the peak force was recorded by the load cells.

The combination of Eq. 1 to 3 gives the weighted pressure, $P_{i,j}$, acting on the (*i,j*) sensel:

$$P_{i,j} = C_{i,j} * P_{LC}$$

Eq. 4

For larger in size sensors, where a sensel-by-sensel calibration can become laborious the use of a global calibration can be advantageous but only when applied on equilibrated sensor. Sensors equipped with ventilation channels can be equilibrated using the proposed calibration rig without any further adjustments. A variety of uniform pressures acting on the sensor can be generated by altering the vacuum level. For equilibrating the sensor a measurement of the acting pressure is not needed as the output of every sensel is compared against the mean output of all sensels and weighting factors forcing the output of each sensel to be equal to the mean

digital output are generated. Although this normalization procedure can involve only one acting pressure a multilevel equilibration is recommended, Tekscan (2008). An equilibration example for the 9500 model sensor is shown in Figure 6.6a, where the equilibrated and not-equilibrated output of the sensor are presented.

6.4.2. Entrapped air effects

The air trapped between the two polyester sheets may prevent the contact of the electrodes and thus deteriorate the quality of the pressure mapping system's output. This is investigated through a series of tests with and without air trapped in the sensor. Initially the non-perforated sensor is subject to 300 water-jet impacts. Soon after, the sensor is perforated and the procedure is repeated. The calibration rig described above is used and for all tests the vacuum level is kept constant at 40 kPa

The peaks of the impact induced pressures on the non-perforated (crosses) and the perforated (circles) sensor are plotted as a function of the sensel digital output in Figure 6.6b.

It is observed that the absence of entrapped air (perforated sensor) leads in reduced data scatter and a steeper response for the sensor, which now returns smaller digital values for higher pressures.
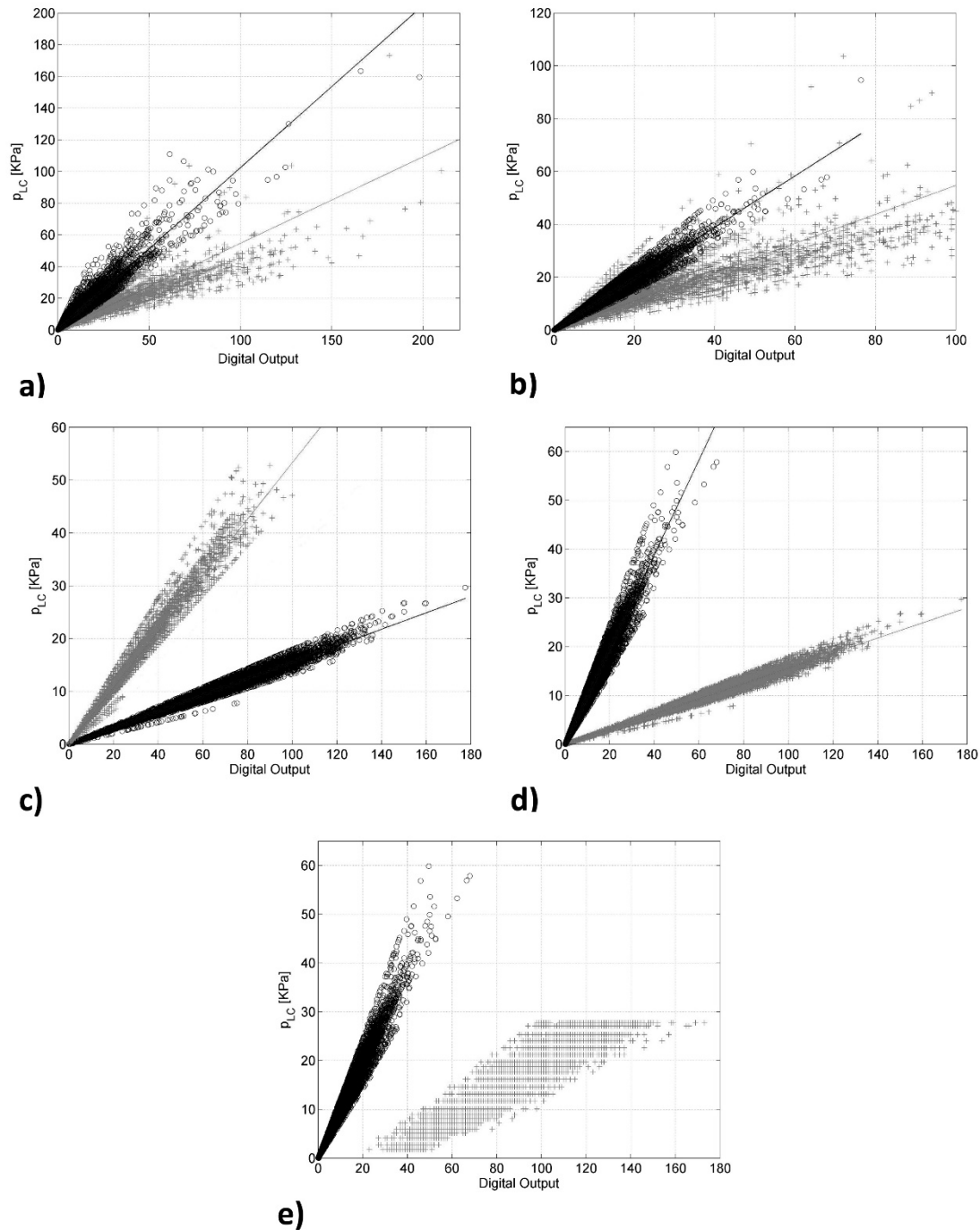
Figure 6.6: a) Water jet calibration – Non equilibrated (grey crosses) and equilibrated (black circles) data and linear fit. – b) Water jet calibration – Non perforated (grey crosses) and Perforated (black circles) data and linear fit (pressures (LC) for non perforated extend up to 120kPa but no such pressures are recorded during the perforated tests). – c) Pendulum calibration - Impacts with (grey crosses) and without (black circles) air trapped in the sensor. – d) Pendulum (grey crosses) and water jets (black circles) calibrations. R2 is the same (0.98) for both test cases. – e) Hydrostatic (grey crosses) and water jets (black circles) calibrations data.

Figure 6.7 presents the area reported by the sensor (crosses: non-perforated, circles: perforated) at the time instant of the peak impact pressure as a function of the P_{LC}; the latter is calculated here from the load measured by the load cells and the area reported by the pressure

mapping system. Although for all tests the area reduces in size as the acting pressure increases and the data scatter reduces when the entrapped air is removed.
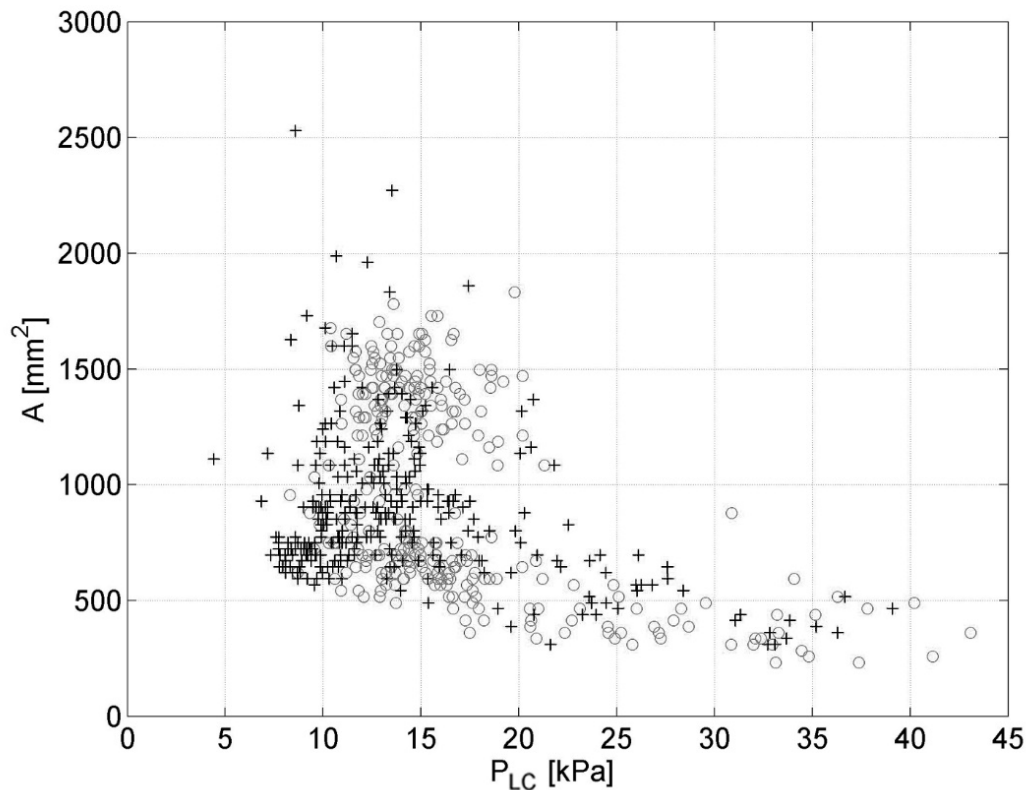
Figure 6.7: Mean acting pressure over impact area (number of activated sensels multiplied by sensel area) for tests with (crosses) and without (circles) entrapped air

A similar set of tests was conducted but with impacts induced by a pendulum equipped with a load cell. A flat, steel plate covered with a 4mm thick sponge layer was mounted on the load cell and the impact force was simultaneously recorded by the pressure mapping system and the load cell, see also in Ramachandran et al (2013) where a similar set-up was used. Compared to the water-jet induced, the pendulum induced impacts cover a larger area of the tactile sensor and thus entrapped air related effects are more pronounced and more clearly illustrated.

For the non-perforated sensor the effect of the entrapped air is manifested as pressure distribution map with a rather poor resolution, left hand side of Figure 6.8. In contradiction and in the absence of air the contact of the electrodes is undisturbed and the details of the impact are reported, right hand side of Figure 6.8.

The impact area recorded for all tests and for the same time instant is plotted over the P_{LC} in Figure 6.9. In a similar manner to the water-jet tests, the trend remains similar but the vertical scatter on the data reduces when the air is removed, while the size of the impact area measured by the pressure mapping system is for the majority of the tests larger than 20% of the pendulum area (2200mm^2). The performance of the system on capturing the impact area is deemed

satisfactory, especially if the presence of the deformable layer on the plate is considered. The digital output of all sensels as a function of the P_{LC} calculated by the load cell measurements is illustrated in Figure 6.6c. For the pendulum impacts, the scatter on the data is reduced for the perforated sensor, which however has now a less steep response.

Overall, the results presented indicate that when the entrapped air is removed the impact induced pressure distribution is reported in more detail and the scatter in the response of the sensels reduces. Accordingly the use of a tactile sensor with ventilation channels is recommended.
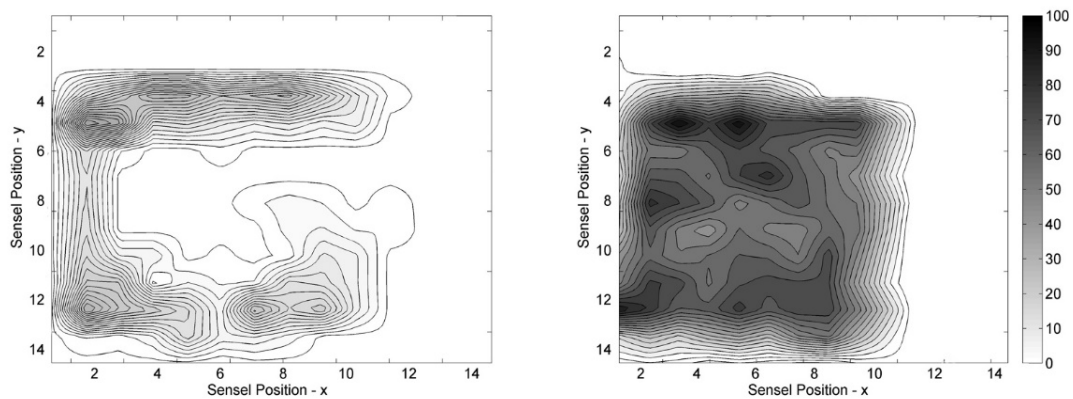
Figure 6.8: Contour plots of the pressure distribution for pendulum tests with (left) and without (right) entrapped air. The distributions presented correspond to the time instant of the peak force acting on the sensor.
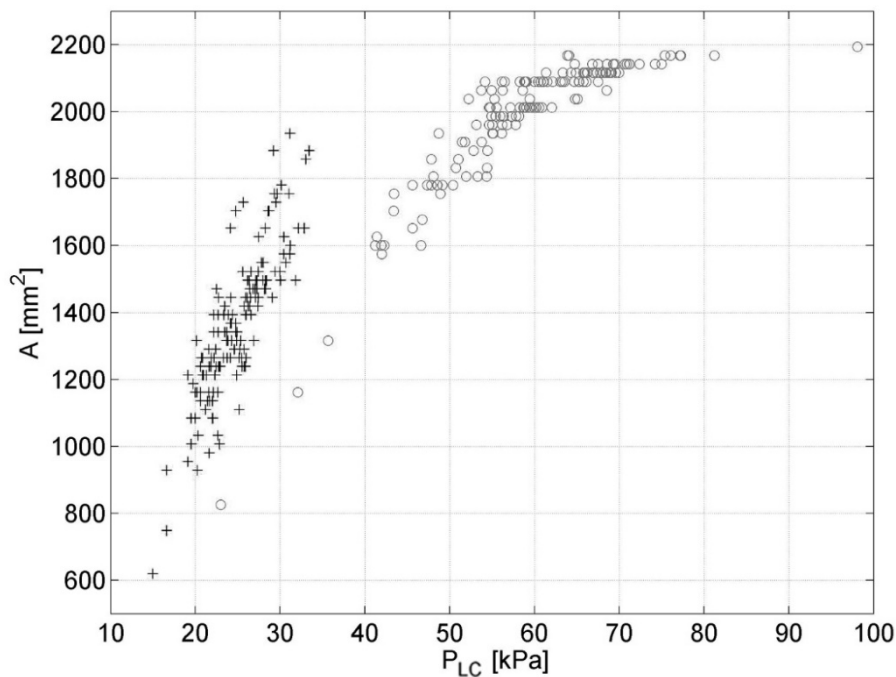
Figure 6.9:Impact area (number of activated sensels x sensel area) recorded by the pressure mapping system for the non-perforated (crosses) and the perforated (circles) sensor plotted over the mean pressure; the latter is calculated as the peak force recorded by the load cell over the impact area reported by the pressure mapping system.

6.4.3. Effects related to the medium generating/transferring the pressure/load

The response of the perforated sensor for impact tests conducted with the pendulum and with water-jets is compared in this section. Both test cases involve dynamic impacts but for the former the load is generated by the impingement of the pendulum and momentum is transferred on the sensor through a deformable sponge layer. For the latter the load is directly generated by the interaction of the sensor with the free falling water-jet. The peak digital output of all sensels for the tests with the pendulum (crosses) and water-jets (circles) is plotted in Figure 6.6d over the peak of the pressure acting on the sensel. The significant difference in the response of the sensor shows beyond any doubt that a water based calibration should be preferred over a pendulum based calibration. Interestingly enough, even when the acting pressure exceeds the nominal range of the sensor (35kPa) saturation is not observed. It is reminded that when the saturation level is reached or exceeded the sensels return a digital output of 255. Hence, the nominal measuring range for a perforated and vacuumed sensel significantly exceeds the range defined by the manufacturer, 0-35kPa for the non-perforated 9500 sensor. Similar results have also been reported in Ramahandran et al. (2013). Nonetheless, establishing the exact pressure range for the perforated sensor falls outside the scope of the present work.

6.4.4. Dynamic and static loads

For pressure transducer a static calibration is used even when tests involving dynamic events are considered but for tactile pressure sensors this does not seem to be a plausible approach, section 6.3. In this section we compare the response of the *Tekscan I-Scan^{TM}* pressure mapping system for dynamic and static loads. The previously described tests with water-jets are used for the former, while for the latter the calibration rig is altered and a 3m high, 15 cm in diameter PVC pipe is placed on top of the perforated sensor and the vacuum pressure was kept constant. The applied hydrostatic pressure was calculated from the known water depth and for a total of 14 water depths ranging from 0.2 to 2.6 m. Examples of the measured time histories for static and impact induced (dynamic) pressures are shown in Figure 6.10
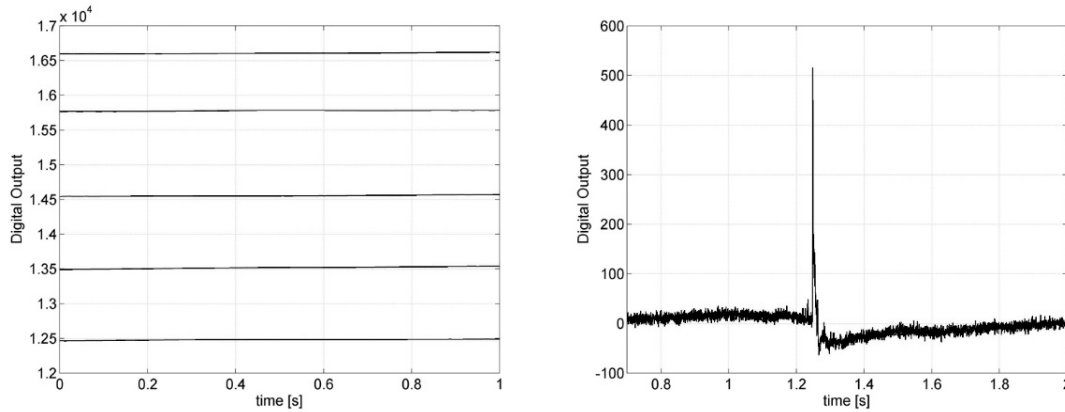
Figure 6.10: Time histories of the digital output of a sensel for various static and an impact-induced pressure, subplot on the left and right hand side, respectively.

The Digital Output (DO) of all sensels for dynamic (circles) and static (crosses) pressures is plotted over the pressure acting on the sensor (P_{LC}) in Figure 6.6e.

Once again, for the water-jet tests the mean pressure on the sensor is calculated as the force measured by the load cells divided with the loaded area of the sensor (eq. 2), while for the static tests the pressure is the hydrostatic pressure. Very significant differences on the response of the sensor are clearly observed and therefore, it is recommended that a static calibration should not be used for experiment involving dynamic conditions, such as wave impacts, and the opposite.

6.4.5. Accuracy of calibration

The review of the existing literature and the results presented so far shows that the selection of the appropriate calibration approach may vary with the nature of the medium generating/transferring the pressure/load, the type (dynamic or static) and range of the pressure/load, and the measuring range of the sensor with respect to the pressures expected at the experiments. In this section results on the accuracy of the proposed calibration methodology are presented.

Initially two calibration approaches, a sensel-by-sensel and a global approach, are compared. A global calibration is acquired by applying a linear regression fit on the equilibrated outputs of all sensels and for all tests. On the contrary, for a sensel-by-sensel calibration a linear fit is separately applied individually on the non-equilibrated outputs of each sensel for all tests, Figure 6.4 and 196 fits are generated, Table 6.1.

Calibration y=ax	a				R2			
Equilibration and global calib	0.97				0.98			
	min	Max	mean	std	min	max	mean	std
No equilibration and calib sbs	0.9	1.29	1.03	0.02	0.81	1	0.94	0.01

Table 6.1: Linear calibration coefficient and R2 values for the global and sensel-by-sensel.

Given the range of the calibration coefficients for the sensel-by-sensel approach, it can be anticipated that a global calibration will yield erroneous results for the pressures measured by individual sensels. The performance of the two calibration approaches is further compared in Figure 6.11, where emphasis is given on the force acting over the whole sensor as simultaneous load cell measurements are available. The acting force is calculated from the integral of the pressures measured by each sensel. The pressure measurements are calibrated using the global and the sensel-by-sensel calibration and the ratio of peak forces is plotted for all tests. It is seen that the global calibration yields results ranging between ±10% of the sensel-by-sensel based calculations.

Accordingly, a sensel-by sensel calibration is recommended but the use of a global calibration should not be disregarded completely. The former has the advantage that each sensel is calibrated individually but this also entails the requirement for a significantly increased number of calibration tests. As such a less laborious global calibration combined with an equilibration of the sensor could be useful for cases focusing on the measurement of the force acting over the sensor and whenever a decreased calibration accuracy can be tolerated.
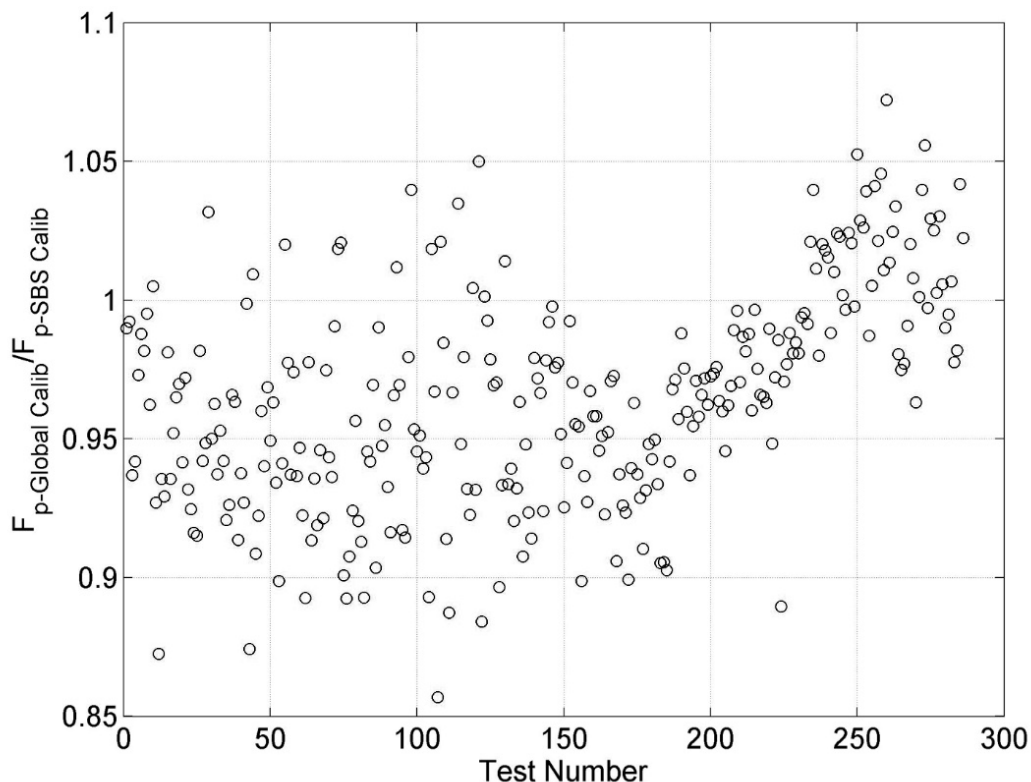
Figure 6.11: Ratio of the peak acting force calculated using a global and a sensel-by-sensel calibration

Following the selection of a sensel-by-sensel calibration approach the selection of the calibration's level (linear or higher order) is discussed. Previously, Brimacombe et al. (2009),

Palmer et al. (2009) among others have shown for a variety of applications that *Tekscan* sensors illustrate a non-linear response over the largest (or the full) part of its measuring range, which can be considered as nearly linear for smaller parts of the range. Accordingly the selection of the most appropriate (linear or higher order) calibration algorithm should depend, on the quality of the fit but also on the range of the pressures expected in the experiments with respect to the calibration range of the sensor. Nevertheless, for the current work pressures exceeding the nominal range by more than 4 times have been applied to the 9500 model sensor without reaching saturation. This in conjunction with the well-known high variability in wave impact induced pressures, see for example Hull and Muller (2002) and Kisacik et al. (2012), makes the a-priori selection of an approximate range for the anticipated pressures rather difficult. Accordingly, the linear and non-linear calibration curves fitted over the full range of data for each sensel are compared. The number of data points and the R^2 values for a linear, a power and a 2nd order polynomial curve are presented for every sensel in Figure 6.12; white in the color range corresponds to the smaller values and black to the largest. For the linear, the power and the 2nd order polynomial calibration the minimum, mean and maximum R^2 is 0.82, 0.94±0.01 (mean±std) and 0.99, 0.82, 0.94±0.01 and 0.995, 0.82, 0.94±0.01 and 0.995, respectively. The minimum, mean and maximum RMS (Root Mean Square) error is 0.15, 1.11±0.58, and 5.3, 0.15, 1.08±0.57 and 5.4, and 0.15, 1.07±0.57 and 5.34kPa.
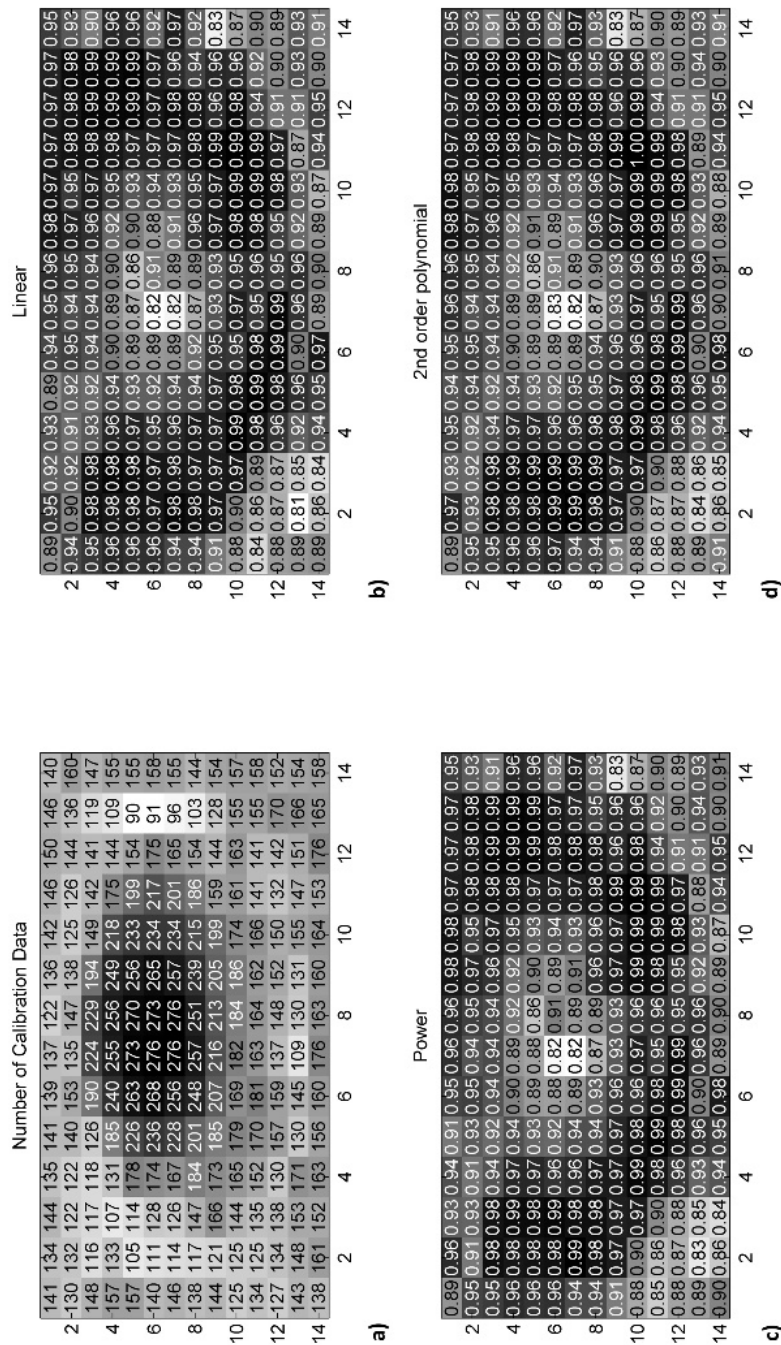
Figure 6.12: From top left and moving clockwise – a) number of calibration data per sensel. - R2per sensel for b) liner calibration, c) power law calibration, d) 2nd order polynomial calibration; white in the color scale corresponds to the smallest and black to the largest values.

The integral of the pressures acting on each sensel is also calculated with the three different calibration algorithms and the results area compared with simultaneous load cell measurements. For forces ranging from about 5 to 50N and for the linear calibration the minimum, mean±std and maximum RMSE is 0.0012, 1.47±1.23 and 6.7N. For the power calibration, 0.0053, 1.49±1.23 and 6.7N, and for the 2nd order polynomial, 0.0021, 1.49±1.23 and 6.72N. Statistically indistinguishable results for the three calibration algorithms are also found (see also caption of Figure 6.13) for the percentage of error calculated as:

$$E_{\%} = \frac{F_{LC} - F_{TEK}}{F_{LC}} \cdot 100$$

<div align="right">*Eq. 5*</div>
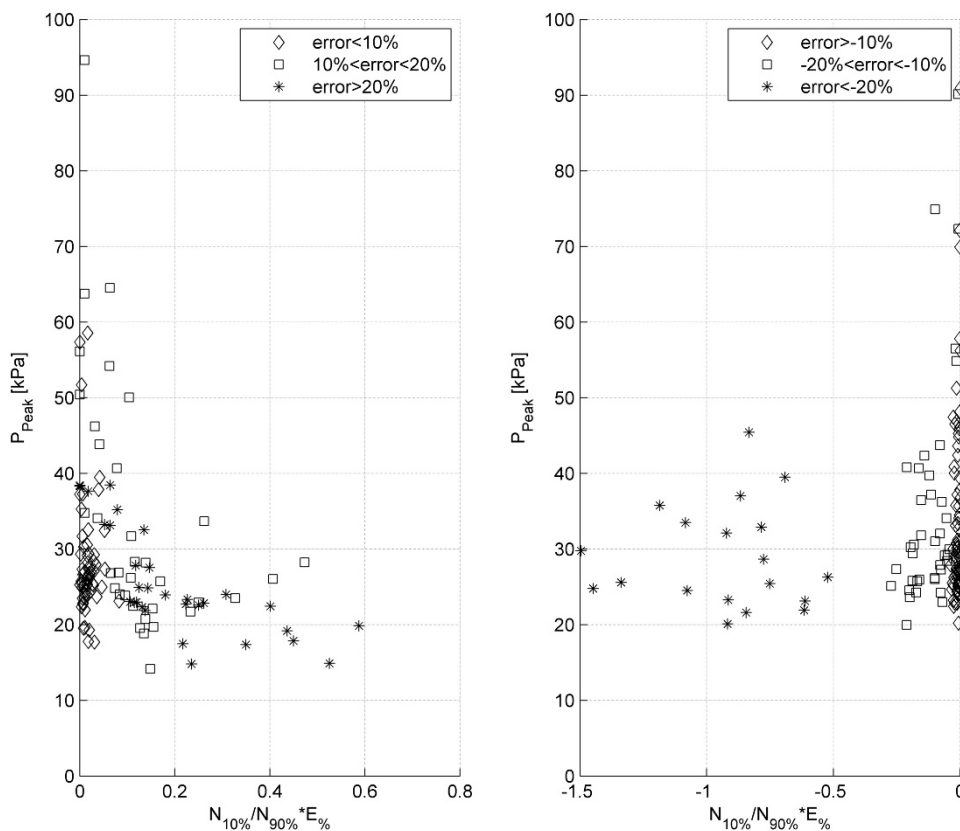
Figure 6.13: Plot of the pressure peaks recorded by a sensel for a given impact over eq. 5, for positive (on the left) and negative (on the right) percentage of error. The minimum, mean±std, and maximum error for the linear, power and 2nd, is -38%, 0.85±15.84% and 44.2%, -37%, 0.98±15.8% and 43.7%, and -37%, 0.8±15.4% and 42.8%.

where:

- F_{LC} : is the peak of the force measured by the load cells
- F_{TEK} : is the peak of the force calculated as the integral of the pressures measured by the *Tekscan* sensor
- $E_{\%}$: is the error percentage

The origin of the error for the overall force calculations is further examined in Figure 6.13, where the highest pressure peak measured by a sensel during a single impact is plotted over:

$$\frac{N_{10\%}}{N_{90\%}} * E_{\%}$$

where,

- $N_{10\%}$: is the number of sensels reporting pressures smaller than 10% of the highest pressures recorded in all tests.

- $N_{90\%}$: is the number of sensels reporting pressures higher than 10% of the highest pressures recorded in all tests

- $E_{\%}$: is the error from Eq. 5

Overall, the error on the force estimation is seen to decrease as the $N_{10\%}$ decreases and as the pressure increases. The latter is, for the majority of the impacts, associated with a higher force acting on the sensor and thus the error decreases as the water-jet induced force increases. In contrast, the highest errors are reported for the combination of low pressures and large $N_{10\%}$. This is in agreement with previous studies reporting that the accuracy of the *Tekscan* sensors decreases for pressures near the lowest nominal range of the sensor, see for example Palmer el al. (2009) and Ouckama and Pearsall (2012) and section 6.6.3.

For the calculation of the overall acting force an error is also introduced due to the consideration of the 'dead' area in the integral of the measured pressure, see section 6.6.2.2. The noise included in the signal of each sensel (2 to 4 digital units) and the residual (after filtering) noise induced by the vacuum pump is an additional source of error, Tekscan (2008) and Figure 6.11. For the time histories a low pass filter was applied and the vacuum pressure has been extracted; it is noteworthy, that a drift in the signal is not observed.

The calibration algorithms appear to be statistically indistinguishable over the full calibration range but their evaluation is based on the goodness of fit and errors associated to the force acting on the sensor and not on individual sensels. Nonetheless, the existing literature and the manufacturer suggest the use of a higher order calibration if the full or a large part of the sensor's measuring range is to be considered, see section 6.3 and Tekscan (2008). Indeed, Marzeddu et al. (2015) uses a power law calibration and reports a satisfactory comparison in wave impact induced pressure/load measurements conducted with the system and pressure transducers/load cells.

A limitation of our study, however, is the small number of calibration data for pressures higher than 50kPa and smaller than 5kPa, areas within which the regression plots of the different algorithms are seen to diverge, subplot on the right in Figure 6.4. A more rigorous calibration is

expected to increase further the accuracy of the calibration. This could provide some justification on the contradiction with the results of Brimacombe et al. (2009), where a cubic calibration was reported to drastically improve the accuracy of the calibration. The discrepancy between the two studies can also be due to the different loading conditions, which for the LIM/UPC wave flume tests involve dynamic loads induced on the sensor by a fully compliant medium (water) instead of static loads generated by a materials testing machine and applied through a semi-compliant polyethylene disk. In addition, a different Tekscan sensor with a much higher pressure range (0-17.2MPa) was employed in the experiments of Brimacombe et al. (2009).

6.5. Conclusions

- This two part work looks at the details of the application of a pressure mapping system in hydraulic model tests involving wave impacts on structures. Part 1 describes and studies the details of an experimental apparatus and a calibration methodology suitable for such applications. It is suggested:

- To employ a water proof arrangement for the sensor.

- To employ a perforated sensor and remove the internal air by maintaining a vacuum throughout the course of the experiments.

- To use water for the calibration of the sensor.

- To use dynamic events, such as the water-jet impacts used here, for the calibration of the sensor

- To prefer a sensel-by-sensel calibration.

- To generated and use as many calibration points as possible

- To prefer a higher order calibration algorithm if the full nominal range of the sensor is considered. The latter is line with the manufacturer's recommendations and it is thus suggested despite the fact that for the data set produced and used here, linear and higher order calibrations over the full pressure range yield statistically indistinguishable results.

For the above, and a power law calibration the minimum, mean and maximum RMS (Root Mean Square) error for pressures 0.15, 1.08±0.57 and 5.4kPa, and for loads 0.0053, 1.49±1.23 and 6.7N. It is also noted, that the nominal pressure range of a perforated and vacuumed tactile sensor extends significantly over the upper limit defined by the manufacturer.

A limitation of this study is the reduced control over the location of the water-jet impact and thus the, comparatively, reduced number of calibration points for sensels located near the edges of the sensor. Nevertheless, using the proposed experimental arrangement and calibration Part

2 (Marzeddu et al. (2015)) reports a satisfactory agreement between the pressure mapping system and pressure transducer and load cell measurements of wave impact induced pressure/loads.

Acknowledgment

References

Bachus, K.N. et al., 2006. Measuring contact area, force, and pressure for bioengineering applications: using Fuji Film and TekScan systems. *Medical engineering & physics*, 28(5), pp.483–488.

Baer, T.E. et al., 2004. Calibrating and monitoring sheet array pressure sensors for intra-articular load measurement. In and E. Societies of Canada, USA, Japan, ed. *Proceedings of the Fifth Combined Meeting of the Orthopaedic Research*. p. 115.

Brimacombe, J.M. et al., 2009. Effect of calibration method on Tekscan sensor accuracy. *Journal of biomechanical engineering*, 131(3), p.34503.

Brown, T.D., Rudert, M.J. & Grosland, N.M., 2004. New methods for assessing cartilage contact stress after articular fracture. *Clinical orthopaedics and related research*, 423, pp.52–58.

Bullock, G.N. et al., 2007. Violent breaking wave impacts. Part 1: Results from large-scale regular wave tests on vertical and sloping walls. *Coastal Engineering*, 54(8), pp.602–617.

Fregly, B.J. & Sawyer, W.G., 2003. Estimation of discretization errors in contact pressure measurements. *Journal of biomechanics*, 36(4), pp.609–613.

Grune, J., 1992. Loads on sloping seadykes and revetments from wave-induced shock pressures. *Coastal Engineering Proceedings*, 1(23).

Hattori, M., Arami, A. & Yui, T., 1994. Wave impact pressure on vertical walls under breaking waves of various types. *Coastal Engineering*, 22(1-2), pp.79–114.

Hoffmann, K. & Decker, K., 2005. Inaccuracies in measurement of contact pressure due to the measuring grid of a foil sensor. *1st International Conference on Sensing Technology November 21-23, 2005 Palmerston North, New Zealand*, 3(1/2), p.80.

Hull, P. & Müller, G., 2002. An investigation of breaker heights, shapes and pressures. *Ocean Engineering*, 29, pp.59–79.

Kim, S.-Y., Kim, K.-H. & Kim, Y., 2015. Comparative study on pressure sensors for sloshing experiment. *Ocean Engineering*, 94, pp.199–212.

Kisacik, D., Troch, P. & Van Bogaert, P., 2012. Description of loading conditions due to violent wave impacts on a vertical structure with an overhanging horizontal cantilever slab. *Coastal Engineering*, 60, pp.201–226.

Lu, W. et al., 2013. Rubble Ice Transport on Arctic Offshore. In *Proceedings of the 22nd international conference on Port and Ocean Engineering under Arctic conditions*. Espoo, finland.

Marzeddu, A. et al., 2015. Measuring wave impact induced pressures with a pressure mapping system, Part 2: Validation. *Coastal Engineering*. (Submitted)

Otto, J.K., Brown, T.D. & Callaghan, J.J., 1999. Static and dynamic response of a multiplexed-array piezoresistive contact sensor. *Experimental Mechanics*, 39(4), pp.317–323.

Ouckama, R. & Pearsall, D.J., 2011. Evaluation of a flexible force sensor for measurement of helmet foam impact performance. *Journal of biomechanics*, 44(5), pp.904–909.

Ouckama, R. & Pearsall, D.J., 2012. Impact performance of ice hockey helmets: head acceleration versus focal force dispersion. *Proceedings of the Institution of Mechanical Engineers, Part P: Journal of Sports Engineering and Technology*, p.1754337111435625.

Oumeraci, H. et al., 2001. *Probabilistic design tools for vertical breakwaters* A. kortenhaus & H. Voortman, eds., Amsterdam : (ndl): Swets & Zeitlinger,.

Paik, J.K. & Shin, Y.S., 2006. Structural damage and strength criteria for ship stiffened panels under impact pressure actions arising from sloshing, slamming and green water loading. *Ships and Offshore Structures*, 1(3), pp.249–256.

Paikowsky, S.G. & Hajduk, E.L., 1997. Calibration and use of grid-based tactile pressure sensors in granular material. *ASTM geotechnical testing journal*, 20(2), pp.218–241.

Palmer, M.C. et al., 2009. Tactile Pressure Sensors for Soil-Structure Interaction Assessment. *Journal of Geotechnical and Geoenvironmental Engineering*, 135(11), pp.1638–1645.

Ramachandran, K. et al., 2013. Measuring Wave Impact on Coastal Structures with High Spatial and Temporal Resolution--Tactile Pressure Sensors a Novel Approach. In *35th IAHR World Congress, Chengdu, China*.

Stagonas, D. et al., 2012. Distribution of impact induced pressures at the face of uniformly sloped sea dikes: Preliminary 2D Experimental Results. *Coastal Engineering Proceedings*, 1(33), p.structures–74.

Stagonas, D., Marzeddu, A., et al., 2014a. Large scale experiments on the interaction of a caisson breakwater with breaking waves. *Proceedings of the HYDRALAB IV Joint User Meeting, Lisbon, July 2014*

Stagonas, D., Lara, J.L., et al., 2014b. Large scale measurements of wave loads and mapping of impact pressure distribution at the underside of wave recurves. *Proceedings of the HYDRALAB IV Joint User Meeting, Lisbon, July 2014*

Tekscan, I., 2008. I-Scan and High speed I-Scan User manual. , pp.1–11.

Vicinanza, D. et al., 2014. Innovative rubble mound breakwaters for overtopping wave energy conversion. *Coastal Engineering*, 88, pp.154–170.

Wienke, J. & Oumeraci, H., 2005. Breaking wave impact force on a vertical and inclined slender pile - Theoretical and large-scale model investigations. *Coastal Engineering*, 52(5), pp.435–462.

Wilson, D.C. et al., 2006. Accuracy and repeatability of a new method for measuring facet loads in the lumbar spine. *Journal of biomechanics*, 39(2), pp.348–353.

Wilson, D.R. et al., 2003. Accuracy and repeatability of a pressure measurement system in the patellofemoral joint. *Journal of biomechanics*, 36(12), pp.1909–1915.

7. Propuesta de una nueva tecnología: validación

Una vez calibrado el sensor táctil, en este capítulo se evalúa su funcionamiento a través de una comparativa directa (resultados registrados en el mismo momento y en la misma área de impacto) con la célula de carga. Se realiza también una comparativa indirecta (misma área y zona de medida pero en ensayos separados) con los sensores de presión. Se evidencían las enormes posibilidades de este tipo de sensor y los problemas asociado a su utilización. La descripción de los ensayos, la presentación y el análisis de estos resultados se encuentran en el artículo *"Measuring wave impact induced pressures with a pressure mapping system, Part 2: Validation" (Submitted)*

Marzeddu, A., Stagonas, D., Gironella, X., Sánchez-Arcilla, A., Muller, G., 2015. Measuring wave impact induced pressures with a pressure mapping system, Part 1: Experimental set-up and calibration. Coast. Eng. (Submitted)

Abstract

The use of a pressure mapping system for measuring wave impact induced pressures is evaluated in this paper. The set-up and calibration methodology suggested in the first part of this work are employed and the system is validated against pressure transducer and load cell measurements and for a variety of breaking condition on a vertical seawall. For a large number (120 measurements for each case considered) of breaking and broken waves interacting with the wall, the peak pressure (P_{peak}) profiles and the pressure distribution maps reported by the system agree well with results acquired using pressure transducers. Although the pressure mapping system tends to underestimate P_{peak}, differences on the mean of the 3, 5 and 10 highest P_{peak} range within ±10%, while for the majority of the measurements the error on the integral of the acting pressures (the acting force compared with the force measured by the load cell) ranges within ±20%. It is concluded, that through careful calibration and set-up the pressure mapping system has the capacity to provide pressure distribution maps with a good accuracy. It is not, however, consider to constitute the absolute alternative to pressure transducers and thus a combined use is suggested for applications where a very high level of accuracy is required.

7.1. Introduction

As knowledge on the mechanics involved in the breaking wave-structure interaction is limited impact induced pressure measurements are one of the most important outcomes hydraulic model tests. Pressure measurements are usually preferred over load measurements as they allow for the location of vulnerable areas on the structure, while the acquisition of global loads

requires at times complicated and expensive experimental layouts, especially in large scale facilities. For most physical model tests involving, e.g., coastal structures an array of pressure transducers is placed vertically at the seaward face of the structure and the data collected are used for the construction of pressure profiles and the calculation wave induced loads and moments, Cuomo et al. (2010).

Nonetheless, pressure transducers provide single point measurements and in most cases financial and practical reasons dictate the use of a relatively small number of transducers. In the same time, the high spatial and temporal variability of wave impact induced pressures, Hattori (1994), Peregrine (2003), Saruwatari et al. (2009), the limited information available even on the coherence pressure profiles, Hull and Müller (2002), and the increased complexity on the geometry of the structures (for example, wave re-curves, wave energy converters and ships) tested, drive the need for experimental measurements with a high spatial resolution.

Additional challenges emerge when cylinders and structures with more complex geometrical shapes are considered. For example, investigating the survivability of wave energy converters, offshore oil platforms or wave recurves requires detailed knowledge of the impact induced pressure distribution. However, due to technical and financial restrictions high resolution pressure maps cannot be produced using pressure transducers.

A pressure mapping system with the potential to provide pressure measurements with a high spatial resolution is described in Stagonas et al. (2015). The system has been used in and validated for, e.g., biomedical and geotechnical applications but never before for measuring wave induced impact pressures. In addition, the existing literature suggests that the accuracy of the system depends mainly on the experimental set-up and the calibration methodology employed. An appropriate set-up and methodology for application in hydraulic model tests are also proposed in Stagonas et al. (2015). In this second part of the work, the performance of the pressure mapping system is validated for measuring wave impact induced pressures. The model of a vertical model seawall is used as the testing structure and the performance of the system is evaluated against pressure transducer and load cell measurements, and for various breaking conditions on the wall.

In the remainder, the equipment used, the experimental arrangement and the wave parameters are described in section 7.2. Results from the tests conducted are presented and discussed in section 7.3 and the work is concluded in section 7.4.

7.2. Methodology

7.2.1. Experimental equipment

7.2.1.1.   Pressure mapping system

The high speed Tekscan Pressure Mapping System (PMS) is used here. The system consists of a tactile pressure sensor (sometime referred to as pressure pad or simply pad), a connection handle and a hub allowing the simultaneous use of more than one handles and triggering from an external signal. The hub is connected to the USB port of any PC equipped with I-Scan software provided by the manufacturer along with the PMS.

A variety of tactile pressure sensors is available with their characteristics ranging in terms of number of measuring points (most commonly referred to as sensels), physical size and maximum sampling frequency. For all tests presented here the tactile sensor with model number 9500 was used. The sensor has 196 sensels spread at equal distances over a square area of 7.1x7.1cm and it allows for a maximum sampling frequency of 4 kHz with and 8bit resolution. At this point it should be highlighted that each sensel consists of an active area and a 'dead' area surrounding the active area. Accordingly an intrinsic disadvantage is entailed, as the pressure is calculated as force over the full (active and 'dead') area of each sense. The pressure mapping system is not provided already calibrated by the manufacturer. For details on the pressure mapping system and the purposely developed and used calibration methodology the reader is referred to Stagonas et al. (2015).

7.2.1.2.   Pressure transducers and load cells

In total, 8 P8AP pressure transducers were available. The P8AP is an absolute pressure transducer suitable for measuring static and dynamic, gas or liquid induced pressures and can be safely immersed to depths down to 1m. Each transducer is composed of a strain-gauge sensor and is provided already calibrated by the manufacturer (HBM); accompanied with a CE declaration of conformity and a test certificate. The P8AP sensors used here have a maximum measuring range of 103kN/m^{2}with a reported accuracy of 0.3% of the maximum load, a 24bit resolution and a natural frequency of the diaphragm of 12 KHz.

Force measurements were conducted using two Z6FC3 bending beam load cells with a nominal load of 50Kg, an accuracy of 0.009% of the maximum load and a resolution of 24bit. As for the pressure transducers   the load cells are provided calibrated and they can be immersed to a maximum depth of 1m. An HBM QuantumX data acquisition system is used to simultaneously sample each load cell and pressure transducer with a sampling frequency of 4.8 kHz. Although the system has the capacity to amplify and sample up to 16 channels with a maximum sampling rate of 19.2 kHz, 4.8 kHz were selected as the rate closest to that of the pressure mapping system

(4 kHz per sensel). For experiments with pressure transducers Marzeddu et al. (2013, 2014) recorded the highest impact pressure with a sampling frequency of 19.2 kHz but they concluded that a satisfactory description of the pressure pulse can be acquired with a minimum of 2.4 kHZ.

7.2.1.3.   Experimental setup

All experiments were carried out in the CIEMito wave flume of the Laboratori d'Enginyeria Maritima (LIM) of the Universitat Politecnica de Catalunya BarcelonaTech (UPC). The flume is 18m long, 0.38m wide and 0.56m deep and a vertical seawall model is placed at the end of a 1:15 smooth slope, Figure 7.1.
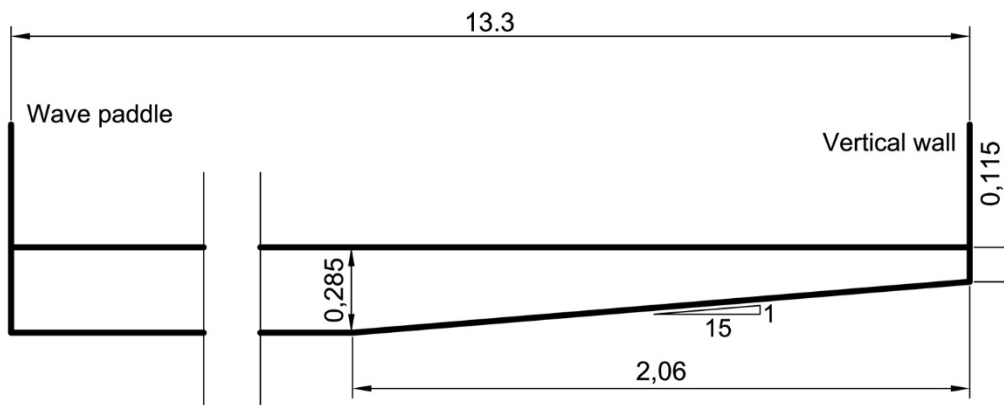
Figure 7.1: Experimental layout - Wave probes were located at 3, 5, 5.08, 5.2, 5.6, 10.5, 10.71, and 11.11 m from the wavemaker. A rectangular box section placed 0.5m from the vertical wall was used for the generation of broken waves at the structure; all dimensions in m.

Groups of regular waves are generated by a computer driven piston type wave maker. For each group the first (ramp-up) wave is always smaller than the target wave height and it is fully reflected at the structure, while the second wave has the height reported in Table 7.1 and results in an impact at the wall. Through small variations of the water depth (d), the wave height (H) and period (T) different breaking conditions are induced on the wall, seeTable 7.1. Broken waves were generated by introducing a 0.2×0.35×0.05m (length×width×depth) block 0.5m from the structure.

H [m]	T [s]	d [m]	N. Repetitions	Breaker type	RMSE [m]	Error [%]
0.16	2.4	0.285	120	Nearly breaking (NB)	0.003	2
0.16	2.3	0.285	120	Large air pocket (LP)	0.004	2.5
0.16	2.3	0.29	120	Small air pocket (SP)	0.003	1.8
0.16	2.3	0.285	120	Broken wave (BW)	0.004	2.5

Table 7.1: Incoming wave parameters and RMSE and percentage of error on surface elevation measurements for 120 waves of each category. The wave height error calculation were computed from wave probe number 1 at 3 m from the wavemaker.

Each breaker type is repeated 120 times. As the 1st wave of the group is always reflected at the structure the impact of the 2nd wave was considered to be the cleanest and most repeatable. For this reason, only the pressures induced by the impact of this wave on the seawall are considered. The repeatability on the generation of the wave groups was also tested and the RMSE (computed on wave height) and percentage of error values are also shown inTable .

In total, 4 experimental arrangements *EA1* to *EA4* are employed for this work and the *Tekscan I-Scan^{TM}* pressure mapping system is validated through the cross-comparison of the different data sets produced. For *EA1* the tactile sensor is placed on top of segment of the vertical wall mounted on a load cell, Figure 7.2. The load cell has a high stiffness and it is in turn mounted on a stiff metallic structure. The segment of the wall is of the same size (7.1 x 7.1 cm) as the tactile sensor and the water-proofing arrangement (Figure 7.2) and the calibration rig proposed in Stagonas et al. (2015) were employed.

For *EA2*, and array of 7 pressure transducers is placed in the middle of the vertical wall. The vertical intervals between the transducers (PT1 to PT3 and PT5 to PT8 near the top of the wall) are shown in Figure 7.2, while an additional transducer (PT4 in Figure 7.2) is placed near SWL and at a distance of 2.5 cm to the left of the array. As for *EA1*, the array is mounted on a segment of the wall (35 x 10 cm) supported this time on two load cells, see Figure 7.2.
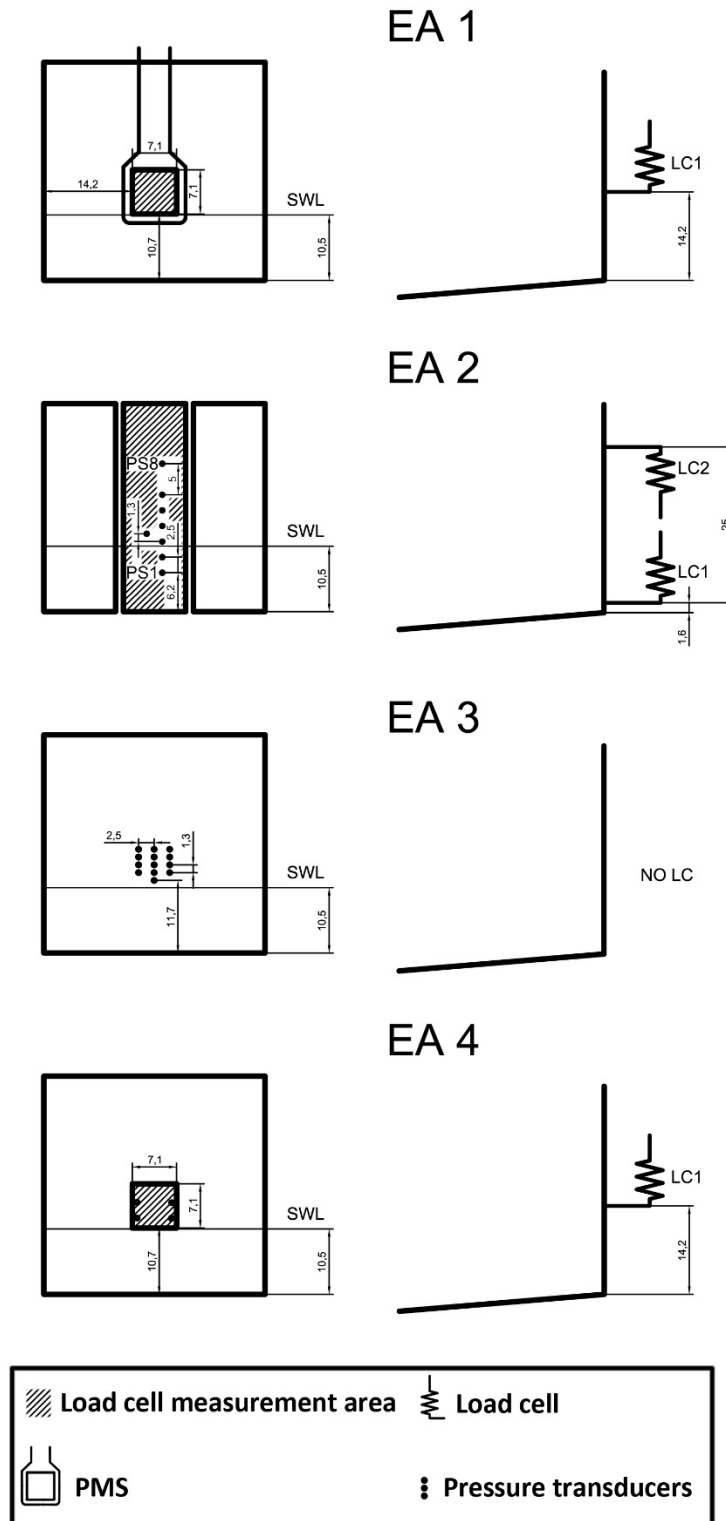
Figure 7.2: Schematics of all experimental arrangements. From top to bottom, EA1, EA2, EA3 and EA4. Inclined lines indicate the measurement zone of the load cell in EA1 (under the pad) and EA4 (with four pressure transducers) - (all dimensions in cm)

In contradiction to *EA1* and *EA2* a not-segmented seawall model is used for *EA3* and matrix of

13 measuring locations is created at the same location as the tactile sensor for *EA1*, Figure 7.2.

Restrictions due to the physical dimensions of the transducers make the simultaneous use of load cells impossible. In addition, and since no more than 7 transducers can be fit on the area of interest 120 impacts of each breaker type are recorded and the tests are repeated with 6 transducers re-located on the remaining 6 positions. This way, a matrix of 13×120 measurements is generated.

Given the aims of this paper, *EA1* allows for the comparison of force measurements acquired by the tactile sensor with simultaneous load cell measurements, while the vertical distribution of the peak pressures (P_{peak}) recorded by the pressure mapping system for *EA1* is evaluated against the transducer measurements for *EA2*. For *EA1* and *EA2* the same incoming wave conditions are used and pressure records are acquired for segments of the wall mounted on load cells.

Nevertheless, impact induced pressures for *EA3* are measured on a non-segmented wall and therefore *EA4* is utilised to evaluate potential effects of the latter difference. For *EA4*, a segment of the seawall model equal in size to that for *EA1* is mounted on the load cell and 4 pressure transducers are fixed near the 4 corners of the plate as shown in Figure 7.2; pressure transducer positions for *EA2* (small circles), *EA3* (small circles) and *EA4* (small circles) are also shown in Figure 7.2.

Indicative results for the comparison between *EA3* and *EA4* for breaking waves with large pocket(LP) and broken waves (BW) are presented in Figure 7.3, where the P_{peak} probability of non-exceedance is plotted for *EA3* (circles) and *EA4* (triangles). For breaking waves, the peaks of the pressures recorded for *EA3* are up to 3.5 times higher than those for *EA4* but they are reported to range within the same order of magnitude for broken waves; similar trends were seen when *EA3* was compared with *EA2* and *EA1* (comparison not presented here). The results of Figure 7.3 are not investigated further within this work but they are used in support of those (results) presented in section 7.3.2.

BREAKING WAVE

a)

b)

c)

d)

BROKEN WAVE

a)

b)

c)

d)
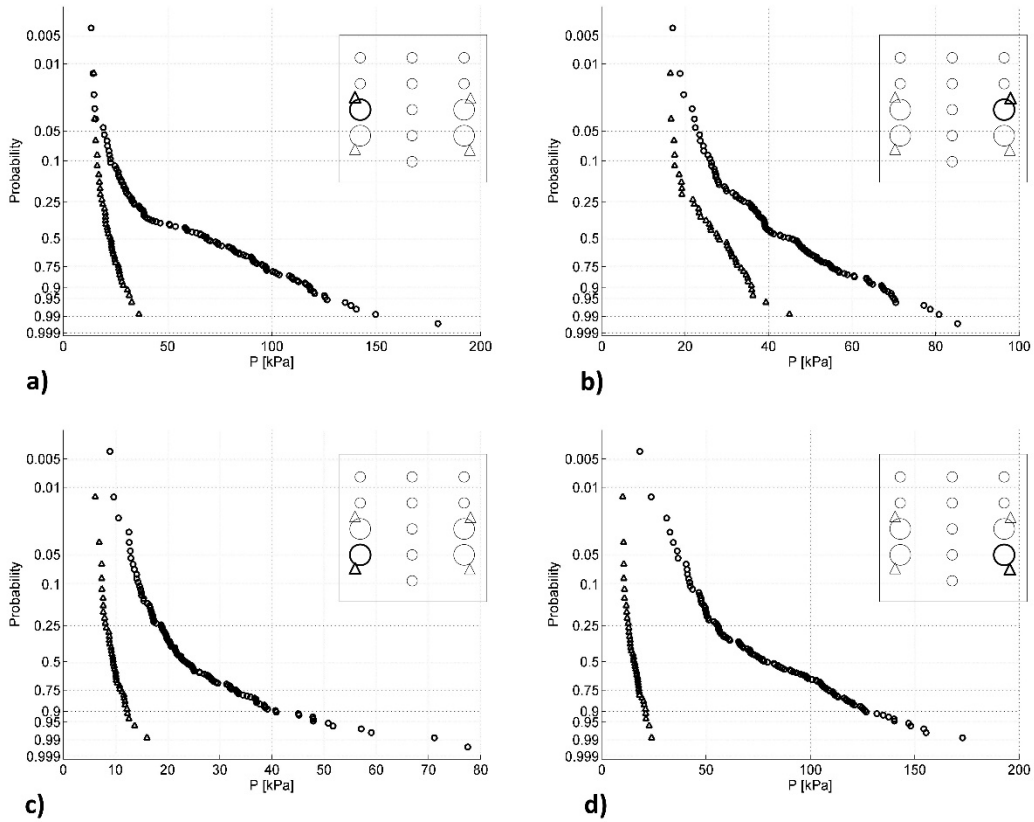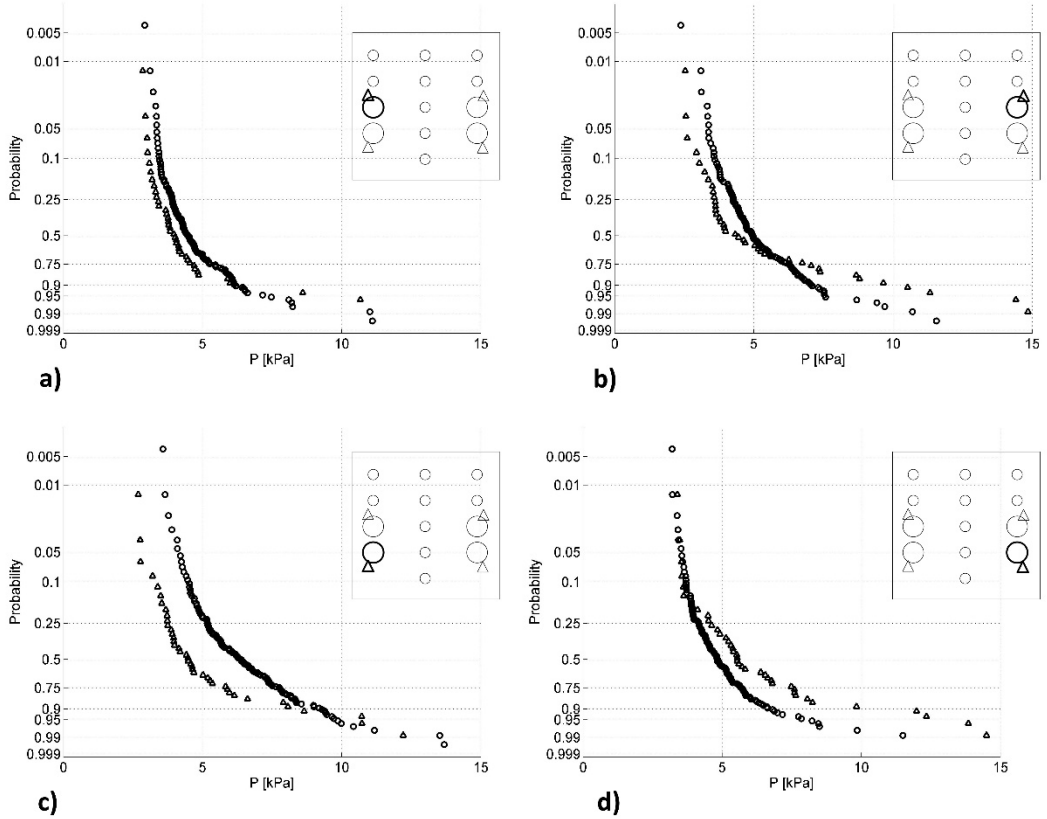
Figure 7.3: Probability plots of P_{peaks} for EA3(circles) and EA4 (triangles). Top subplots results for breaking wave (LP). Bottom subplots results for broken waves (BW).

7.3. Results and discussion

7.3.1. Vertical distribution and pressure rise time

Hull and Muller (2002), have shown that for waves shoaling over a slope and breaking on a vertical wall maximum impact pressures are located at and near Still Water Level (SWL). This was later on confirmed by several researchers conducting tests in similar or larger scales, see for example Kisacik et al. (2012), Bullock et al. (2007) and Cuomo et al. (2010).

The vertical distribution of the highest peak pressures (P_{peak}) measured by 14 vertical arrays of 14 sensels (dashed grey to black lines) is compared with those reported by the array of 7 pressure transducers (solid black line) in Figure 7.4.
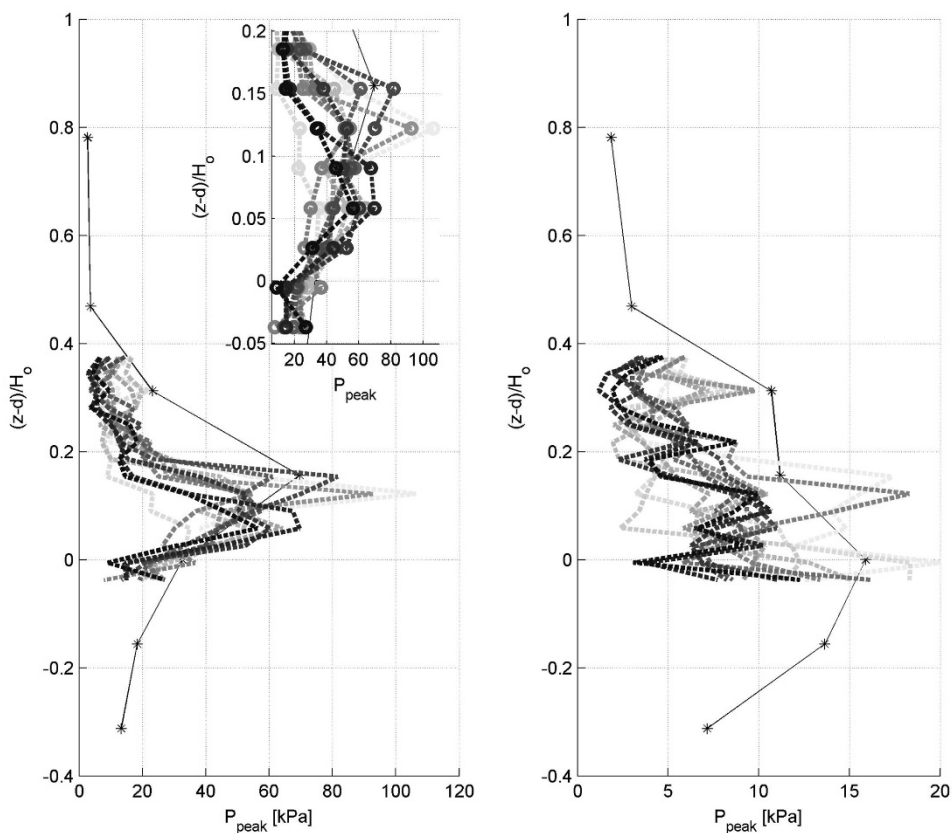
Figure 7.4: Vertical distribution comparison – breaking wave (LP) and zoom in the impact zone (left), broken wave (BW right) – PMS sensels EA1 (dashed grey to black lines) and pressure transducers EA2 (solid black line). z is the distance from the toe of the structure.

A reasonable agreement is observed between the pressure profiles induced by breaking waves forming a large air pocket (left subplot) and broken waves (right subplot). For both instruments, and in line with previous works, the highest pressures are located at and slightly above SWL. Sensels positioned at locations similar (dashed black line with P_{peak} = 82kPa on the left hand side of Figure 7.4) to those of the pressure transducers report the highest P_{peak} for (z-d)/H = 0.18, which is increased by 14% compared to the P_{peak} for the transducer array. In principle, profiles

with increased P_{peak} (grey and light grey lines) are reported for sensel arrays the coordinates of which do not overlap with those of the pressure transducer array. It is however noteworthy that all profiles maintain a coherent shape as P_{peak} values on each side of the maximum P_{peak} decrease gradually. Broken wave impacts result in more irregular pressure profiles with reduced coherence but a reasonably good overall agreement between the pressure profiles is still observed.

Pressure transducers PT3, PT4, PT5 and PT6 are located inside the impact zone for breaking and broken waves and the P_{peaks} recorded for 120 impacts are compared with measurements from sensels at similar locations in Figure 7.5 and Figure 7.6.
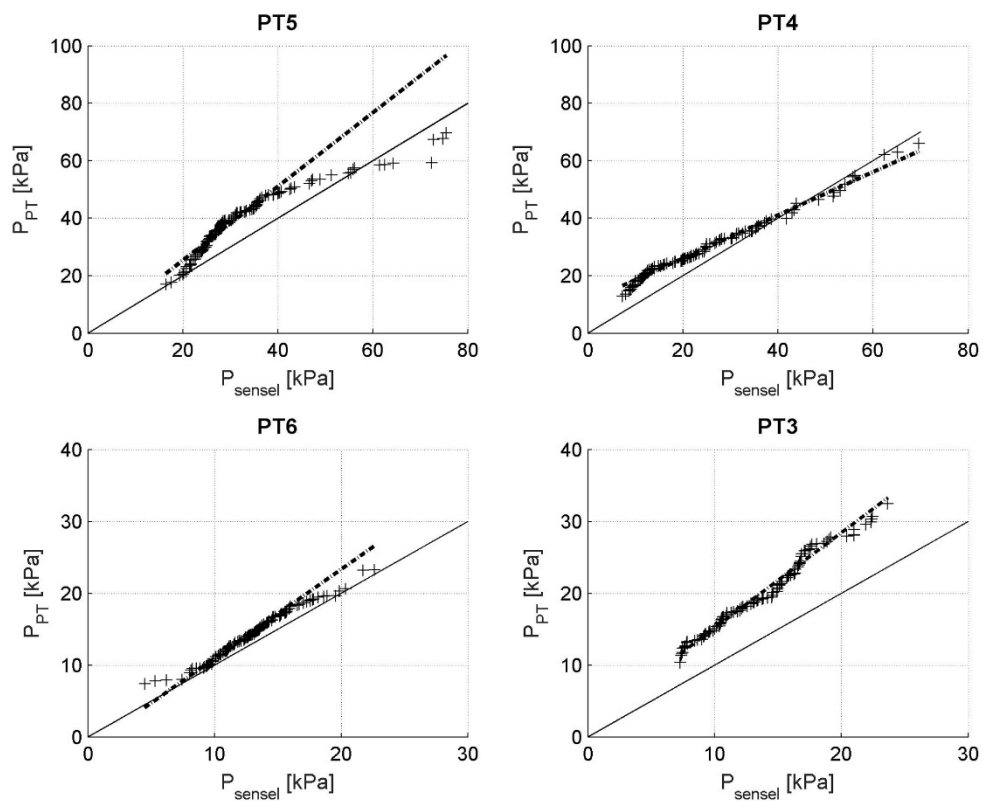
Figure 7.5: qqplots of sensels (EA1) and pressure transducers (EA2) at similar location in the impact zone against - breaking wave (LP)
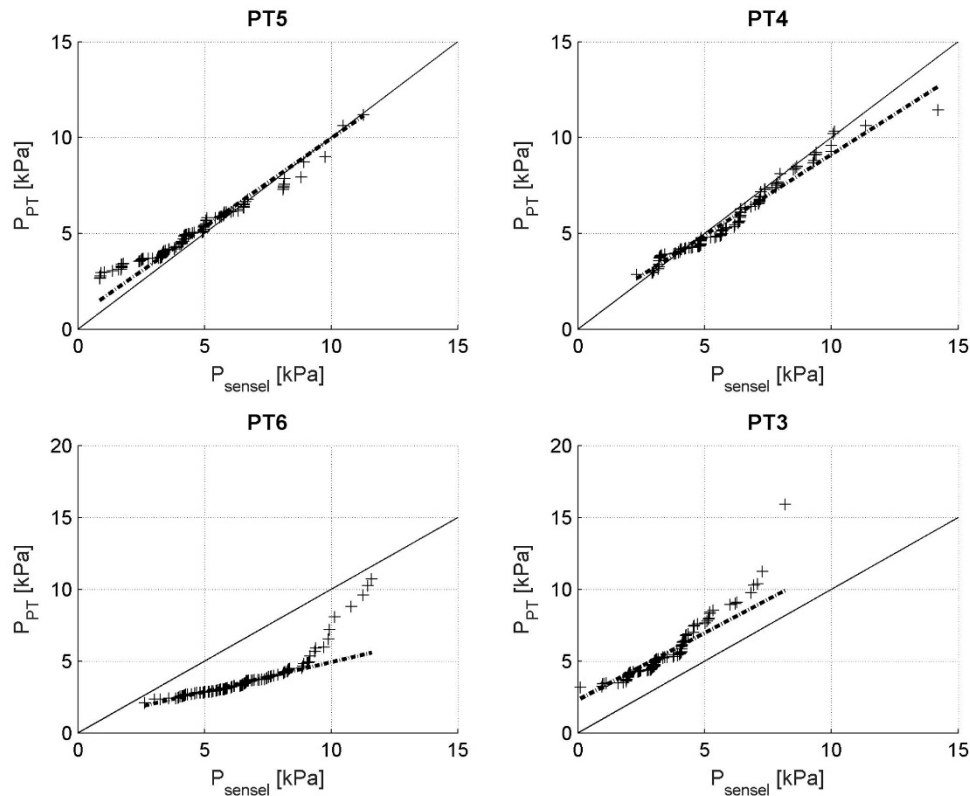
Figure 7.6: qqplots of sensels (EA1) and pressure transducers (EA2) at similar location in the impact zone - broken wave (BW)

The quantiles calculated for each data set are shown in the Quantile-Quantile plots (QQplot) of Figure 7.5 and Figure 7.6 along with a reference (dashed) line joining the 1st and 3rd quartile of each distribution. Since the majority of the plotted quantiles form the line it can be said that the data recorded by the sensels and those recorded by the pressure transducers come from the same distribution family and they have similar mean and standard deviation (STD).

Indeed, and for example, the mean and STD for PT4 and PT5 and the corresponding sensels is 28.43kPa and 10.88, 39.3kPa and 11.05, and 23.58kPa and 13.98, 33.04kPa and 12.4, respectively. Similar results are found for PT3 and PT6, while for broken waves the mean and STD are 5.62kPa and 1.9, 4.9kPa and 1.53, and 5.89kPa and 2.07, 4.88kPa and 2.02. Nonetheless, the mean of the recorded P_{peak} is of little value from a design point of view, for which the highest values of P_{peak} are more useful. The average of the 3, 5 and 10 highest P_{peak} for PT4 and PT5 and breaking waves is 63.2kPa, 60.02kPa and 54.54kPa, and 68.27kPa, 64.6kPa and 61.1kPa, while for the sensels of the tactile sensor is 65.7kPa, 61.8kPa and 56.8kPa, and 74.4kPa, 71.2kPa, and 65.13kPa, respectively.

The *y=ax* (black solid) line is also plotted in Figure 7.5 and Figure 7.6. Although a reasonable agreement between sensels and pressure transducers is seen for the aforementioned mean and

highest P_{peak} the vast majority of quantiles fall above the *y=ax* line. Thus a tendency of the pressure mapping system to underestimate pressures is clearly indicated. Given the similar sampling rates (4kHz for the tactile sensor and 4.8kHz for the pressure transducers) and the large number of impacts considered this tendency can be attributed to the low digital resolution of the tactile sensor and to calibration inaccuracies discussed in detail in Stagonas et al. (2015). In addition the largest discrepancies refer to the smaller P_{peak} measured. This is in-line to results presented in the literature for a variety of different applications showing that the accuracy of the Tekscan tactile sensors reduces for pressures closer the lower end of the their nominal range, for more details and references see also Stagonas et al. (2015).

On the other hand, Kim et al. (2015) compared the performance of pressure sensors for sloshing induced impact pressures. Interestingly enough, the authors presented measurements showing that two ICP (Integrated Circuit Piezoelectric) sensors of the same type, the sensing diameter and linearity return different results on peak pressure measurements; the characteristics of both ICP sensors are similar to those of the pressure transducers used here. Kim et al. (2015) presented also pressure pulse time histories for both ICP sensors and highlighted differences on the sharpness/spikiness of the pressure signal, pressure drops and significant differences on rise time measurements.

Pressure time history examples for pressure transducers and sensels located above and below SWL are illustrated in Figure 7.7.
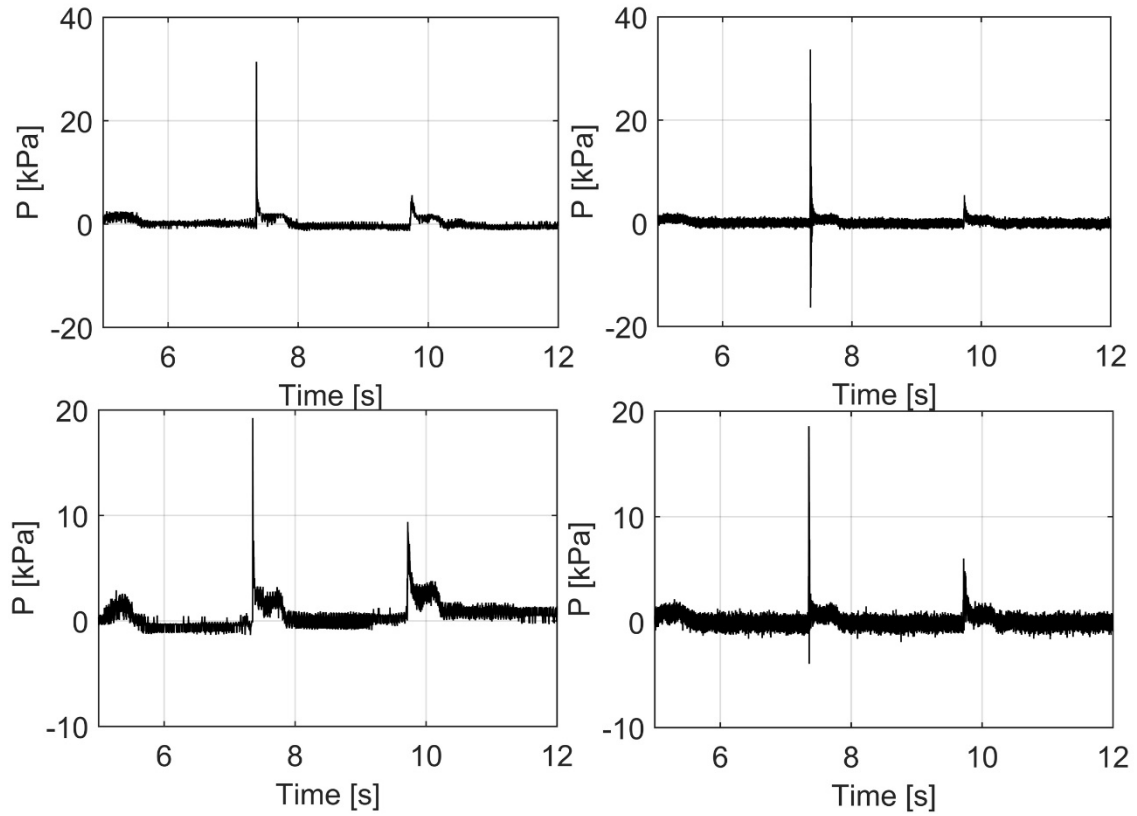
Figure 7.7: Pressure time series comparison – PMS (left) and PT (right) – Above SWL (top) and below SWL (bottom)

It is noteworthy that a signal drift is not observed for the tactile sensor time histories shown on the lefts hand side of Figure 7.7. When focusing in the details of a single impact, Figure 7.8, it becomes apparent that high frequency oscillations are not reported by the sensels of the pressure mapping system.
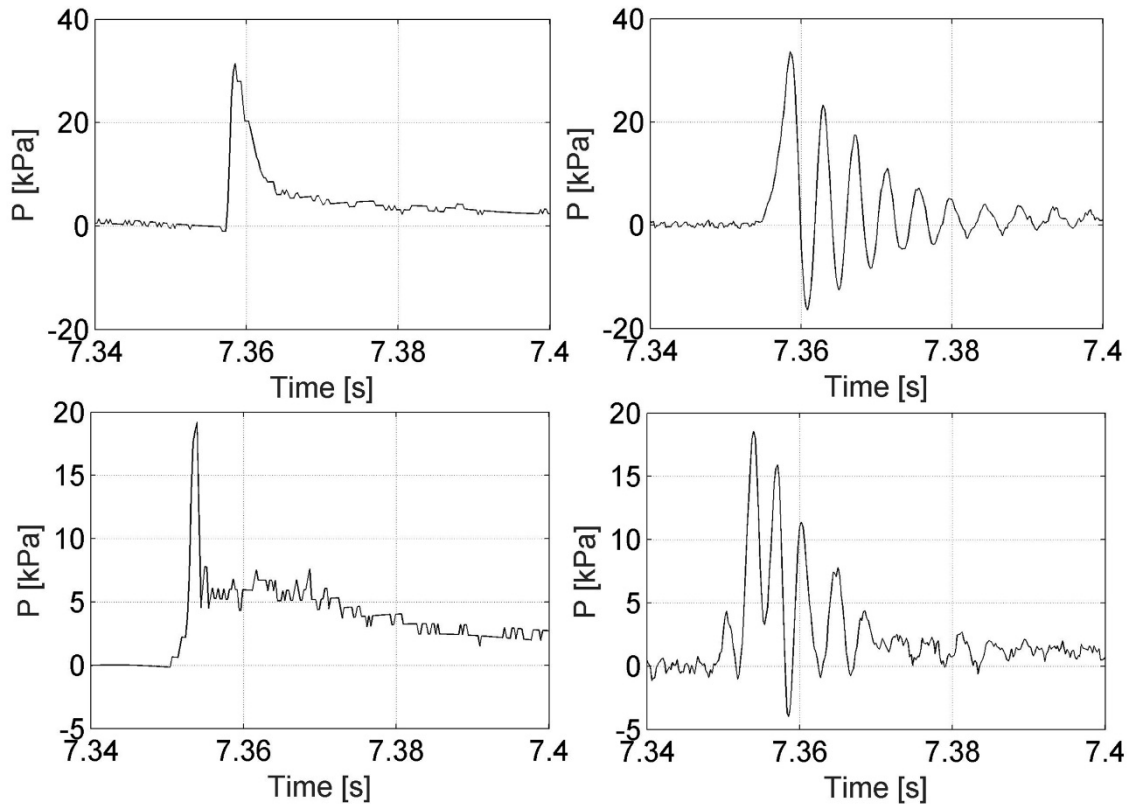
Figure 7.8: Detail of a single impact– PMS (left) and PT (right) – Above SWL (top) and below SWL (bottom)

Such high frequency oscillations have been associated with the presence of air bubbles entrained in the fluid during the impact, and can be clearly observed in the pressure transducer time histories.

In the same time histories, the rise time (t_r) is defined as the time required for the pressure to increase from 0 to its peak value. The rise time is linked to the response for the structure and its importance in the design process of, e.g., coastal structures is emphasised in contemporary design guidelines, Oumeraci et al. (2001). All t_r measurements for pressure transducers (crosses) and sensels (circles) are presented in Figure 7.9 as a function of P_{peak}.
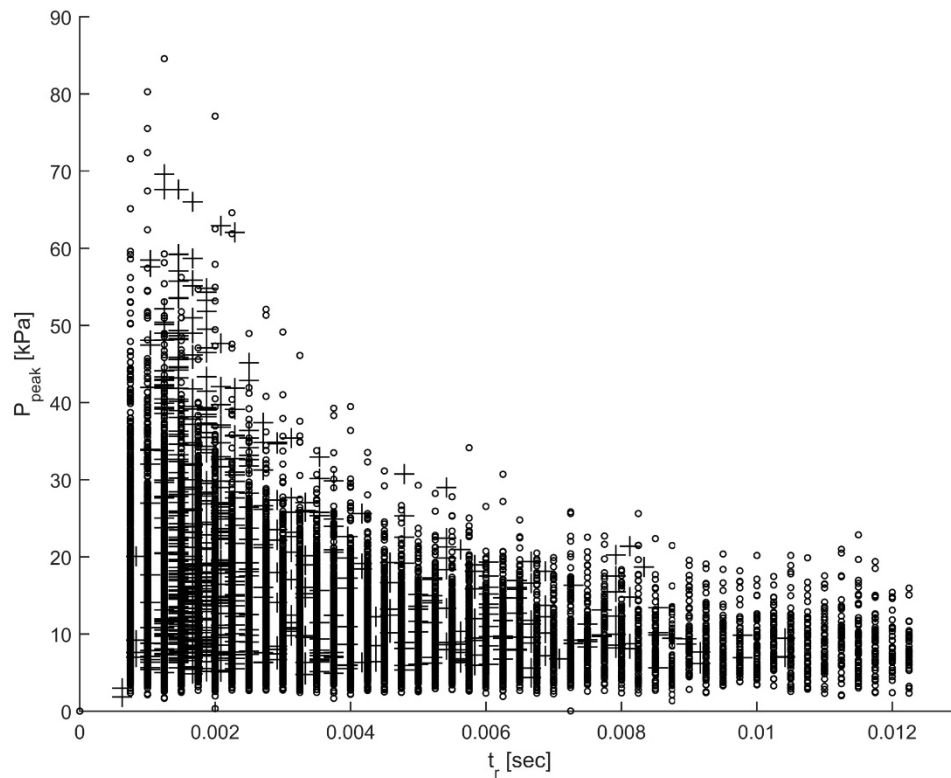
Figure 7.9: Rise time comparison for Tekscan sensels (circles) and transducers (crosses)

Overall, the exponential relation (the rise time increases as the pressure reduces) between P_{peak} and t_r observed for the pressure mapping system is in good qualitative agreement with that reported for the pressure transducer measurements but also with that presented elsewhere for similar experiments, see for example Kisacik et al. (2012). In principle, however, shorter rise times are seen for the tactile sensor and the average of t_r for the 3, 5 and 10 highest P_{peak} recorded for LP (breaking wave forming a large air pocket with the wall) range between 1.8ms and 2ms, and 1.3ms and 1.4ms for PT4 and PT5, and 0.6-1.2ms for the corresponding sensels.

The differences in t_r can be attributed to disadvantages explicit to the *Tekscan I-Scan^{TM}* pressure mapping system, like the low digital resolution (8bit). The latter entails that a smaller number of measurements is available to capture the (rapidly increasing) rising part of the pressure pulse resulting in a sharper and overall poorer description. The effect of the sampling frequency on the comparison between the two instruments is considered to be negligible as a similar rate is used; 4kHz (the maximum available rate the model 9500 tactile sensor) for the pressure mapping system and 4.8kHz for the pressure transducers.

On the other hand, the definition of the rise time used here in combination with the shape of the pressure time history records can also introduce errors. Very recently Kim et al. (2015) reported differences (up to 100%) on t_r measurements conducted by two pressure transducers

with similar technical specifications and a sole difference on the natural frequency, 250kHz and 300kHz. These were attributed to alterations on the shape of the time history prior to P_{peak}, e.g. negative signal drops, due to thermal shocks and/or sudden medium changes (air to water).

In summary, the discrepancies on tr measurements presented (Figure 7.9) and discussed are not considered significant enough in order to disregard the use of the *Tekscan I-Scan^{TM}* pressure mapping system.

7.3.2. Pressure distribution map

The high spatial variability of impact induced pressures is by now well recognised, see for example Hofland et al. (2010) and Stansberg et al. (2012), but the mechanisms of the wave impact on a structure remain largely unknown and thus the distribution of impact pressures unpredictable. Accordingly the capability of the pressure mapping system to provide high resolution maps of the impact induced pressure distribution becomes appealing. In this section, the distribution map of the maximum P_{peak} recorded by the pressure mapping system is compared with measurements by 3 vertical arrays of pressure transducers and a first evaluation step is made.

An example of the pressure map time history for a breaking wave is given in Figure 7.10, where the instantaneous pressure measurements for all sensels are illustrated as contour plots.
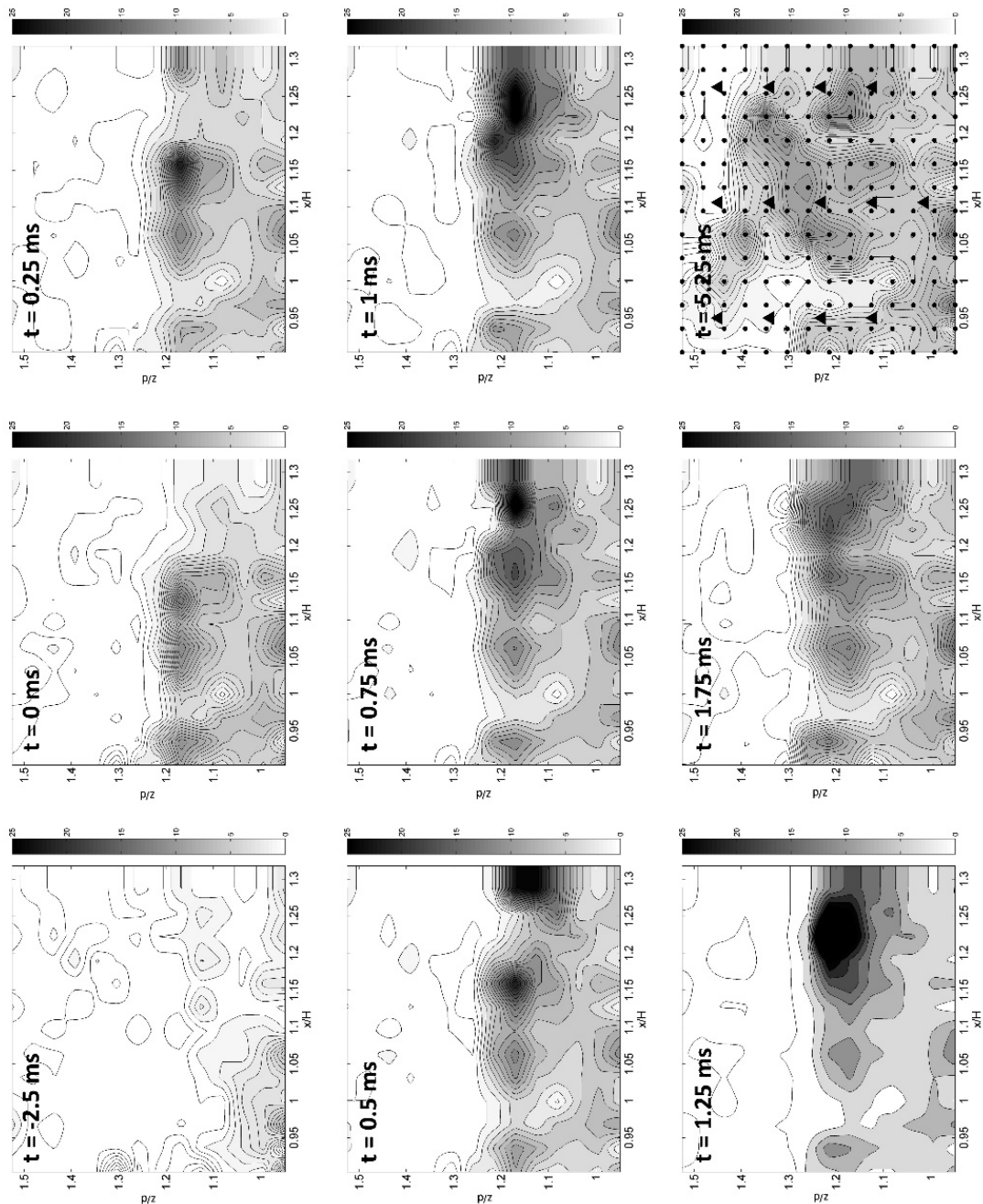
Figure 7.10: Tactile sensor - spatial pressure distribution time history. x-axis relative x position to the wave height. Y-axis relative position to the SWL. Z-axis P_{peak}/rgH

In agreement with previous works, the highest pressures are seen to occur near SWL but their spatial distribution is seen to vary with time. This spatial and temporal variability of impact induced pressures is potentially associated to the shape of the wave crest during breaking, see for example Peregrine (2003) and Saruwatari et al. (2009).

The map of the highest pressures recorded by all sensels (*EA1*) for 120 impacts is compared with pressure transducer measurements (*EA3*) in Figure 7.11.

Left (Tekscan), z/d vertical axis (1.5 to 1), Sensel Position – x (0.14 to 0.21):

14.1	17.1	17.1	23.6	16.7	13.7	13.5	12.5	8.18	9.51	14.9	10.2	6.77	6.84
5.25	6.25	8.93	11.4	14.7	10.9	8.19	9.82	10.8	4.63	5.27	3.26	2.71	4.27
11.8	12.9	22	16.1	19.8	16.6	10.6	6.12	3.5	6.03	3.74	5.01	5.9	9.44
12.7	10.4	6.31	13.7	17.8	18	10.9	10.5	9.76	16.9	9.14	5.98	4.04	3.44
12.1	10.5	11.2	7.95	8.36	6.41	10.1	12.1	11.8	14.7	19.6	10.8	9.93	16
20.9	9.67	7.85	7.5	7.14	14.4	18.4	20.8	22.5	19.4	12.4	12.5	14	18.2
49	29.6	10.1	5.68	10	29.2	26.3	20.8	19.8	26.7	23.7	15.3	13	12.6
22.4	54	8.8	20.4	44.6	31.2	27.4	25.1	32.9	61	81.6	37.9	16.9	14.5
54	106	23.3	33.4	53.3	54.5	92.7	54.4	51.3	51.8	69.9	52.4	34.8	33.9
74.4	53	22.5	27.6	37.9	48.6	44.6	36.8	54.7	57.4	54.8	50.2	67.4	45.7
17.2	38.3	34.9	11	53	64.2	43.3	30.1	43	44.2	44.2	60.1	69.6	56.2
20.4	44.4	33.4	43.8	45.2	41.5	41.5	26.3	41.8	33.2	39.7	52.4	44.1	31
22.2	22.6	20.4	18.1	28	24.3	20.6	36.5	22.1	21.7	20.9	15.3	14.3	8.92
29.1	20.1	20.4	14.9	19.6	22.8	26.8	7.86	24.8	19.1	13.5	14.9	14.9	26.9

Right (Pressure Transducers), z/d vertical axis (1.5 to 1), Sensel Position – x (0.14 to 0.21):

0	0	0	0	0	0	0	0	0	0	0	0	0	0
0	0	0	0	0	0	0	0	0	0	0	0	0	0
0	0	0	37.3	0	0	38.1	0	0	0	34.8	0	0	0
0	0	0	0	0	0	0	0	0	0	0	0	0	0
0	0	0	94.9	0	0	85.5	0	0	0	70.7	0	0	0
0	0	0	0	0	0	0	0	0	0	0	0	0	0
0	0	0	180	0	0	133	0	0	0	85.3	0	0	0
0	0	0	0	0	0	0	0	0	0	0	0	0	0
0	0	0	77.5	0	0	92.6	0	0	0	200	0	0	0
0	0	0	0	0	0	48.9	0	0	0	0	0	0	0
0	0	0	0	0	0	0	0	0	0	0	0	0	0
0	0	0	0	0	0	0	0	0	0	0	0	0	0
0	0	0	0	0	0	0	0	0	0	0	0	0	0
0	0	0	0	0	0	0	0	0	0	0	0	0	0

Figure 7.11: Map of the highest pressure recorded by the two instruments for the breaking wave (LP) – Left Tekscan, Right Pressure Transducers

Two different arrangements (7 and 6 transducers respectively) and 2×120 wave impacts were used to construct the results matrix on the right hand side of Figure 7.11. For EA3 pressures were measured on a solid wall while for every other arrangement impact pressures were measured on a segment of the wall mounted on load cells. The comparison between EA1, EA2 and EA4 (see section 7.2) clearly shows that for the tests with a solid wall the magnitudes of the impact pressures induced for the same incoming wave conditions are consistently higher. P_{peak} within the impact zone for EA3 are up to 3.5 times higher than those for EA2 and EA4.

With that in mind, a reasonable qualitative agreement can be observed for the results presented in Figure 7.11. The maximum P_{peak} recorded by each sensel (image on the left) and pressure transducer (image on the right) for 120 and 2×120 impacts of a breaking wave is plotted in Figure 7.11 as a function of each instruments location. The distance from the side wall is used for x (horizontal), y coordinates (vertical) are presented in relevance to the water depth, and the color scale (white to black) corresponds to increasing values of P_{peak}. For both sensors the impact zone is located above SWL although for the pressure transducers it appears to extend up to about z/d=1.35 instead of z/d=1.3 for the PMS. However, this small discrepancy is justifiable by the differences on the positioning, size and shape of the measuring area of sensels and transducers. The impact zone is very clearly depicted by the tactile sensor and maximum peak pressures (dark grey to black) occur for 0.14≤x≤0.15, 0.17≤x ≤0.18, and 0.195≤x≤0.205, similar to the location of the transducer arrays for EA3. Interestingly enough, for both instruments pressure values around the highest P_{peak} reduced by more than 50% within a distance smaller or equal to about 2.5cm. On the opposite side, the most striking difference between the two instruments is the drastically higher (up to 2 or even 3 times) P_{peak} measurements for pressure transducers. These discrepancies could, in parts, be attributed to the disadvantages explicit to the pressure mapping system (e.g. lower digital resolution) and to calibration inaccuracies. However, the results

presented in the previous section and mainly the comparison between EA2, EA1 and EA4 discussed above (see also Figure 7.4) indicate a strong effect related to the experimental set-up. A favorable comparison between the P_{peak} map of the pressure system and the pressure transducer measurements can be seen in Figure 7.12.

Left (Tekscan), z/d axis (1 to 1.5), Sensel Position - x (0.15 to 0.21):

5.11	4.7	6.79	6.38	4.3	5.66	7.39	5.59	5.44	3.41	4.69	4.41	5.25	4
7.22	6.25	6.57	4.6	6.03	4.26	4.02	3.72	4.13	3.37	2.48	2.48	2.2	3.55
4.33	6.54	7.86	8.03	7.56	6.26	14.1	2.06	2.03	2.16	2.2	3.1	1.43	3.52
3.46	5.07	2.81	4.13	6.04	5.63	4.48	3.4	3.6	4.7	5.54	2.34	3.63	2.86
4.11	2.8	3.6	3.09	4.87	2.97	7.65	3.52	4.34	5.57	5.31	2.46	4.68	4.74
12.9	4.3	6.74	4.98	2.51	4.34	6.3	10	7.47	6.43	6.05	4.26	5.23	14.3
11.7	9.09	4.99	4.94	3.11	6	7.78	9.18	6.39	7.15	9.21	1.75	3.73	6.91
6.67	6.3	4.88	5.48	9.89	11.2	12.2	10.2	8.01	6.83	7.59	4.57	5.4	4.01
13.6	4.47	3.69	4.74	14	1.68	5.91	4.66	12.7	9.23	3.03	7.76	7.82	6.13
13.6	13.6	8.57	5.86	8.56	3.05	2.36	7.91	11.1	8.13	10.1	10.2	10.7	7.17
4.94	7.08	12.7	3.23	8.92	11.7	8.06	12.1	12.4	12.4	11.4	11.1	9.49	5.09
8.51	6.61	13.4	4.69	8.23	14.4	13.4	9.92	10.2	11.3	8.53	10.6	3.22	7.21
9.39	8.8	4.88	6.28	4.84	14.9	13.6	11.9	9.7	12.5	10.9	9.2	4.68	3.61
7.85	13.8	4.12	7.15	7.39	3.25	14.4	1.69	5.58	5.39	9.6	13.7	8.91	6.35

Right (Pressure Transducers), z/d axis (1 to 1.5), Sensel Position - x (0.14 to 0.21):

0	0	0	0	0	0	0	0	0	0	0	0	0	0
0	0	0	0	0	0	0	0	0	0	0	0	0	0
0	0	0	8.84	0	0	0	5.79	0	0	0	7.48	0	0
0	0	0	0	0	0	0	0	0	0	0	0	0	0
0	0	0	8.96	0	0	0	10.7	0	0	0	13.9	0	0
0	0	0	0	0	0	0	0	0	0	0	0	0	0
0	0	0	11.1	0	0	0	15.9	0	0	0	11.6	0	0
0	0	0	0	0	0	0	0	0	0	0	0	0	0
0	0	0	13.7	0	0	0	13.3	0	0	0	15.3	0	0
0	0	0	0	0	0	0	0	0	0	0	0	0	0
0	0	0	0	0	0	0	19.7	0	0	0	0	0	0
0	0	0	0	0	0	0	0	0	0	0	0	0	0
0	0	0	0	0	0	0	0	0	0	0	0	0	0
0	0	0	0	0	0	0	0	0	0	0	0	0	0

*Figure 7.12: Map of the highest pressure recorded by the two instruments for the broken wave (BW) – Left Tekscan, Right Pressure Transducers*

As expected for broken waves pressure peaks are randomly scattered and pressure magnitudes are significantly smaller than those for breaking waves. Nevertheless, for both instruments the highest P_{peaks} are reported for y<0.15 with maximum values of about 20kPa, which reduce to $P_{peak} \leq 16$ for $0.15 \leq y \leq 0.25$ and to less than 10kPa for 0.15<y; similar results (not presented) were found for NB and SP. In contradiction to the results presented in Figure 7.11 for breaking waves, a very good qualitative and quantitative agreement is seen for broken waves, Figure 7.12. P_{peak} measured for EA3 and broken waves were also found to be in-line to those for EA4 and supporting therefore the accuracy of the results presented in Figure 7.12.

Overall, the comparison of the peak pressure distribution recorded by the pressure mapping system and the matrix of pressure transducers shows a reasonably good, qualitative at the very least, agreement and encourages the use of the *Tekscan I-Scan^{TM}* system for the acquisition of high resolution pressure maps.

7.3.3. Force measurements

The accuracy of the system is evaluated further in this subsection, where the force measured by the tactile sensor is compared with simultaneous load cell measurements. The force on the sensor is calculated as the integral of the pressures acting on each sensel with, however, the area considered for each measuring point (sensel) being larger (5.1x5.1mm) than the area over which the acting pressure is measured (approx. 3.1x3.1mm).

 An example of the force time history as recorded by the load cell and the pressure mapping system, for the first reflected wave and the second and third breaking waves is shown in Figure 7.13.
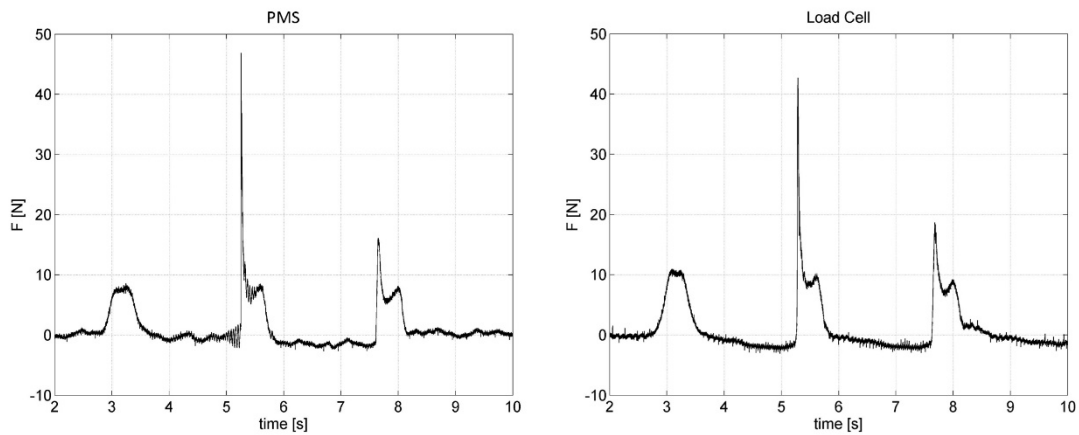
Figure 7.13: Force time series comparison breaking wave (LP) attack

Despite small differences on the maximum force values reported, a good agreement is seen between the two time histories, especially with regards to the temporal location and shape of the force pulse. The peaks of the forces recorded for all 120 events for breaking and broken waves are compared in Figure 7.14.
14.
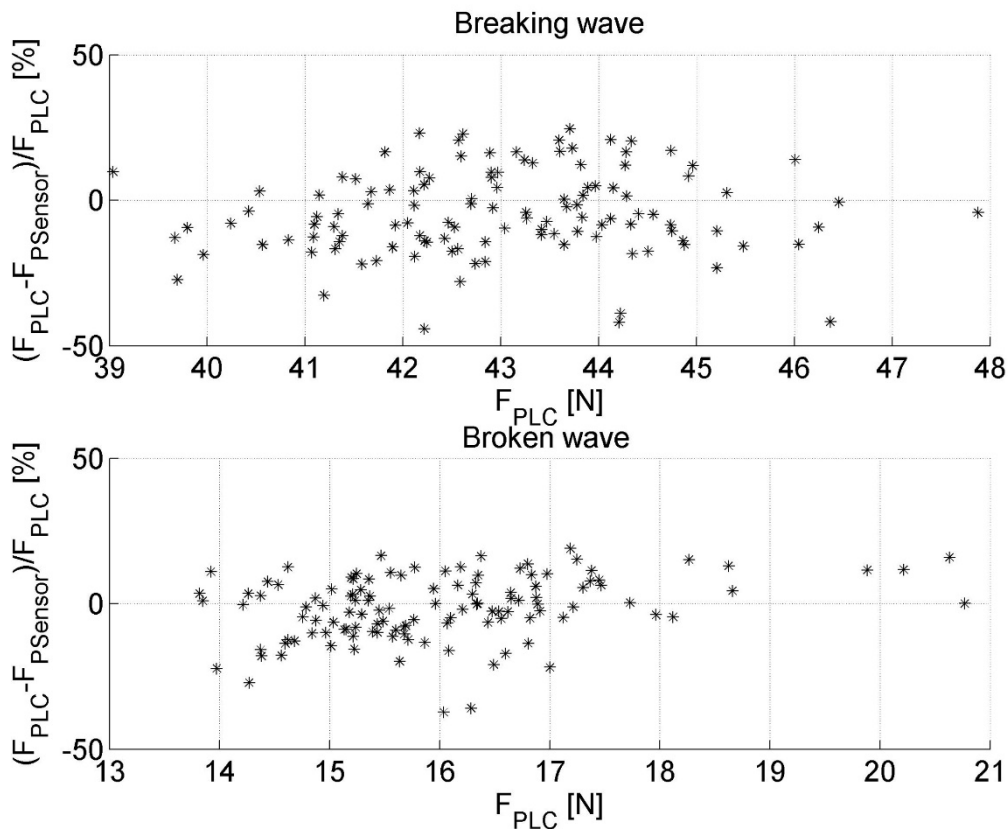
Figure 7.14: Comparison of the force peak for breaking (LP) and broken (BW) wave attacks

The majority of the force values calculated for the tactile sensor ($F_{PSensor}$) range within ±20% of the load cell measurements (F_{PLC}), while 55% and 70% of these measurements are scattered between ±10%, for breaking and broken waves respectively. For only 9% and 5% (breaking and broken waves) of all measurements the force calculated for the tactile sensor differs by more than ±20% of the corresponding load cell results; similar results (not presented) were acquired for NB and SP.

For the pressure mapping system, the above mentioned discrepancies can be attributed to sensel (pressure) calibration inaccuracies and to errors introduced by the calculation of the applied force as the integral of pressures acting on parts of and not over the whole sensor. Nevertheless with the majority of the errors ranging within ±20% the performance of the *Tekscan I-scan*^{TM} system is deemed satisfactory. In addition, the force results presented provide further support to the argument that the drastic disagreement between pressure peaks presented in section 7.3.2 for the tactile sensor and pressure transducers are mainly due to the differences in the experimental set-ups EA1 and EA3.

7.4. Conclusions

This two part work looks at the details of the application of the *Tekscan I-Scan*^{TM} pressure mapping system in hydraulic model tests involving wave impacts on rigid structures. The system is described in detail in the 1st part, where an appropriate experimental set-up and calibration methodology are proposed. In the 2nd part the pressure mapping system is used to measure wave impact induced pressures and loads on a model seawall and the results are used to validate the system against pressure transducer and load cell measurements.

The comparison between pressure mapping system and pressure transducer measurements shows:

*. A good agreement between the P_{peak} profile shapes presented for the pressure mapping system and the pressure transducers. P_{peak} magnitudes agree reasonably well and coherent profiles are reported for the mapping system.

*. That for all breaker types considered, the pressure mapping system tends to underestimate P_{peak}, especially for pressures closer the lower end of the nominal range of the tactile sensor used. However, differences between the system and pressure transducer measurements for the mean and std of P_{peak} range between ±15%, while the average values of the 3, 5 and 10 highest P_{peak} differ by up to ±10%.

*. An encouraging agreement for the spatial distribution (horizontal and vertical) of P_{peak}. The highest P_{peak} are reported at similar locations and the reduction trends shown for adjacent

pressures agree equally well. It is noteworthy that for breaking waves, the significantly higher pressure transducer measurements are due to differences in the experimental set-up.

*. That, especially for the strongest impacts, the pressure mapping system in combination with the tactile sensor (model 9500) used here reports shorter t_r than pressure transducers. Nonetheless, a good qualitative agreement on the $P_{peak} - t_r$ relation is shown and the overall differences are not considered significant enough to disregard the use of the system.

*. For the majority of the experiments conducted the integral of pressures (the force applied over the whole sensor) acting on the tactile sensor differ from simultaneous load cell measurements by less than ±20%.

*. High frequency pressure oscillations, potentially, related to the presence of bubbles are not recorded by the pressure mapping system.

*. Signal drifts related to the operation of the pressure mapping system and/or due to thermal and medium change shocks do not occur for application times used here.

Overall, the experimental results presented here encourage the use of the *Tekscan I-Scan^{TM}* pressure mapping system in combination with the experimental set-up and the calibration methodology suggested in Stagonas et al. (2015). Potential users, however, should be aware that applying the system in hydraulic model tests involving breaking waves can be laborious and requires careful planning and cautious use. It is also highlighted that to the authors' opinion the system, with its current limitations, it does not constitute an alternative to pressure transducers but it has the capacity to provide unique information referring to the spatial distribution of impact induced pressures. Therefore, and if the highest level of accuracy is sought after, the combined use with pressure transducers is suggested. As an example the pressure mapping system can be used to acquire knowledge on the location of high/extreme pressures and then pressure transducers can be used to collect pressure measurements.

Acknowledgement

References

Bullock, G. N., Obhrai, C., Peregrine, D. H., & Bredmose, H. (2007). Violent breaking wave impacts. Part 1: Results from large-scale regular wave tests on vertical and sloping walls. *Coastal Engineering*, *54*(8), 602–617. doi:10.1016/j.coastaleng.2006.12.002

Cuomo, G., Allsop, N. W. H., Bruce, T., & Pearson, J. (2010). Breaking wave loads at vertical seawalls and breakwaters. *Coastal Engineering*, *57*(4), 424–439. doi:10.1016/j.coastaleng.2009.11.005

Hattori, M., Arami, A., & Yui, T. (1994). Wave impact pressure on vertical walls under breaking waves of various types. *Coastal Engineering*, *22*(1-2), 79–114. doi:10.1016/0378-3839(94)90049-3

Hofland, B., Lech Kaminski, M., & Wolters, G. (2010). LARGE SCALE WAVE IMPACTS ON A VERTICAL WALL. *Proceedings of the 25th Coastal Engineering Conference*.

Hull, P., & Müller, G. (2002). An investigation of breaker heights, shapes and pressures. *Ocean Engineering*, *29*, 59–79. doi:10.1016/S0029-8018(00)00075-5

Kim, S.-Y., Kim, K.-H., & Kim, Y. (2015). Comparative study on pressure sensors for sloshing experiment. *Ocean Engineering*, *94*, 199–212. doi:10.1016/j.oceaneng.2014.11.014

Kisacik, D., Troch, P., & Philippe Van Bogaert. (2012). Experimental study of pressure distributions due to the breaking wave impacts. *Coastal Engineering*.

Oumeraci, H., Allsop, N. W. H., De Groot, M., Crouch, R., Voortman, H., & Vrijling, H. (2001). *Probabilistic design tools for vertical breakwaters*. (A. kortenhaus & H. Voortman, Eds.). Amsterdam : (ndl): Swets & Zeitlinger,.

Peregrine, D. H. (2003). Water - Wave Impact on walls. *Annual Review of Fluid Mechanics*, *35*(1939), 23–43. doi:10.1146/annurev.fluid.35.101101.161153

Saruwatari, A., Watanabe, Y., & Ingram, D. M. (2009). Scarifying and fingering surfaces of plunging jets. *Coastal Engineering*, *56*, 1109–1122. doi:10.1016/j.coastaleng.2009.08.007

Stagonas, D., Marzeddu, A., Gironella, X., Sánchez-Arcilla, A., & Muller, G. (2015). Measuring wave impact induced pressures with a pressure mapping system, Part 1: Experimental set-up and calibration. *Coastal Engineering*. (Submitted)

Stansberg, C., Berget, K., Graczyk, M., Muthanna, C., & Pakozdi, C. (2012). Breaking wave kinematics and resulting slamming pressures on a vertical column. In *Proceedings of the*

ASME 2012 31st International Conference on Ocean, Offshore and Arctic Engineering. Rio de Janeiro, Brazil.

8. Resumen y Conclusiones

8.1. Resumen

Para la redacción de esta tesis se han llevado a cabo más de 4000 ensayos en el canal físico de pequeña escala CIEMito (LIM-UPC) durante aproximadamente dos años (primer ensayo 06/11/13). Durante estos dos años se ha realizado un proceso de aprendizaje que ha derivado, después de un atento análisis de los resultados, a varias modificaciones en la geometría, en los oleajes, en la metodología, en la instalación y en los tipos de sensores ensayados. Durante este proceso se han generado dudas y respuestas, pero persiste la sensación que aún hay mucho trabajo a realizar para poder entender, en su totalidad, el fenómeno del impacto de las olas que rompen violentamente encima de estructuras marítimas rígidas. Seguramente el principal punto de partida es la necesidad de confianza en el método y en la metodología de ensayo y medida de este fenómeno. Tal como se ha dicho varias veces a lo largo de este trabajo, este fenómeno se distingue por su corta duración, elevada magnitud y elevada turbulencia. Esta última característica conlleva, aunque se garantice una casi perfecta repetitividad del oleaje incidente, las siguientes propiedades:

- Gran variabilidad de magnitudes,
- Gran variabilidad espacial
- Incorporación de aire en el fluido

Todas estas características hacen que la medida deba ser:

- Rápida (altas frecuencias de muestreo y bajos tiempos de respuesta de los instrumentos de medida)
- Densa (alta densidad espacial de puntos de medida)
- Extensa (es necesario cubrir una zona más grande de la de impacto para no perder puntos concentradosde altas presiones)
- No ser afectada por la presencia de una mezcla de aire y agua (zona de medida con un contacto directo con el fenómeno).

8.2. Conclusiones

El análisis de los resultados de todos los ensayos realizados durante este trabajo muestra que:

8.2.1. Metodologia

- La gran variabilidad en la magnitud de fuerzas y presiones impulsivas hace que sea necesario un gran número de repeticiones del mismo oleaje para garantizar un resultado estadísticamente valido.

- La fiabilidad de los resultados (sobre todo en magnitudes) de los sensores táctiles depende en gran parte de su *set-up* y de la calibración realizada. Para garantizar la validez de los resultados es importante utilizar:
  - Un *set-up* estanco para mantener el sensor seco durante las pruebas.
  - Un sensor adecuadamente perforado de manera que se pueda quitar el aire atrapado en su interior, manteniendo al mismo tiempo el vacío en su interior durante toda la duración de los experimentos.
  - Impacto dinámico con agua, como por ejemplo la caída de un volumen controlado de agua desde un altura predeterminada
  - Una calibración única para cada sensor (196 en el sensor utilizado para estos test)
  - El mayor número posible de puntos de calibración
- Una calibración de orden superior si se puede cubrir todo el rango de presiones (como aconseja la empresa constructora del sensor), aunque prácticamente se han obtenido idénticos resultados utilizando una calibración lineal. Esta última es preferible para aquellos sensores donde no se pueda cubrir todo el rango de presiones.

8.2.2. Muestreo

- A bajas frecuencias de muestreo corresponden bajas probabilidades de muestrear correctamente el pico de fuerza/presión impulsiva. En el caso particular de estos ensayos se ha comprobado que a frecuencias de muestreo menores de 1 kHz se corresponden reducciones en el promedio de las fuerzas/presiones medidas de más del 10%. Claramente esta consideración depende de la duración del fenómeno a medir. Como consideración general se puede analizar la cantidad de puntos medidos durante el transitorio y asociarla con el máximo error de medida posible.

$$E_{max} = \frac{50}{n_{points}}$$

Con:

E_{max} = máxima reducción del pico de fuerza/presión posible (en %)

n_{points} = número de puntos registrados durante el transitorio

Se aconseja así el uso de una frecuencia cercana a 4 kHz optimizando el equilibrio entre la velocidad de muestreo y cantidad de datos registrados

- Considerando que se ha trabajado con una escala de trabajo entre 1/50 y 1/100, se propone una frecuencia de muestreo a escala prototipo de 500 Hz.

8.2.3. Incertidumbre

- La gran variabilidad espacial no permite extrapolar los valores de presión medidos en un punto a una gran área de influencia sin cometer arriesgados errores. La fuerza medida con la célula de carga utilizando como área de medición todo el ancho del canal (y toda la vertical) infravalora el valor de fuerza extrapolado da la distribución vertical de presiones. Por otro lado, la fuerza medida utilizando como área de medición sólo los diez centímetros centrales, en promedio, es comparable con el valor de fuerza extrapolado da la distribución vertical de presiones. Igualmente, la desviación típica aumenta si se utilizan medidas puntuales de presión, con resultados superiores al 25%. El uso del sensor táctil ha proporcionado información acerca de la coherencia tanto vertical como horizontal de las distribuciones de presión. Se han evidenciado "puntos calientes" de presiones de pequeñas dimensiones. La probabilidad de capturar estos puntos calientes disminuye al bajar la densidad espacial de medida.

- La comparación exhaustiva de todos los sistemas de medida ha evidenciado que:
    - En la mayoría de los experimentos realizados, la integral de las presiones medidas del sensor táctil (equivalente a la fuerza aplicada sobre todo el sensor) difiere de las medidas simultáneas de la célula de carga por debajo de un ±20%.
    - Existe una buena correlación espacial entre las medidas de los sensores de presión y del sensor táctil. Se han registrados perfiles de presión coherentes.
    - La comparación entre sensores de presión y sensor táctil, acoplados con células de carga, evidencia diferencias en el promedio de los picos de presión en un ±15%, que se reduce a un ±10% si se consideran sólo los 10 valores más elevados.
    - En el caso del oleaje con impacto más violento, cuando los sensores de presión no están acoplados con la célula de carga, se registran medidas mucho más elevadas. Aunque las diferencias sean elevadas sigue habiendo buena correlación espacial. Esto evidencia el efecto de un set-up diferente con la célula de carga que deformándose (fenómeno necesario para su correcta medición), genera un efecto amortiguador sobre las presiones medidas.
    - Oscilaciones de presión de altas frecuencias presentes en las series temporales de los sensores de presión no están presentes en las series temporales de los sensores del sensor táctil. Estas oscilaciones se atribuyen a la presencia de burbujas de aire y de un volumen "muerto" de aire delante de la membrana de medición del sensor de presión.

8.2.4. Extrapolación al diseño de estructuras rígidas

Los resultados aquí presentados deben ser interpretados como unas directrices para realizar una mejor, lo más correcta posible, campaña de medidas para estudiar el fenómeno impulsivo del oleaje que pueda romper directamente sobre una estructura rígida. Se evidencían las necesidades de hardware específico para la ejecución de este tipo de medida analizando posibles efectos relacionados con la tipología de sensores, los sistemas de adquisición y la metodología de ensayo y análisis. No se desaconseja/aconseja a priori la utilización de ningún sistema de medida, aunque se observa un gran potencial en la utilización de los sistemas táctiles, condicionado a su correcta puesta a punto y calibración.

Destacar quizás que una pobre resolución espacial de sensores de presiones clásicos, puedan dar lugar a subestimación del orden del 75 % en el valor de la resultante de fuerzas durante el instante impulsivo del oleaje sobre la estructura.

Con este estudio se quiere también hacer resaltar las posibles repercusiones de una incorrecta campaña de medición sobre el diseño de estructuras rígidas. Se ha identificado grandes diferencias entre medidas tomadas con los mismos sensores con *set-up* diferentes. Esto puede llevar a fallos estructurales importantes en las obras reales o a diseños exageradamente seguros que conllevan unos gastos económicos totalmente inútiles y a veces inasumibles.

8.2.5. Limitaciones y trabajos futuros

Uno de los avances mas importante de este trabajo es la implementación de una nueva técnica de medida de fuerzas y presiones basada en el uso de un sensor de presión tactil (pressure mapping system by Tekscan) que permite medidas de presión con una elevadisima densidad espacial (4 puntos por cm2). Este sensor también destaca para su flexibilidad. El sensor táctil puede adaptar su forma a prácticamente cualquier superficie y se abren así nuevas perspectivas para la medida de presiones en estructuras con geometrias complejas. La posibilidad de adquirir "paneles de medida de presión" de grandes dimensiones acoplables al mismo hardware, permite su uso también en infraestructuras de gran escala y en el campo. Claramente se han identificado varias limitaciones. En primer lugar, para una correcta medición de las presiones, hay que manipular el sensor de forma tal que deje salir el aire atrapado entre las dos membranas de medida. Si no se deja escapar este aire se genera un efecto almohada y el sensor no mide corectamente. Esta manipulación, aunque sencilla (abrir unos pequeños cortes en la membrana superior con un cutter), deja al sensor permeable y expuesto a la entrada del agua. Los electrodos mojados cambian la propia resistividad y el sensor acaba siendo inutilizable. Existen sensores de grandes dimensiones, ya preparados por la empresa constructora del sensor, con

canales de ventilación que permiten la salida del aire manteniendo la estanqueidad del sistema. Desafortunadamente no existen sensores de pequeñas dimensiones (utilizables en canales de pequeña escala) con esta característica. Esta pérdida de estanqueidad genera un aumento importante de la complejidad del *set-up* y de los riesgos de pérdida de funcionalidad del sensor. Hay que destactar también que la realización del mismo sistema de calibración (caída de un volumen controlado de agua), utilizado para estos ensayos, a gran escala comportaría problemas constructivos importantes.

Otra limitación en el uso del sensor táctil es la medida de presiones en un ambiente donde esta presente una mezcla de aire y agua típica de las olas rompiente. Los sensores de presión clásicos en su mayoria tienen la unidad de medición (membrana) alejada de la boca del propio sensor. Este volumen añadido de aire (comprimible) entre la membrana y la boca del sensor puede tener un efecto almohada o un efecto de magnificación de las presiones (explosión de la burbuja de aire). Ademas, a consecuencia de este volumen de aire se pueden iniciar incontrolables (e incuantificables) efectos de vibración de la membrana que puedan alterar la medida. También aparecen dudas en la tipologia de calibración que se utiliza para estos sensores. Los sensores de presión vienen calibrados (y certificados) por el constructor, pero esta calibración, dinámica y estática, se realiza en cámaras de aire a presión controlada. Este ambiente parece lejos de rapresentar corectamente la mezcla de aire y agua en la que se encontrarán al medir los sensores de presión. Pruebas realizadas con columna de agua han corroborado la exactitud de la calibración en caso de presiones estáticas, pero ha sido imposible comprobar la parte dinámica de la calibración en condiciones de impacto de una mezcla de aire y agua.

Vistos los resultados de todos los ensayos en los cuales se han acoplado células de cargas y sensores de presión (sean los clásicos transductores o el sensor táctil) se ha notado una disminución no irrelevante de las presiones medidas. Una parte de trabajos futuros sería volver a testear el sensor tactil encima de un soporte totalmente rigido y no de una celula de carga. Desafortunadamente esto no se ha podido realizar durante esta serie de ensayos.

Al mismo tiempo, utilizando el set-up EA2 (Figura 7.2) y con los oleajee regulares LP y BW (Tabla 7.1), se han realizado una serie de ensayos utilizando teoría de generación de orden superior. Los resultados estan todavía en fase de análisis, pero se ha podido notar una variación de la distribución de presión. El uso del sensor tactil habría dado información adiciona importantísima con la elevada densidad espacial que permite.

Ahora que la fase de test de este innovador sensor se ha acabado, sería muy importante empezar a ensayar oleajes irregulares y corroborar todas las formulaciones extrapoladas a partir

de ensayos anteriores. Este sistema de medida puede aportar, sobre todo en la zona de impacto, una mejora importante en la definición de los diagramas de presión. Se abre también la posibilidad de ensayar en piscina oleajes oblicuos e intentar entender los complejos fenómenos de interación oleaje estructura en el caso de impacto con un angulo no normal difícilmente estudiables con arrays de sensores de presión.